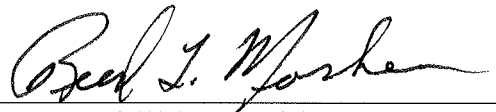
EXPERT REPORT

Prepared for United States Department of Justice
Robinson v. United States

Prepared by:



REED L. MOSHER
December 18, 2008

Table of Contents

Executive Summary…..…… 5

I. Assessment of Levee Erosion and Scour Along the Mississippi River Gulf Outlet…….. 9

Introduction 9

1. Failure Patterns..... 15

a. Evidence of overtopping erosion of Levees 15
b. Evidence of wave damage of levees..... 17
c. Evidence of overtopping damage of floodwalls 20
c. Evidence of overtopping damage of floodwall/levee transitions..... 24

2. Soils and Erodibility..... 25

Hydraulic Placement of fill for the Levee Construction..... 25
a. Hydraulic Fill..... 25
b. Soil Type..... 26
c. Erodibility 30

3. Post-Katrina Erosion Observations along MRGO 31

a. Levees 33
b. Sheetpile Walls 47
c. Transitions 49
d. Soil Quality and Erosion..... 53

4. Summary 54
References 56

II. Assessment of Breaches along the Inner Harbor Navigation Canal…….57

Introduction 57

1. Observations and Possible Modes of Failure..... 60

2. Stratigraphy..... 67
a. IHNC East Bank – Lower 9th Ward..... 67
b. Shear Strength - IHNC – East Bank 72
c. Original Design Strengths - East Bank 79

3. IHNC East Bank North and South Failures 84

4. Analysis of GDM Cross section 96
Summary 100

III. Assessment of Erosion Potential for MRGO Hypothetical Alternative Conditions ... ……..101

Appendix A: Oblique Photos - MRGO Reach 2 Levees and Floodwalls……..110

Appendix B: Inner Harbor Navigation Canal (IHNC) Seepage Analysis 161

CV ……..189

Executive Summary

Hurricane Katrina's unprecedented storm surge and waves overwhelmed the Lake Pontchartrain and Vicinity Hurricane Protection Project ("LPV") flood works on August 29, 2005. These levees, floodwalls, and control structures had not been designed to withstand a storm as powerful as Hurricane Katrina. Based on my study of the available and pertinent evidence and information, it is my opinion to a reasonable degree of scientific certainty that:

(1) The Mississippi River-Gulf Outlet ("MRGO") did not cause the breaching of the LPV levees and floodwalls adjacent to St. Bernard Parish, New Orleans East, and the Lower Ninth Ward;

(2) The hydraulic forces of the waves and the surge that overtopped the LPV levees and floodwalls on the south side of the MRGO and the east side of the IHNC were sufficiently powerful to cause the breaches that occurred even if the MRGO had been no larger than its design dimensions or had not even been in existence when Hurricane Katrina struck. Erosion of the protected side of these levees precipitated by overtopping flow and waves was the principal failure mechanism for the breaches in the LPV levee on the south side of the MRGO. Even if the MRGO had been smaller when Katrina struck---or had not even existed---the large volumes of water and the significant velocities of this water washing over the levees for prolonged periods under either of those scenarios would have been sufficient to erode the protected side of the levees catastrophically. In numerous locations this erosion progressed from the protected side, resulting eventually in erosion of the crown the levees, resulting in loss of crown elevation (*i.e.,* breaches) in these locations. These initial breach formations allowed even greater volumes of water to flow over the levees and through the breaches, resulting in enlargement of the breaches. Parametric studies support my opinion that large breaches would have been caused by protected-side erosion even if the MRGO had been no larger than it was designed to be or had not even existed at all when Hurricane Katrina struck;

(3) Neither wave-induced flood side breaching nor seepage was the principal cause of the breaching that occurred in the LPV levees on the south side of Reach 2, and there insufficient evidence or information to conclude that either of these mechanisms was even a secondary cause of the breaching that occurred; and

(4) The hydraulic forces exerted by storm surge and waves in the IHNC caused the LPV floodwall on the east side of the canal just south of Florida Avenue to collapse before the surge and waves

reached the top of the wall (colloquially referred to as the "north breach"). Even if the MRGO had been no larger than its design dimensions or if the MRGO had not even existed, Hurricane Katrina would have forced sufficient surge and waves into the IHNC through the GIWW to cause the LPV floodwall to collapse at this location.

(5) The hydraulic forces exerted by storm surge and waves in the IHNC caused the LPV floodwall on the east side of the canal north of Claiborne Avenue to collapse after the surge and waves overtopped the wall (colloquially referred to as the "south breach"). Even if the MRGO had been no larger than its design dimensions or if the MRGO had not even existed, Hurricane Katrina would have forced sufficient surge and waves into the IHNC through the GIWW to overtop the LPV floodwall and cause its collapse at this location.

(6) The hydraulic forces exerted by Hurricane Katrina on the LPV levees on the south side of the MRGO and the north side of the GIWW and on the floodwalls on the east side of the IHNC exceeded those that they were designed to withstand. Even if the MRGO had been at its design dimensions when the storm struck—or had not even existed at all—the hydraulic forces generated by the hurricane would have exceeded those that the LPV levees and floodwalls in these locations were designed to withstand. These flood control structures were designed to provide hurricane protection only until they were overtopped. Hurricane Katrina generated sufficient surge and waves to overtop the LPV levees and floodwalls for a prolonged period and would have done so even if the MRGO had not been in existence or had been at its design dimensions.

The principal failure mechanism for the breaches of the levees and other flood control structures on the south side of Reach 2 of the MRGO was overtopping. The volume and velocity of water cascading over the levees far exceeded the shear stresses necessary to trigger soil erosion. Numerous and detailed analyses of the soils used for levee construction in this area validate this opinion. There is no valid scientific basis, or physical evidence, to support any significant wave-induced flood side erosion or seepage as causes of breaching.

Subsequent parametric studies in which the MRGO is modified or removed from the topographical landscape of Southeastern Louisiana were performed to determine the effects of this channel on storm surge and wave propagation. (Ebersole 2008). Analyses of overtopping rates and shear velocities were also performed for these parametric studies. (Resio 2008). This data was then applied to the results of analyses of the levees performed in support of the Interagency Performance Evaluation Task Force ("IPET"),

particularly Volume V: The Performance – Levees and Floodwalls. The reports demonstrated that removal or modification of the MRGO did not prevent prolonged overtopping of these structures and exposure to shear stresses high enough to trigger significant erosion.

There is no evidence to support that wave-induced flood side erosion was a failure mechanism during the hurricane. Post-storm investigations performed with the IPET team found only minor flood side erosion of the Reach 2 levee in the area south of the Bayou Dupre Control Structure. This portion of the levee was several feet higher than the average heights of the levee portion between the Bayous Bienvenue and Dupre Control Structures and did not experience overtopping. Based on the hydrographic data, this levee portion was exposed to wave attack for a longer period than the rest of the Reach 2 levee. The minor erosion on this face is consistent with this prolonged exposure. The fact that there was no wave-induced flood side breaching in this area is illustrative of the likelihood that the rest of the levee, composed of similar soil materials and grass covering, breached due to overtopping.

There were two floodwall breaches adjacent to the Lower Ninth Ward at issue in this case. They are colloquially known as the north and south breaches. The cause of failure for the south breach, located near Claiborne Avenue, was overtopping. As floodwaters traveled through the GIWW/MRGO junction (known as Reach 1) into the Inner Harbor Navigation Canal ("IHNC"), they overtopped the floodwall adjacent to the Lower Ninth Ward. Prolonged exposure to these powerful forces caused significant erosion on the protected side of the floodwall, characterized in post-hurricane photographs by a long and contiguous U-shaped trench behind the floodwall. This erosion diminished the stability of the floodwall, causing it to deflect laterally towards the protected side. As the floodwall lost stability, the force of the water against the floodwall exacerbated the deflection, ultimately causing a breach.

The north breach, near the Florida Avenue bridge, breached prior to overtopping. This was due to a gap that formed between the levee and the floodwall as the floodwall deflected under hydraulic loading and from the ground surface at the levee toe and beyond being lower than the ground surface used in the original design. The development of this gap and lower ground surface destabilized the wall, causing its collapse and allowing floodwaters to flow through the breach into the Lower Ninth Ward and beyond.

Seepage was not a cause of failure for these two breaches. Analyses were performed using a finite element model accepted and validated in the civil engineering community to determine whether this was a failure mode. The soils in the foundation for the floodwalls were analyzed with both high and low permeability values for the soil. Seepage was ruled out as a cause of failure in each of these scenarios. The data inputs Plaintiffs' expert Dr. Bob Bea uses in support of his opinion are based on unrealistic and unproven permeability values and unverified and inaccurate soil stratification. This flawed data produced equally flawed results. Dr. Bea violates the principle of effective stress, soil mechanics most basic concept, by using the soils undrained shear strength in

combination with pore water pressures when performing the slope stability analyses using the limit equilibrium method. The very use of undrained shear strength for the soils implicitly implies that the permeability of the soil is nearly impervious.

I am an employee of the United States Army Corps of Engineers and am not receiving additional compensation for the preparation of this report.

I have yet to read the depositions of Plaintiffs' experts. Therefore, I may have additional opinions.

I. Assessment of Levee Erosion and Scour Along the Mississippi River Gulf Outlet

Introduction

The levees along the Mississippi River Gulf Outlet (MRGO) on the northeast side of St. Bernard Parish, had numerous breaches and were washed out over considerable lengths during Hurricane Katrina, on the morning of August 29th. The performance of levees varied significantly throughout the New Orleans area, but levees along MRGO suffered more damage from erosion and scour than any other part of the New Orleans area hurricane protection system. The MRGO levees were overtopped by as much as 5 ft of water from the hurricane surge and waves for extended time period. These levees were built using a hydraulic filling construction method which contributed to their vulnerability to erosion. Over the years since the construction of the levees along the MRGO, subsidence of the New Orleans area and the consolidation of the soils below the levees resulting in their settlement have led to a reduction in the protection elevation level below that of the original design protection level for the MRGO which increased the amount of overtopping, erosion and subsequent flooding.

Figure 1 shows the breach locations for St. Bernard Parish, which includes nearly 70% of the levee along MRGO. Figure 2 highlights the levee's construction methods, including hauled, hydraulically filled, and walled reaches. Note the breach locations in Figures 1 and 2 coincide with the reaches constructed using hydraulic fill. The elevations of the pre-Katrina hurricane protection levees and floodwalls are significantly below the originally designed heights in part from errors in initial constructed elevations, in part from rapid subsidence, and in part from sections where the authorized hurricane protection levees and floodwalls are not yet been completed. Figure 3 shows the LIDAR stationing map for a segment of MRGO levee. Figures 4 shows the pre- and post-elevations of the levee along the MRGO. The figure is taken from the IPET report and shows pre- and post-Katrina conditions that would be similar to the base conditions used in this litigation. It depicts the degree to which levee elevations just prior to Katrina deviated from the authorized levels.

Based on my review of the available data, I have reached the following opinions:

1. To a reasonable degree of scientific certainty, breaching and erosion which occurred along the levees adjacent to Reach 2 of the MRGO were primarily caused by overtopping. The available data does not support a conclusion as to whether front side erosion from waves was a cause of the breaching along Reach 2.

2. To a reasonable degree of scientific certainty, a primary factor that led to the erosion and breaching of the levees from overtopping along Reach 2 of the

MRGO was the construction of the levees using hydraulic placement of the soil. Breaching and erosion of levees in the New Orleans area from Hurricane Katrina only occurred along sections where the soil for the levee was placed by hydraulic dredging of the channel and hydraulically placing the soil to form the levees. Where the levees were constructed by placing clay soils at controlled water content and compacted, no breaching occurred.

3. To a reasonable degree of scientific certainty, the erosion and breaching of the levees and the subsequent flooding which occurred along Reach 2 was more severe because the protective elevation of levees were below the authorized elevations. Sections of the levees between Bayous Bienvenue and Dupre control structures were 2 ft below the authorized protective elevation for the levees.

.



Figure 1. St. Bernard Parish breach locations.

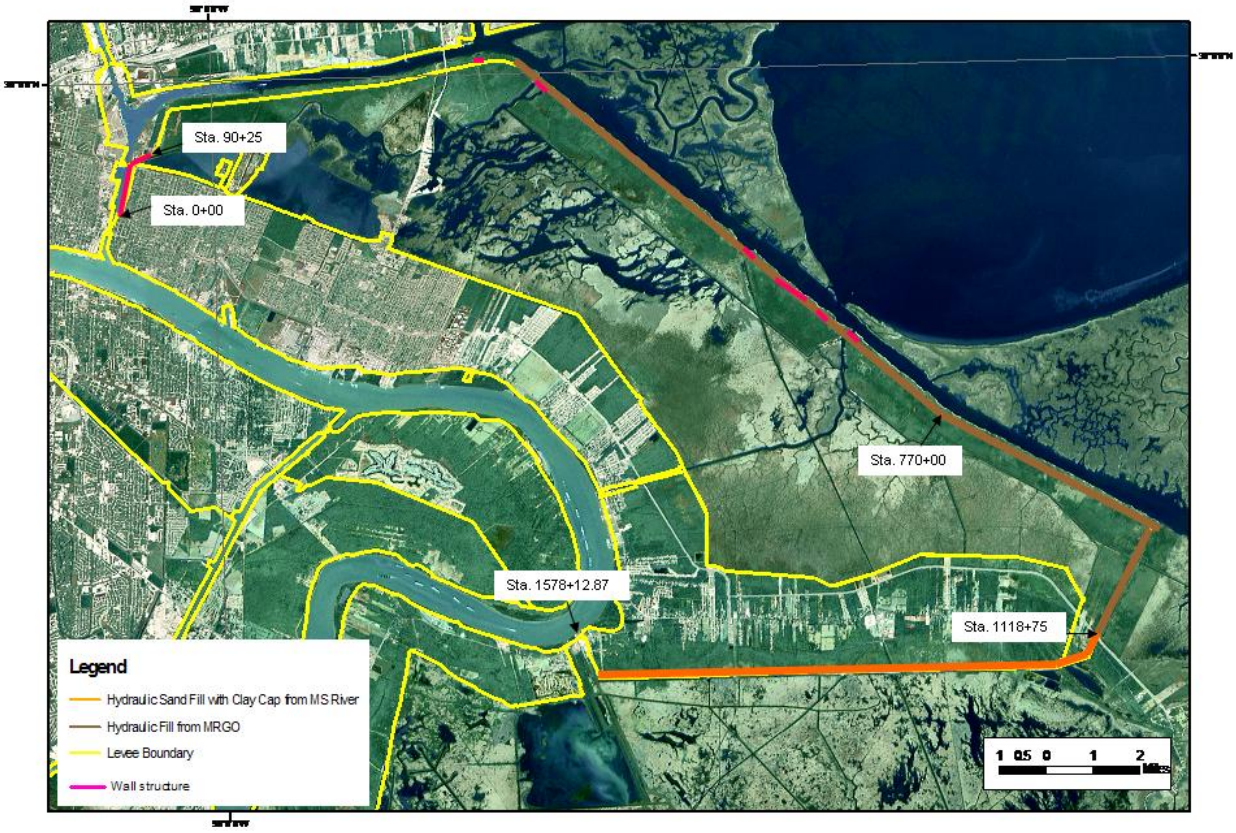


Figure 2. Constructed levee soil sources.

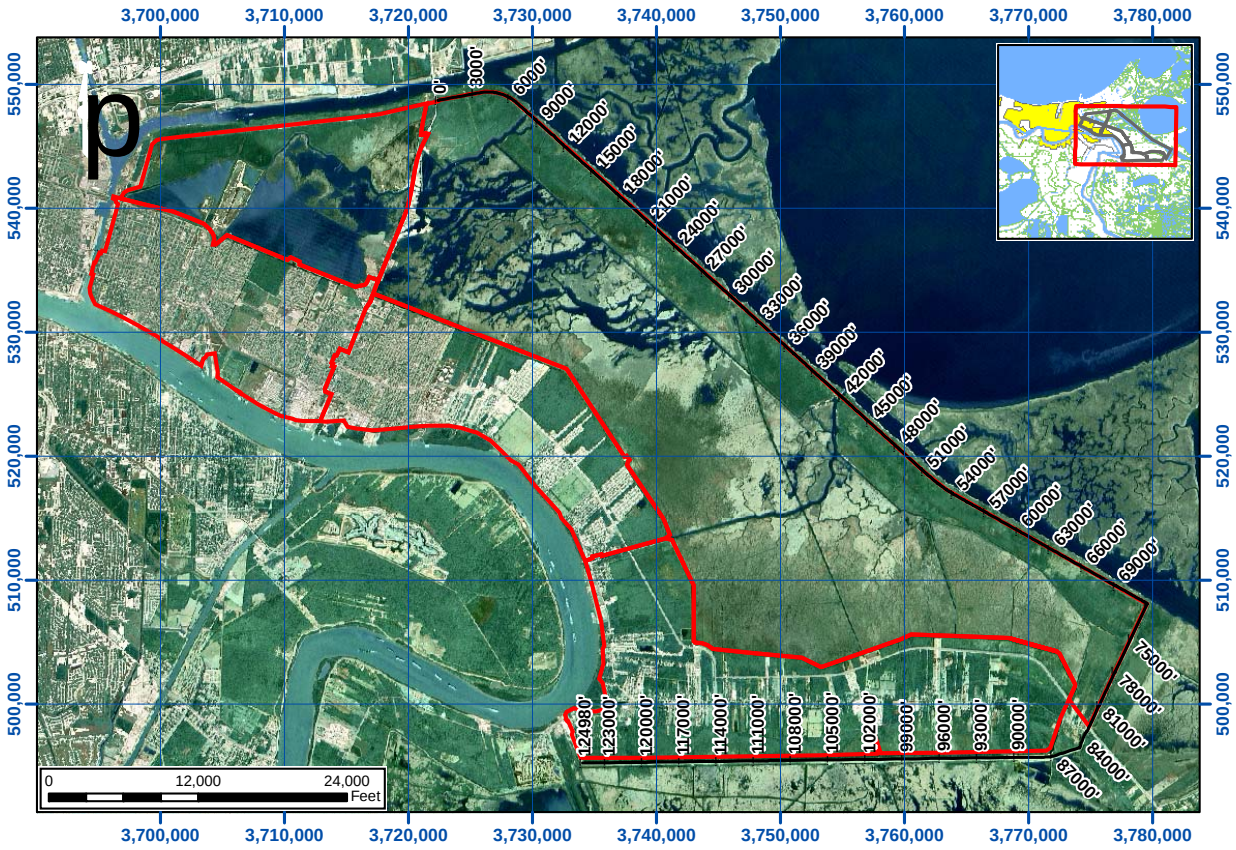


Figure 3. St. Bernard Parish LIDAR stationing map with ERDC erosion test locations.

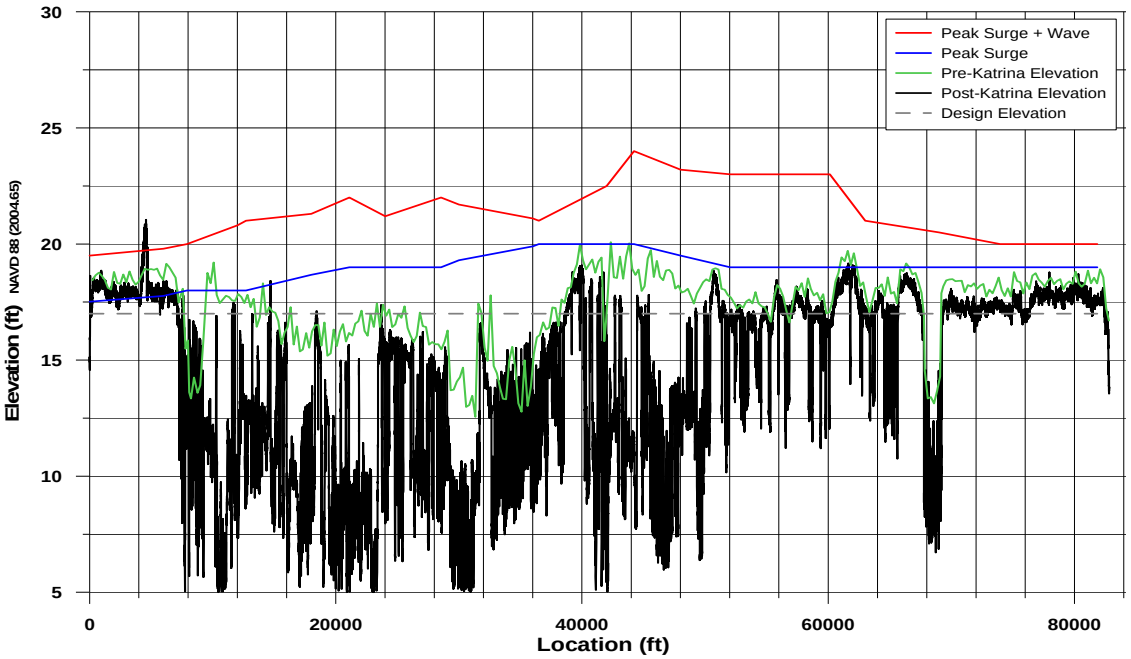


Figure 4. Pre- and post-elevation of the levee with water levels along the MRGO. (IPET 2007).

1. Failure Patterns

The erosion and scour of levees and floodwalls along Reach 2 of MRGO area was caused by overtopping. The available data does not support a conclusion as to whether front side erosion from waves was a cause of the breaching along Reach 2.

a. Evidence of overtopping erosion of Levees

Protected side (backside or landside) erosion patterns were observed along the breached and unbreached levees in the New Orleans area after Hurricane Katrina. Figure 5 shows a generalized cross section of a levee being overtopped by the storm surge. The water overtopping the levee increases in velocity as it flows down the protected side of the levee causing shear stresses to the levee surface. If the shear stresses are high enough, erosion will occur. With overtopping producing high velocity flow down the protected side of the levee, erosion is initiated where there are changes in the surface geometry or irregularities in the surface of the levee causing turbulent flow that erodes the soil. As the erosion zone develops, the flow becomes more turbulent resulting in even greater erosion. The continued overtopping sustains the growth of the erosion zone, increasing the turbulence of the flow. This process of erosion is called head cutting. The face of the erosion zone nearest the levee crest will become nearly vertical for cohesive soils (clay or clayey silts) and sloping for non-cohesive soils (silts and sandy silts). The following overtopping and breaching damage patterns were observed along the MRGO.

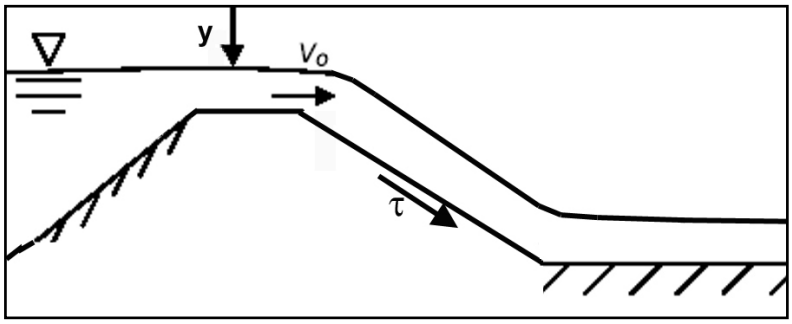


Figure 5. Conceptual diagram of water surge (without waves) overtopping an earthen levee.

As the earthen levee is overtopped, it will exhibit identifiable stages of progressive erosion on the protected side of the levee. The four stages of progressive erosion are illustrated in Figure 6 (Hunt et al 2005, Fukuoka and Fujita 1988).

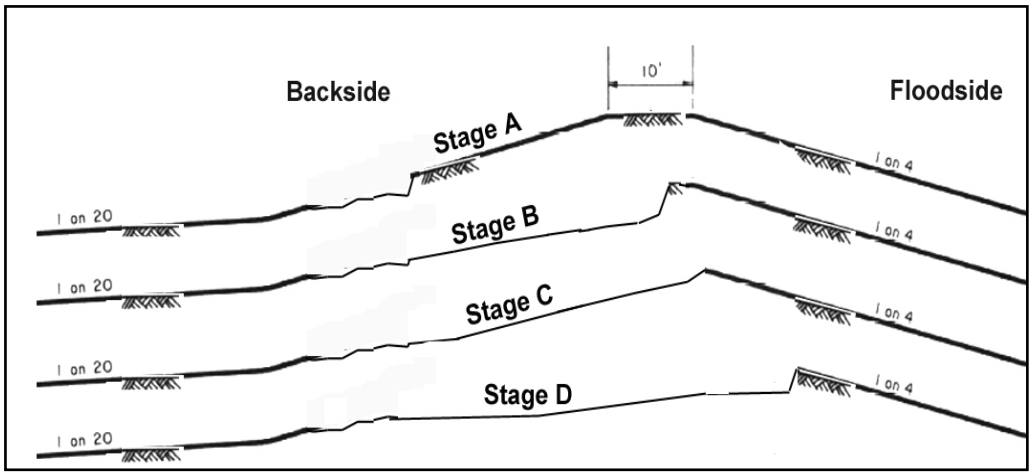


Figure 6. Erosion progression stages.

Figure 7 is a photograph from Reach 2 along the MRGO that shows all four stages of progressive erosion:

Stage A. *Initial overtopping causes surface sheet and rill erosion which develops into a series of cascading overfalls. The highest forces develop from the backside slope down to the backside toe, and the crown is not initially exposed to these large hydraulic forces. The cascading overfalls develop into one large headcut that migrates from the slope to the crest such that the erosion width approximately matches the overtopping width.*

Stage B. *The headcut continues to migrate from the backside crest (crown) to the floodside crest.*

Stage C. *The crest drops as a breach begins to develop.*

Stage D. *The breach opening erodes out to the toe and the breach widens.*



Figure 7. Four stages of progressive erosion along Reach 2 of Mississippi River Gulf Outlet.

b. Evidence of wave damage of levees

There are several locations along the levees adjacent to the MRGO facing Lake Borgne that show signs of some minor front side erosion from wave action, Figure 8. Figure 9 shows the only observed case of front side erosion from wave action that affected the levee crest. It resulted in a narrow cut through the crest of the levee with minor loss of protective elevation. Figure 10 shows an aerial photograph of the area shown in Figure 8 and 9. Figure 11 shows the elevation of the levee before and after Katrina and the water levels due to the hurricane. The pre-Katrina levee elevations along this section where the front side erosion occurred are the highest along MRGO facing Lake Borgne and would have been the location with the longest period of time with the waves breaking on the front side of the levee. This is most likely the reason why there was erosion on the front side of the levee at this location.



Figure 8. Front side levee damage along the Mississippi River Gulf Outlet.



Figure 9. Front side wave erosion of the crest along the MRGO.



Figure 10. Aerial photo of front side erosion on the MRGO.

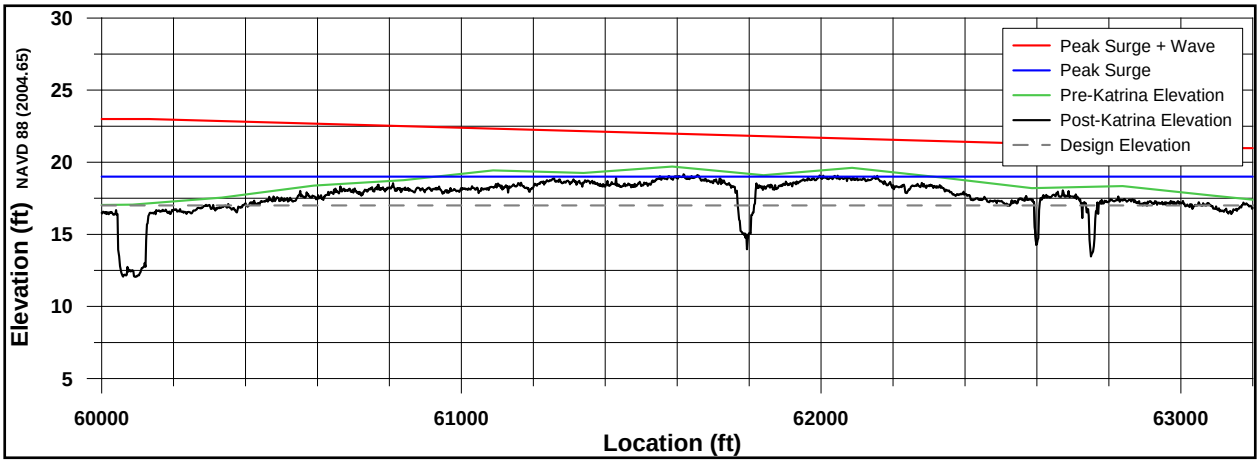


Figure 11. Pre- and post-elevation of the levee with water levels along the MRGO.

c. Evidence of overtopping damage of floodwalls

Figure 12 shows a conceptual diagram illustrating the water overtopping plunging velocity and force of impact on the wall's backside. The high velocity water overtopping the wall froms a plunging jet on the soil adjacent to the protected side of the wall. This jet creates large eddies that erodes the unprotected soil adjacent to the wall. Figures 13 through 15 show the different stages of erosion as a result of floodwall overtopping along the MRGO.

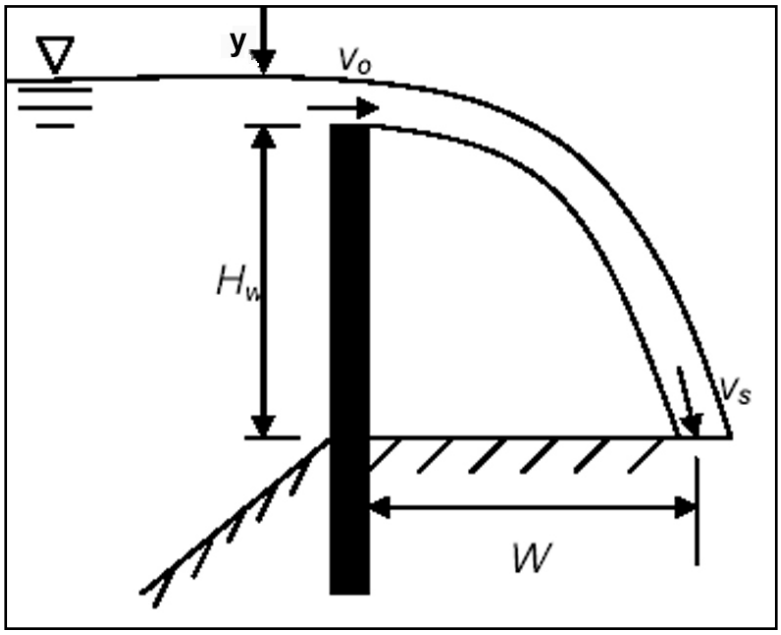


Figure 12. Conceptual diagram of water overtopping a floodwall or exposed sheet pile.

Exposed sheetpile reaches along the MRGO in St. Bernard Parish (Chalmette and Chalmette Extension Hurricane Protection Plans) experienced scouring on the backside, and several locations were breached.



Figure 13. View Looking Southeast from the Bayou Bienvenue Control Structure Showing Backside Scour Beyond the Structure



Figure 14. Sheetpile Between Bienvenue and Dupre Control Structures. Note the sheetpile elevation differences



Figure 15. Closeup of Adjacent Breached Sheetpile with Backside Scour. Note the stratified layers in the soil profile representing existing hydraulic fill historically dredged from the MRGO

c. Evidence of overtopping damage of floodwall/levee transitions

Numerous transition breaches were observed post-Katrina, and they overtopped due to elevation differences. After overtopping, the soil either scoured on the backside of the vertical structure or eroded the levee. The overtopping erosion / scour followed the progressive stages for the levee and/or the impact scour pattern for the floodwall, both as described above. Figure 16 is a diagram of the flow patterns that develop as overtopping occurs. The backside has increased erosion due to local increases in overtopping velocity, especially if the levee crest is lower than the floodwall. As the overtopping height increases above the floodwall height, backside erosion develops along the floodwall.

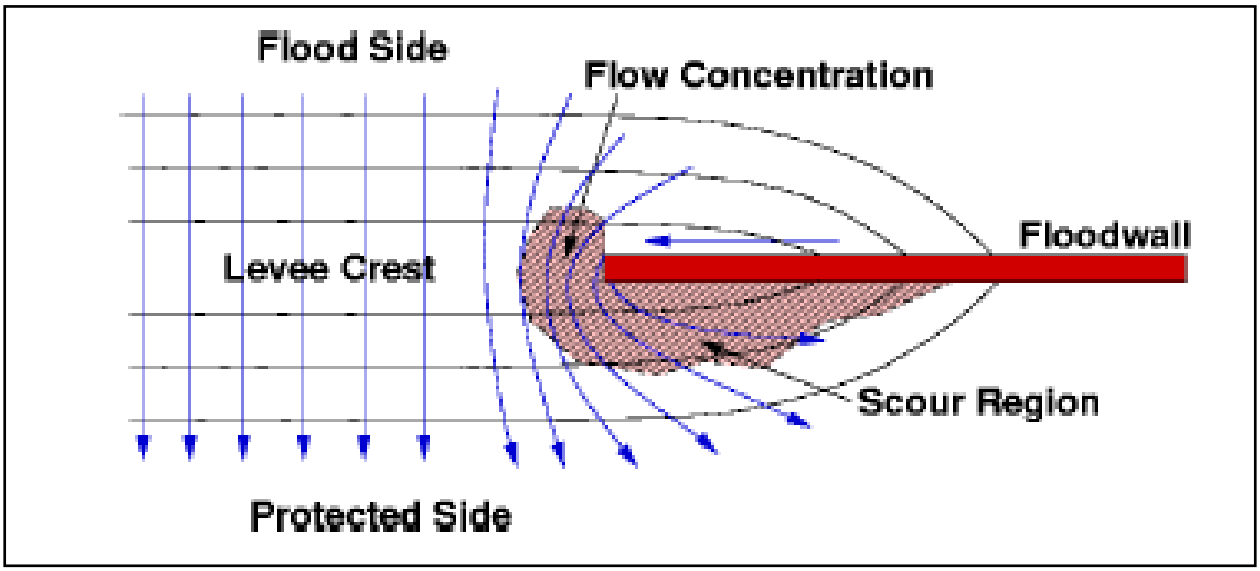


Figure 16. Diagram of Overtopping Erosion at Levee - Floodwall Transition (from Hughes 2006)

2. Soils and Erodibility

The breaches which occurred along Reach 2 occurred only in places where the levees were constructed using hydraulically placement of the soil. Where the levees were constructed with compacted clay soils, breaches did not occur.

Hydraulic Placement of fill for the Levee Construction –

a. Hydraulic Fill

The use of hydraulic placement of fill for the construction of levees dates back to the late 1800's and had been commonly use for levee construction up until the 1980's. It is a cost effective construction method when the material (soil) for the levee is dredged from an adjacent channel by a hydraulic dredge. Indeed, it was within engineering standards of practice at the time of the MRGO levees were designed and constructed to use hydraulic fill to construct levees. The dredged material is pumped to a containment area to allow the water to drain off and the fill to dry and solidify. The containment area is formed by constructing two dikes of dry material outside the toe of levee on either side of the planned centerline of the levee and parallel to it. Discharge pipes with openings in the bottom of them are run on top of the dikes, allowing the fluid material from the hydraulic dredge to flow into the foot print of the levee. With the fluid material flowing from the dikes to the centerline of the levee, the denser particles, coarse gain, will fallout

of solution closer to the dike while the less dense fine grain material settles out in the center of the containment area. The distribution of coarse grain to fine grain material across the containment area is dependent on the geological deposit being dredged from the channel. In general, the geological deposit to be chosen for the construction of a levee will be primarily cohesive material, clay, silty clay or clayey silt, in order to make the levee an impervious barrier. The greater the amount of fine grain material (clay or silt) the lower the permeability of the levee cross-section.

The levee is brought to its desired height through a series of construction lifts. Once the wet fill reaches the top of the dikes, the fill is allowed to drain and solidify. New dikes are constructed at the edge of the newly placed fill and the process is repeated until the desired height is reached. Once the fill has reached the desired height and has solidified sufficiently to allow earthmoving equipment on it, the fill is reworked to shape it into desired levee cross-section.

The hydraulic fill placement method will result in a levee cross-section that is uncompacted and has a low density. The cross-section will have a degree of zone formation with coarse grain materials (non-cohesive materials – sand and silts) at the toes and fine grain materials (cohesive materials – clays and silty clays) at the centerline and a distribution of these materials in between the toes and centerline depending the amount these materials found in the original geological deposits. The levee cross-section may not be uniform along the levee's length because the original geological deposits may contain larger or smaller amounts of these materials along its length. It is not uncommon to find pockets of coarse grain materials in the levee cross-section along its length.

The levee cross-section will be susceptible to erosion starting at the toe or at the pockets of coarse grain materials when overtopped. Once the erosion starts, the uncompacted fill will be more likely to continue to erode with continued overtopping than a semi-compacted or compacted fill placed at its optimum water content.

b. Soil Type

To help the reader to understand the presentation of the information in this report, the terms used to describe the soil types are defined in this section. Soils can be divided into two major categories based on the origin of their principal constituents, those which consist chiefly of the results of chemical and physical rock weathering, and those which consist chiefly of the results of organic origin. Soils resulting from rock weathering are further subdivided into residual soils for those that are located where they originated and transported soils for those that moved from their origination regardless of the mode of transportation, hydraulic or mechanical. Soils of organic origin are formed chiefly in place, termed in situ, either by the growth and subsequent decay of plants such as peat mosses, or by the accumulation of fragments of inorganic skeletons or shells of organisms. Hence a soil of organic origin can be either organic or inorganic. The term organic soil ordinarily refers to a transported soil consisting of the products of rock weathering with a more or less conspicuous admixture of decayed vegetation. Civil

engineers further breakdown soils by classifying them into soil types based on some general physical and behavioral characteristics.

Sand and gravel are cohesionless aggregates of rounded subangular or angular fragments of more or less unaltered rocks or minerals. Particles with a size up to eighth of an inch are referred to as sand, and those with a size from eighth of an inch to eight inches as gravel. The permeability of sands and gravels are relatively high. Soil mixtures with relatively high amounts of sands will feel gritty when rubbed between your fingers.

Clay is an aggregate of microscopic and submicroscopic particles derived from the chemical decomposition of rock constituents. It is plastic, ability to be molded or shaped, within a moderate to wide range of water contents. Dry specimens are very hard, and no powder can be detached by rubbing the surface with dry pats of the fingers. The permeability of clays is extremely low. At higher water contents, clays are conspicuously sticky. Organic clay is a clay that owes some of its significant physical properties to the presence of finely divided organic matter. When saturated, organic clay is likely to be very compressible, but when dry its strength is very high. It is usually dark gray or black in color, and it may have a conspicuous odor.

Silt is a fine grained soil with more or less equidimensional grains of quartz, sometimes called rock flour, with little or no plasticity or flake shaped particles that result in a high degree of plasticity. These inorganic silts are often mistaken for clays because of their smooth texture, but they may be readily distinguished from clays by shaken a patty of the materials in the palm of the hand and seeing if the surface of the patty becomes glossy. After drying, the patty will be brittle and dust can be detached by rubbing it with a finger. Silts are relatively impervious. Organic silt is a fine-grained more or less plastic soil with an admixture of finely divided particles of organic matter. Shells and visible fragments of partly decayed plant matter may also be present. The soil ranges in color from light to very dark gray and may have a character ristic odor dependent on gaseous products from the decay of the organic matter. The permeability of organic silts is very low and its compressibility very high.

Peat is a somewhat fibrous aggregate of macroscopic and microscopic fragments of decayed plant matter. Its color ranges between light brown and black. Peat is extremely compressible and settlement of embankments built on them is likely to be large and to continue at a decreasing rate for many years.

If a soil is made up of a combination of two different soil types, the predominant ingredient is expressed as a noun, and the less prominent ingredient as a modifying adjective. For example, silty sand indicates a soil which is predominantly sand but contains a small amount of silt. A sandy clay is a soil which exhibits the properties of a clay but contains an appreciable amount of sand. The more nearly a soil approaches the characteristics of a clay, the greater is the variety of states of consistency in which it may be found. The degree of plasticity is sometimes expressed by the terms fat and lean, high and low plasticity, respectively. A lean clay is one that is only slightly plastic because it contains a large proportion of silt or sand.

The aggregate properties of sand and gravel are described qualitatively and quantitatively by the terms loose, medium, and dense based on density and indicates the relative strength whereas those of clays are described by hard, stiff, medium, and soft based on their shear strength and compressibility. In the United States, soils are classified using the Unified Soil Classification System (USCS) which describes the texture and grain size. The USCS has three major classification groups: (1) coarse-grained soils (e.g. sands and gravels); (2) fine-grained soils (e.g. silts and clays); and (3) highly organic soils (referred to as "peat"). The USCS further subdivides the three major soil classes for clarification, Figure 17. Figure 18 shows the boring log symbols for the USCS subdivisions.

Unified Soil Classification (USC) System (from ASTM D 2487)				
Major Divisions			**Group Symbol**	**Typical Names**
Course-Grained Soils More than 50% retained on the No. 4 sieve	**Gravels** 50% or more of course fraction retained on the No. 4 sieve	Clean Gravels	GW	Well-graded gravels and gravel-sand mixtures, little or no fines
			GP	Poorly graded gravels and gravel-sand mixtures, little or no fines
		Gravels with Fines	GM	Silty gravels, gravel-sand-silt mixtures
			GC	Clayey gravels, gravel-sand-clay mixtures
	Sands 50% or more of course fraction passes the No. 4 sieve	Clean Sands	SW	Well-graded sands and gravelly sands, little or no fines
			SP	Poorly graded sands and gravelly sands, little or no fines
		Sands with Fines	SM	Silty sands, sand-silt mixtures
			SC	Clayey sands, sand-clay mixtures
Fine-Grained Soils More than 50% passes the No. 200 sieve	**Silts and Clays** Liquid Limit 50% or less		ML	Inorganic silts, very fine sands, rock four, silty or clayey fine sands
			CL	Inorganic clays of low to medium plasticity, gravelly/sandy/silty/lean clays
			OL	Organic silts and organic silty clays of low plasticity
	Silts and Clays Liquid Limit greater than 50%		MH	Inorganic silts, micaceous or diatomaceous fine sands or silts, elastic silts
			CH	Inorganic clays or high plasticity, fat clays
			OH	Organic clays of medium to high plasticity
Highly Organic Soils			PT	Peat, muck, and other highly organic soils

Prefix: G = Gravel, S = Sand, M = Silt, C = Clay, O = Organic
Suffix: W = Well Graded, P = Poorly Graded, M = Silty, L = Clay, LL < 50%, H = Clay, LL > 50%

Figure 17. Unified Soil Classification System

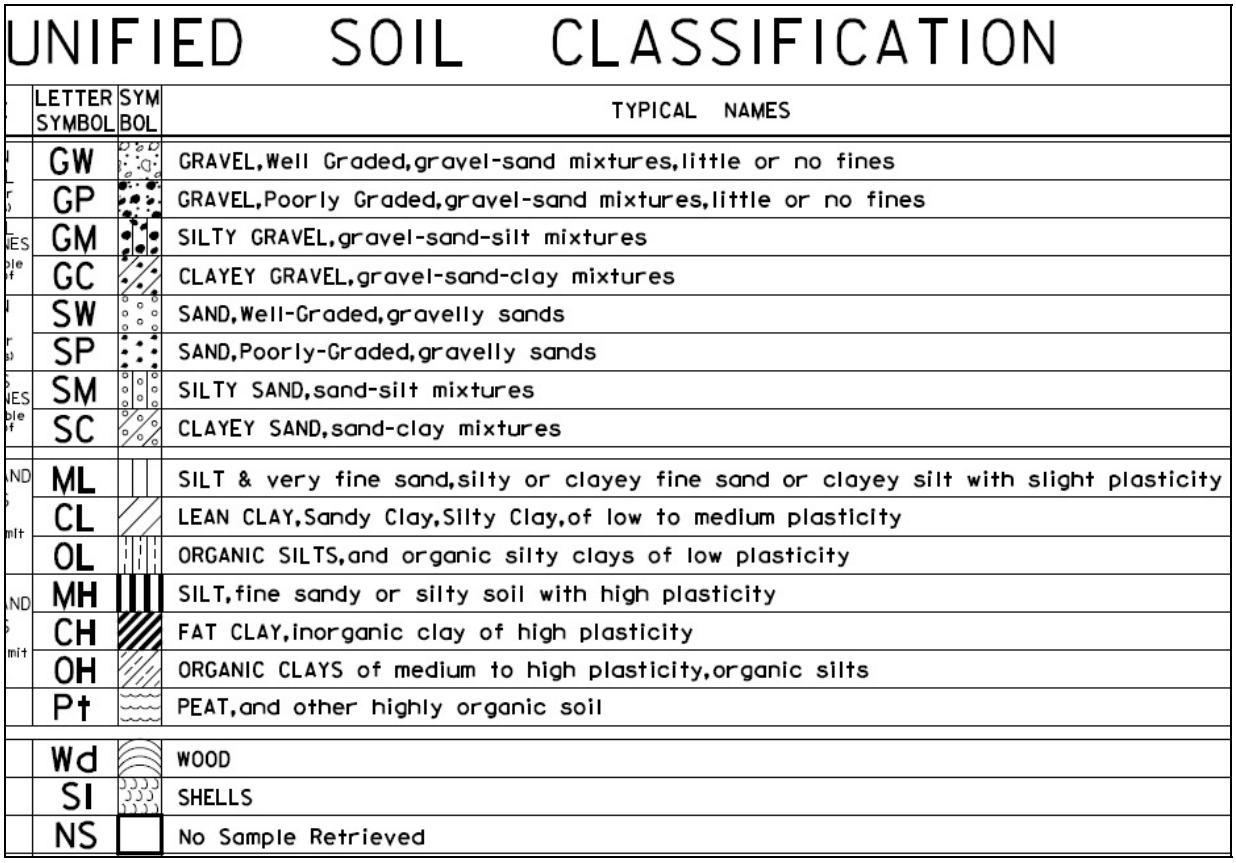


Figure 18. Description of boring log symbols

c. Erodibility

Assessing soil erodibility is a complex matter, due to spatial (horizontal and vertical) non-homogeneity and uncertainty, difficulty in selecting accurate engineering properties needed to determine erodibility, and temporal effects during erosion progression such as changes in surface roughness which in turn affect the hydraulic stress and turbulence conditions. Soil properties affecting erodibility are soil constituents (gravel, sand, silt, clay proportions); water content (antecedent moisture); clay mineralogy and proportion; soil structure; organic content; pore water chemistry (salinity, hardness, quality, pH); in-situ density; in-situ shear strength, and compaction effort during construction.

The rate of erosion is proportional to the applied hydraulic shear stress in excess of a critical shear stress required to initiate soil particle detachment and is also proportional to an erodibility coefficient (Hanson and Simon 2001). Soils with a lower critical shear stress tend to have a higher erodibility coefficient.

Levee geometry is important when analyzing erosion probability. A 1:3 side slope is steeper than a 1:4 slope, and a stabilizing berm slope acts as an overtopping energy dissipator. Water cascading down a 1:3 slope impacting a 1:20 berm slope would be more likely to initiate erosion than that on a 1:4 slope, and would also depend on slope distance between the crest and the toe, surface roughness, and water depth. In addition, a more erodible embankment will need a higher level of protection than a less erodible embankment to reduce or prevent backside overtopping erosion.

Answering the question of why one section of levee eroded compared to another section is difficult to do as a significant amount of forensic evidence was washed away during the hurricane. The pre-Katrina soil boring data (where available) provides an initial, although limited, observation of soil types, stratigraphy, and strength along the centerline of the levees. Forensically assessing the general causational reasons for the erosion along Reach 2 of the MRGO using the pre-Katrina soil parameters and post-Katrina observation can be accomplished within a reasonable degree of scientific certainty. For example, the levees constructed of hydraulic fill (noncompacted) along the MRGO were more erodible than those areas along the MRGO and the Mississippi River that had truck-hauled semicompacted fill. The levees constructed with lower-plasticity surface soils instead of fat clay had more erosion. The following sections provide the basis for reaching my opinions for the cause of the breaching along Reach 2 of the MRGO.

3. Post-Katrina Erosion Observations along MRGO

As discussed previously, an earthen levee that is overtopped will exhibit identifiable stages of backside (landside or protected side) erosion progression. Photographs taken along the Reach 2 adjacent to the MRGO after the storm are included to provide examples of observed erosion stages. The following photographs used as examples are correlated to nearest boring in order understand the in situ soil properties prior to the Hurricane Katrina. Figure 19 shows the location of boring.

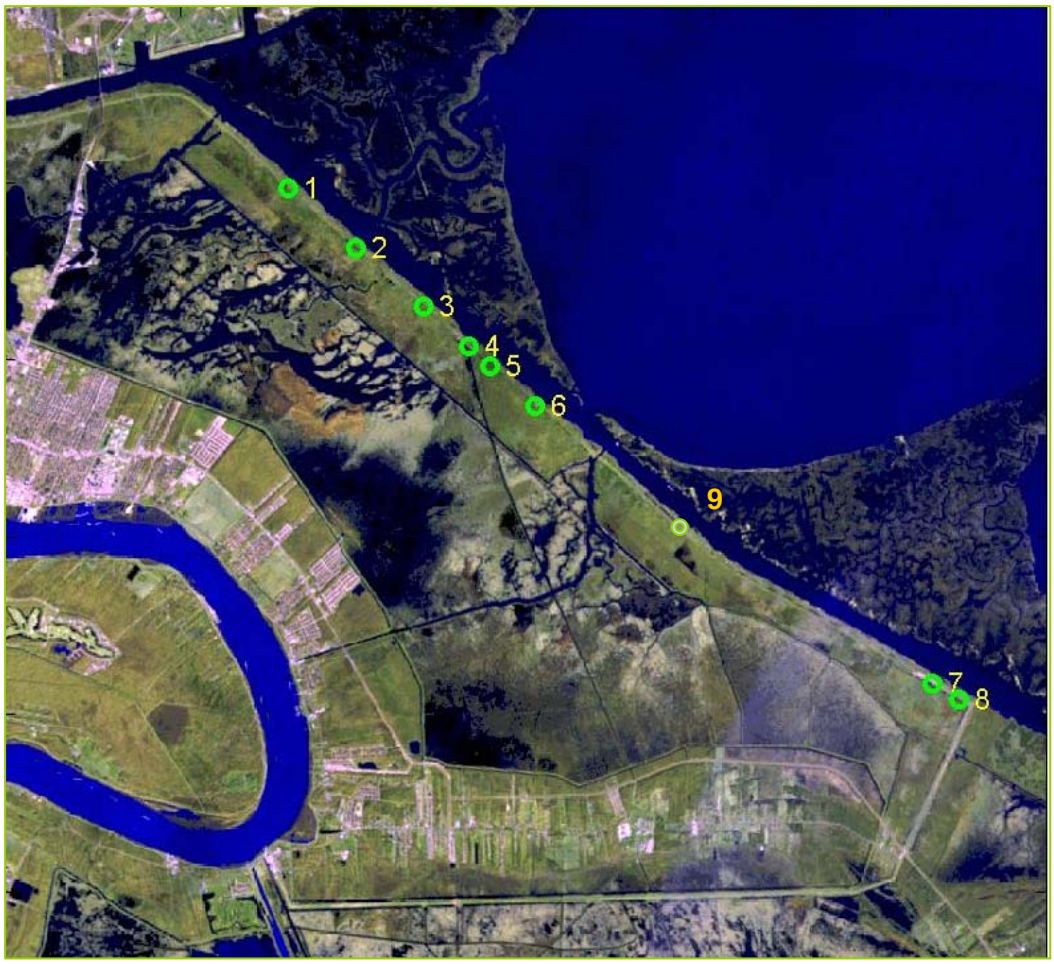


Figure 19. Boring locations along the centerline of the levees of Reach 2 of the MRGO

Storm surge crest elevations are approximated based on actual high water marks and IPET simulations to provide the distribution across several reaches, and the overtopping waterfall heights are approximated based on available pre-Katrina levee/floodwall elevations presumably referenced to local mean sea level datum.

a. Levees

Stage A. *Initial overtopping causes surface sheet and rill erosion which develops into a series of cascading overfalls. The highest forces develop from the backside slope down to the backside toe, and the crown is not initially exposed to these large hydraulic forces. The cascading overfalls develop into one large headcut that migrates from the slope to the crest such that the erosion width approximately matches the overtopping width.*

Figure 20 shows an example of initial overtopping erosion on the backside along the southern portion of MRGO Reach 2 St. Bernard Parish. The levee crown was elevation 17 to 18 ft and storm surge was 18 to 19 ft and the surge and wave were 20 ft to 21 ft so the overtopping crest depth was approximately 3 to 5 ft. The closest soil boring to this location is shown in Figure 21. This 1985 boring at Sta 989+00 (about 800 ft south of the sheetpile/levee transition) showed the levee section was composed of fat clay (CH) with interbedded silt lenses. Figure 22 shows the LIDAR profile along the reach where boring 10 CUI was taken. Maximum wave and surge overtopping was approximately 2.5 to 3.0 ft, with no scouring or erosion of the levee crest.



Figure 20. Backside Levee Erosion Pattern “A” on the southern portion of MRGO Reach 2, St. Bernard Parish

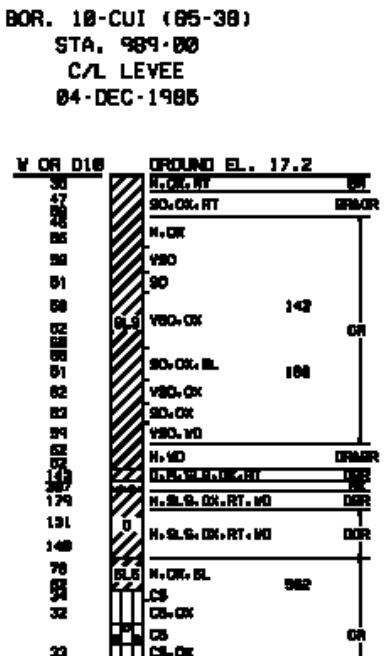


Figure 21. Boring 10-CUI beyond the sheetpile transition to levee. Top layer is fat clay – Location 8.

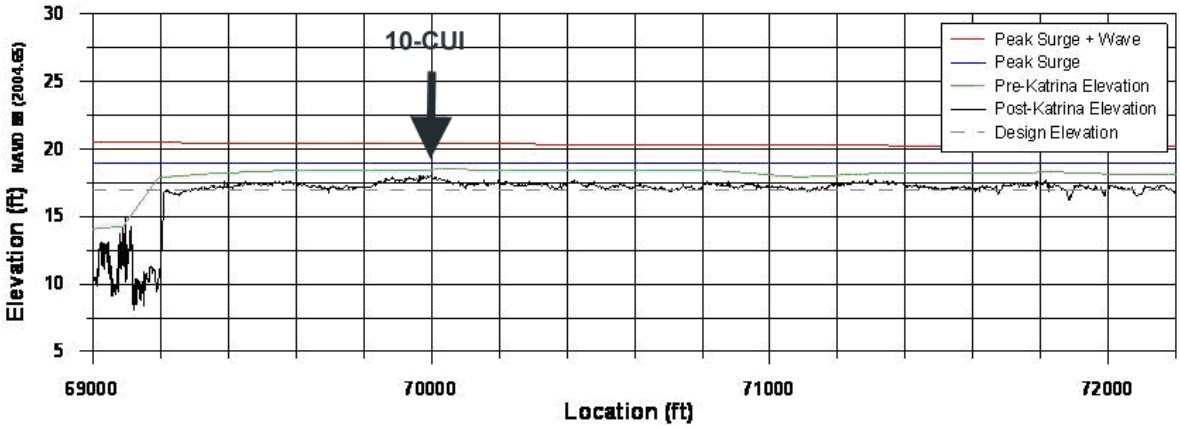


Figure 22. LIDAR plot showing minimal erosion at 10-CUI location.

Stage B. *The headcut continues to migrate from the backside crest (crown) to the floodside crest.*

Figure 23 shows a small section of the levee between Bayous Bienvenue and Dupre, viewed to the south from approximate B/L Sta 570+00. The MRGO is to the left of photo. Approximately 6.2 miles of levee along the MRGO were overtopped and breached at numerous locations. Storm surge plus waves along the MRGO was approximately up to 21 ft, so the approximate overtopping depth was about 5 ft along this reach.

Soil boring 12BU-CHBD (01-16834) from 2001 at Sta 570+00 (Figure 24) shows the top 1.4 ft of levee (at crown elevation 16) was composed of lean clay (CL), with fat clay (CH) layers underneath. Soil tests from this boring show a low shear strengths in the levee profile. The indicates that the levee's ability to withstand water loading would be seriously impaired if the levee footprint was reduced. There were numerous locations along this reach where the footprint was significantly reduced due to soil loss on the backside, which most likely accelerated breaching progression.



Figure 23. Stage B crown erosion on remaining levee southeast of Bienvenue Control Structure

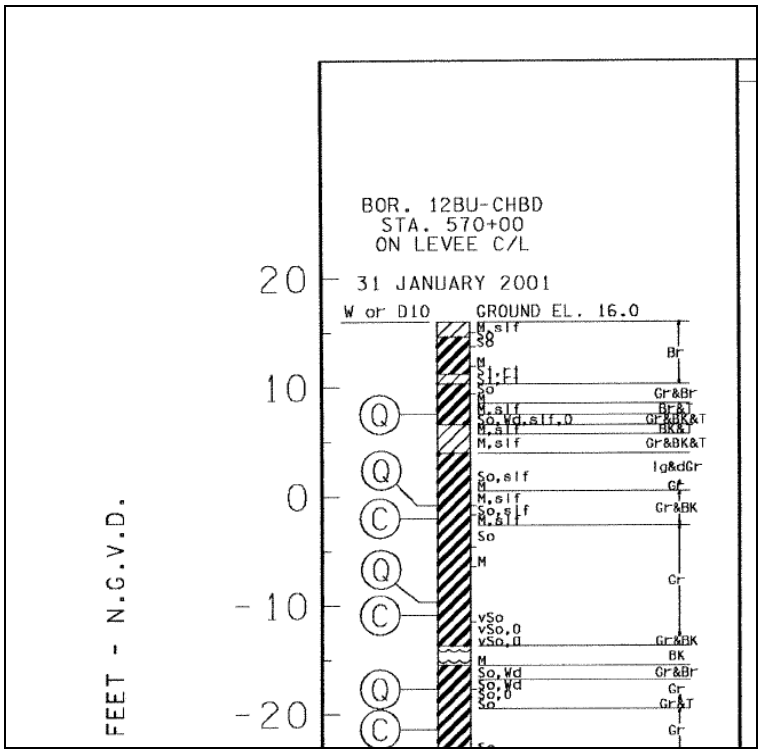


Figure 24. Soil boring 12BU-CHBD approximately located in above Figure – Location 3.

Figure 25 shows the LIDAR profile along the reach where boring 12BU-CHBD was taken. Maximum wave and surge overtopping was approximately 5 ft, with scour depth approximately 6 ft.

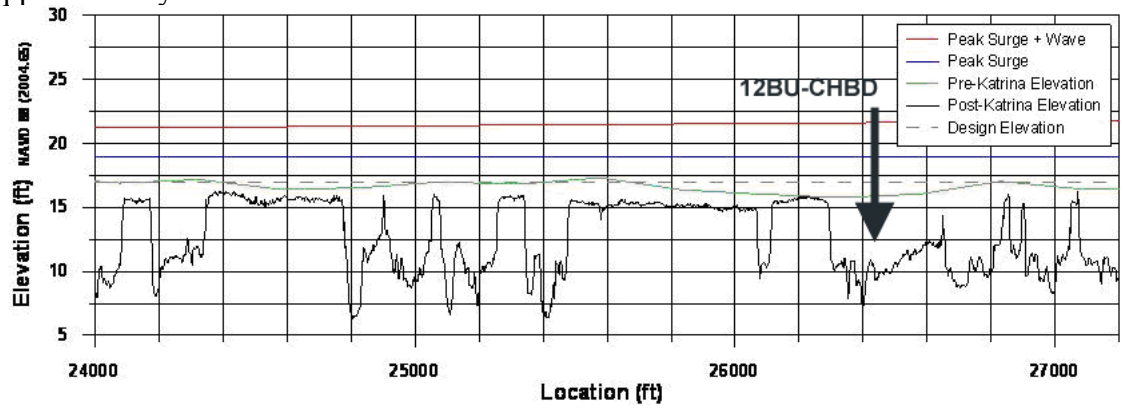


Figure 25. LIDAR plot showing approximate location of soil boring 12BU-CHBD, scour depths, and hydraulic loading (from IPET 2006).

***Stage C**. The crest drops as a breach begins to develop.*

Figure 26 shows Stage C crown scour along approximate B/L Sta 1203+00 to Sta 1230+00 on the St. Bernard levee between the MRGO and the Mississippi River. Crown elevation was approximately 15 ft, but dropped to about 12 ft for about a mile in this

eroded section. Storm surge and wave heights were up to 3 ft higher than the levee along this reach, and this was the only significant breach between Verret and Caervarnon.

The levee along this reach was constructed of Mississippi River hydraulic sand fill, capped with local borrow material fat clay intebedded with silt and/or sand lenses, and shaped to grade with Mississippi River batture soil (truck-hauled fill). Similar to other levees' construction materials and history, this section contains heterogeneous soil layering where the hydraulic placed sands have reached variable degrees of densities in the cross-section from natural processes over a half-century or so timeframe. Figure 27 shows a pre-Katrina boring at Sta 1225+61 with a thin surface layer of very stiff lean clay underlain by very stiff fat clay and the hydraulic fill sand.



Figure 26. Stage C breach development on short reach of levee between Verret and Caernarvon

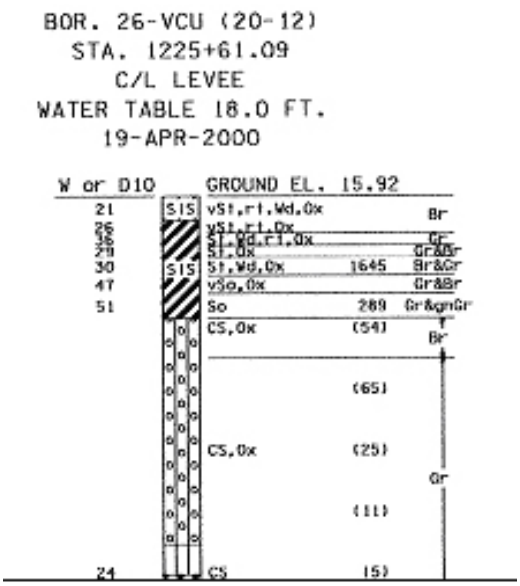


Figure 27. Soil boring taken along the reach between Verret and Caervarnon. Crown height approximately equaled the surge height at this soil boring location.

Stage D. *The breach opening erodes out to the toe and the breach widens.*

Figures 28 and 29 are photos of a 19,000 ft. levee reach between Bayou Bienvenue (Sta 383+00) and Bayou Dupre (Sta 704+00) that lost approximately 12' of levee height from its original (design) height 17.5 ft, and a 2300 ft levee reach that only lost about 8 ft height. Storm surge and wave overtopping between Bienvenue and Dupre ranged from approximately 3 ft to 7 ft, with the highest overtopping occurring closer to Bayou Dupre (IPET 2006).



Figure 28. Stage D erosion between Bienvenue and Dupre structures, St. Bernard Parish



Figure 29. 2,300 ft. of levee between Bayou Bienvenue (Sta 383+00) and Bayou Dupre (Sta 704+00) that only lost 50% of original height.

Hydraulic fill from the MRGO channel formed the levee between Bienvenue and Dupre. Soil boring 9BU-CHBD (Figure 30) from 2001 at Sta 445+00 shows the top 1.5 ft of the levee (elevation 18.1 ft) was composed of medium stiff lean clay (CL). The underlying layers are mostly fat clay (CH) with interbedded lean clay layers. At a depth of 9.7 ft below the crown, a shear Q test indicated cohesion value 238 psf at 32% water content and 88 pcf dry density in a CH layer. Figure 31 shows the approximate location on the LIDAR plot, indicating approximately 5 ft erosion depth.

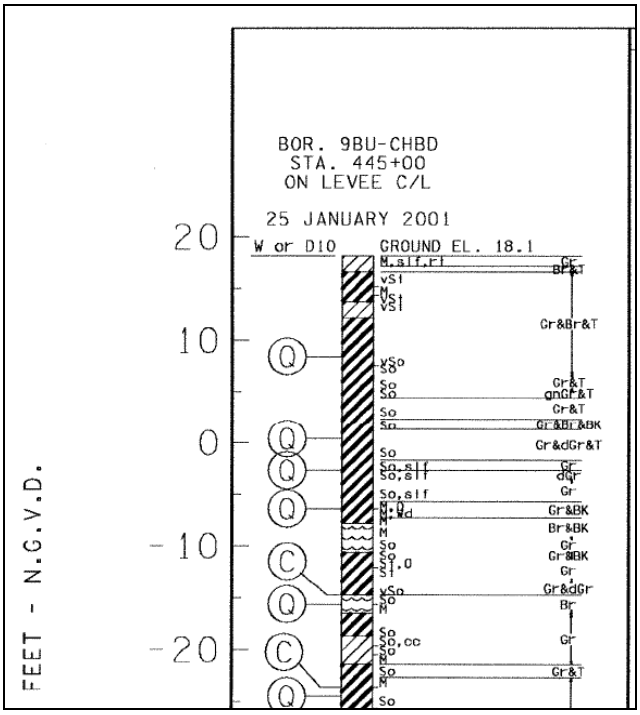


Figure 30. Soil boring 9BU-CHBD at Sta 445+00 – Location 1.

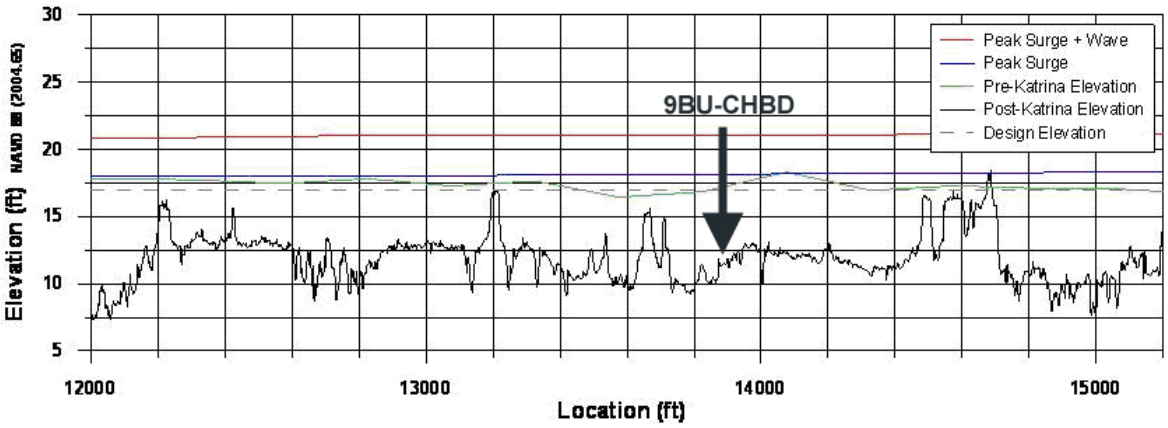


Figure 31. Approximate location of soil boring 9BU-CHBD with scour depth approximately 5 ft from overtopping surge plus wave height 3ft above crown.

Soil boring 11BU-CHBD (Figure 32) from 2001 at Sta 509+00 shows the top 2 ft of levee (elevation 17.4) was composed of soft fat clay (CH), with a 1-ft thick layer of poorly graded sand (SP) underneath. At a depth of 15.4 ft below the crown, a shear Q

test indicated cohesion value 238 psf at 56% water content and 64 pcf dry density in a CH layer. Figure 32 shows the approximate location on the LIDAR plot, indicating approximately 10 ft erosion depth. Storm surge plus wave heights were approximately 5ft above the levee crown.

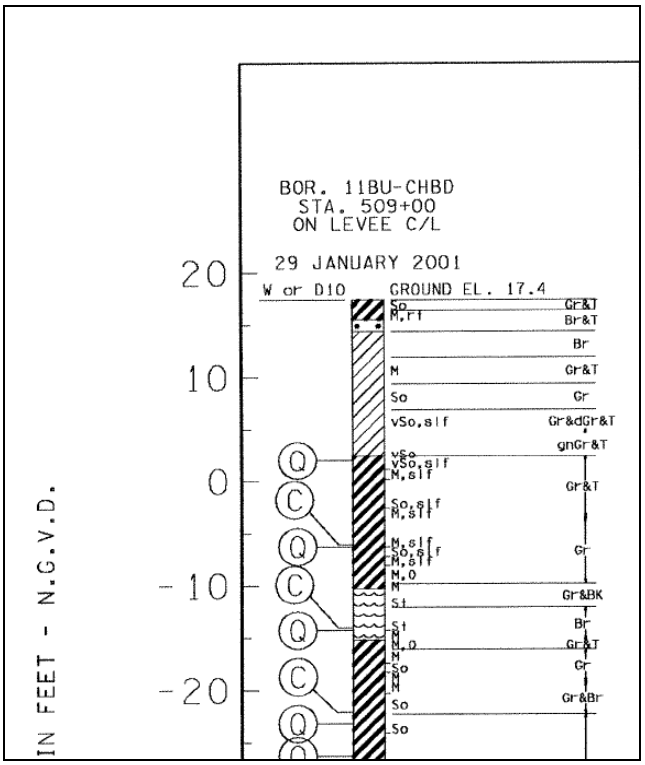


Figure 32. Soil boring 11BU-CHBD at Sta 509+00 with soft clay surface – Location 2

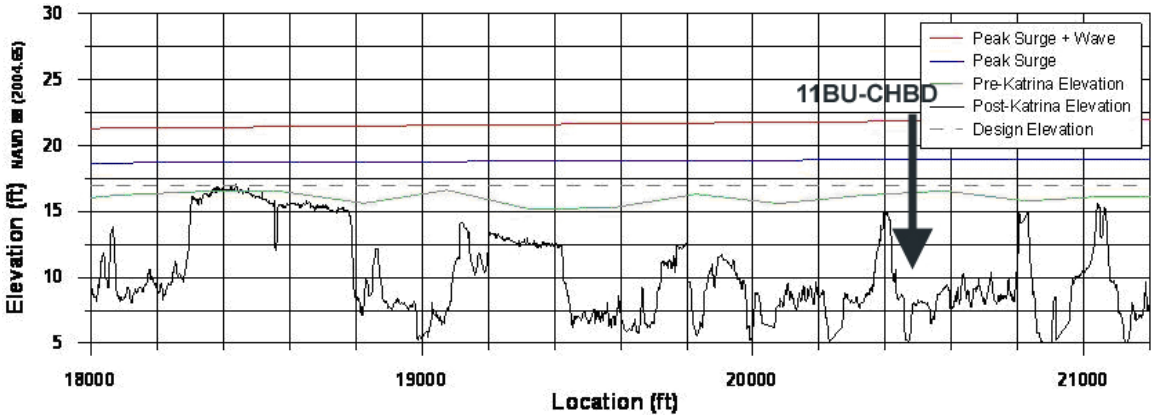


Figure 33. Approximate location and scour near soil boring 11BU-CHBD

Soil boring 18-UBD (Figure 34) at B/L Sta 596+00 shows the top 5.8 ft of levee (elevation 14.4) was composed of sandy silt (SM), with CH layers underneath. At a depth of 12 ft below the crown, a shear Q test indicated cohesion value 396 psf at 27% water content and 95 pcf dry density in a CL layer. Figure 35 shows the LIDAR plot with approximate location and scour depth.

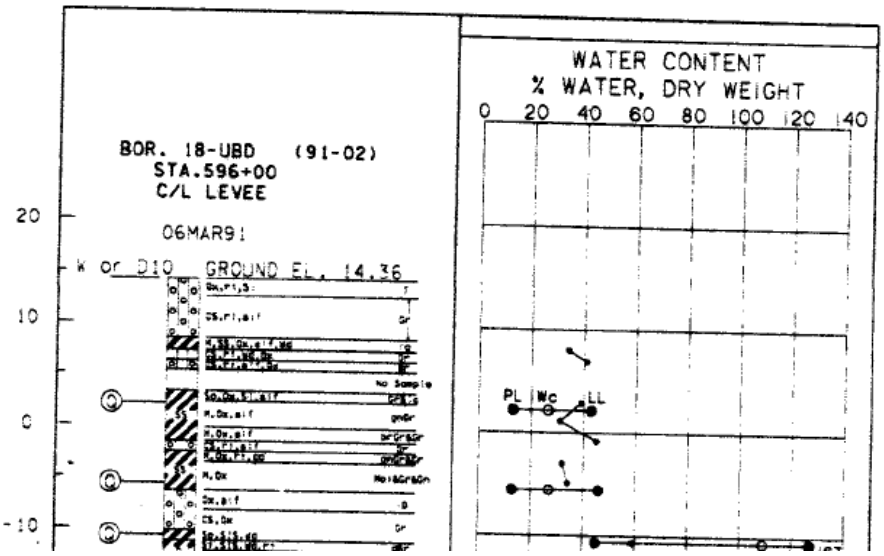


Figure 34. Soil boring 18-UBD – Location 4.

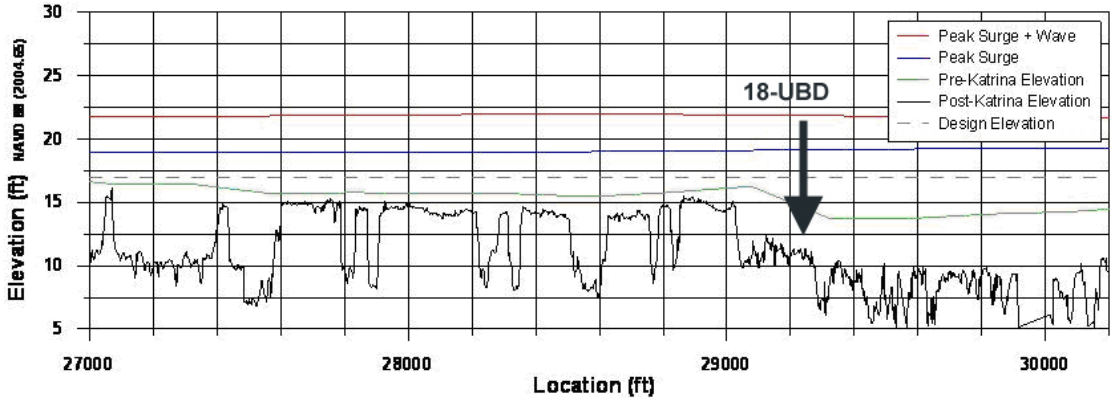


Figure 35. LIDAR plot showing scour depth of approximately 6 ft from 7ft water overtopping (surge plus waves)

Soil boring 13BU-CHBD (Figure 36) at Sta 614+00 shows the top 25 ft of levee (elevation 15.4) was composed of medium fat clay (CH), with organic clays and peats underneath. At a depth of 5 ft below the crown, a shear Q test indicated cohesion value 632 psf at 29% water content and 92 pcf dry density in the CH layer. Figure 37 shows the LIDAR plot with approximate location and scour depth (less than 1ft). Surge plus wave loading was about 7ft.

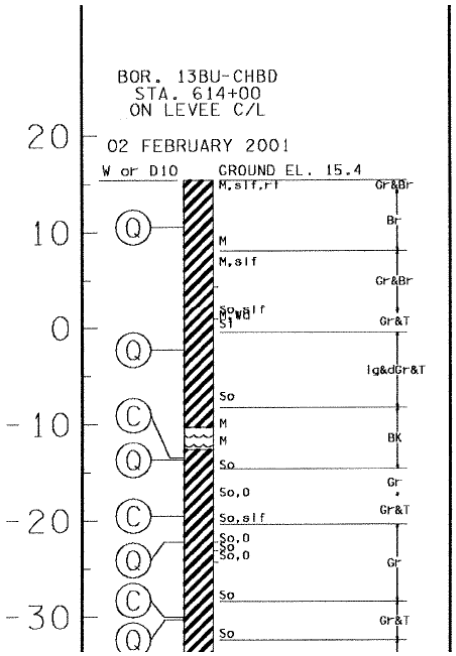


Figure 36. Soil boring 13BU-CHBD at Sta 614+00 – Location 5

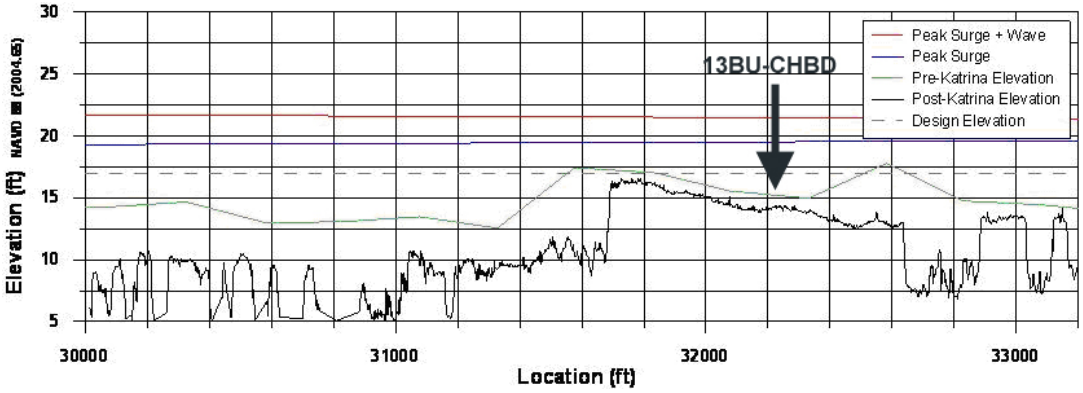


Figure 37. LIDAR plot showing approximate location and scour depth

Figure 38 shows a portion of the 8,000 ft. section of the levee immediately southeast of Bayou Dupre (St. Bernard Parish) that was severely damaged and not only lost approximately 12 feet of original levee height but also part of the original levee foundation. The storm surge and waves overtopping this section of levee were approximately 7 ft. above the crown height. Figure 39 shows another portion of the levee southeast of Dupre.



Figure 38. Stage D erosion southeast of Dupre Control Structure



Figure 39. 2,500 ft. of levee from Dupre Control Structure to Sta 1007+91 that lost approximately 8' of elevation.

A soil boring (Figure 40) through the levee crown southeast of Dupre (7600 ft distant) was logged in 1981 and showed the top 3 ft consisted of stiff lean clay (CL), fat clay (CH), silt (ML or MH), and intebedded lenses of silt and/or sand. Any of these layered soil materials may have contributed to erosion initiation and progression. Surge

plus wave overtopping was approximately 5 ft along this reach, and the scour depth was approximately 7 ft (Figure 41).

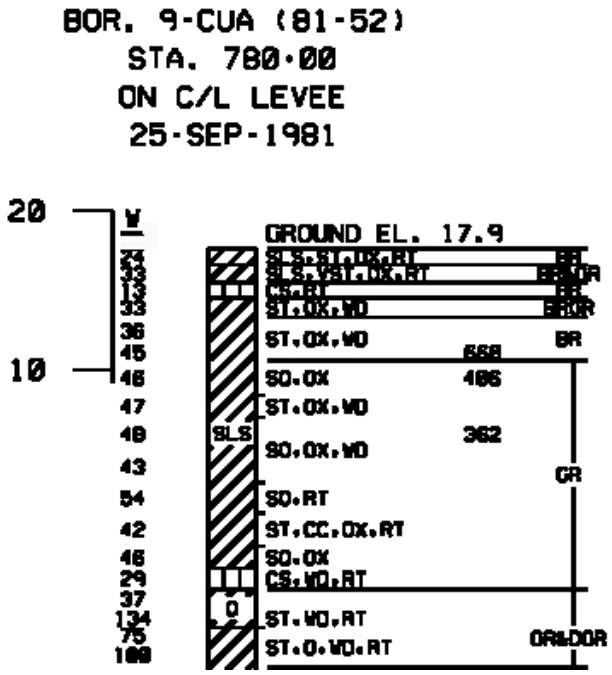


Figure 40. 1981 soil boring at Sta 780+00, approximately 6000 ft south of Bayou Dupre Control Structure, shows top layer of lean clay (CL) underlain by fat clay (CH), silt (ML or MH), and silt / sand lenses (SLS) in the CH material (from drawing 9 of 10, TFG contract solicitation W912P8-06-R-0002) – Location 9.

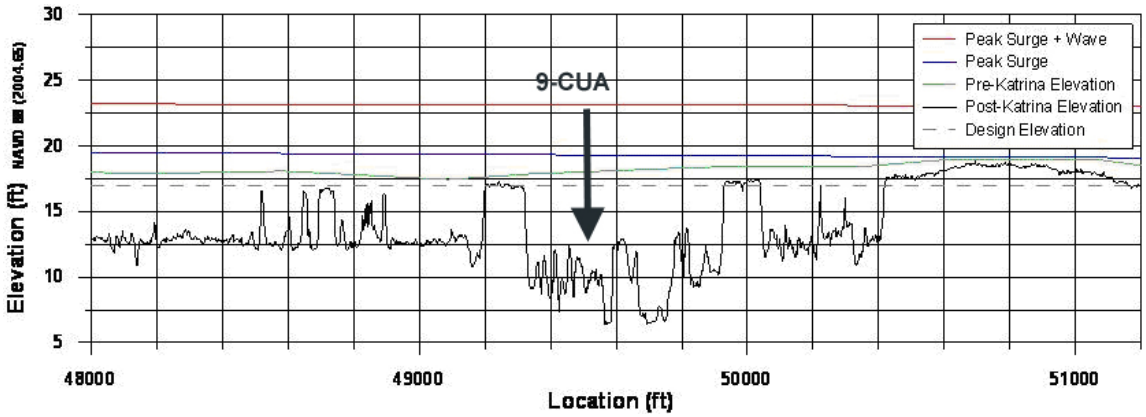


Figure 41. LIDAR plot of approximate location and scour depth.

b. Sheetpile Walls

Figure 42 thru Figure 44 show sheetpile wall sections located between Bayou Bienvenue and Dupre Control Structures at various stages of scour and erosion on the protected side of the wall. The sheetpile wall in Figure 42 shows signs of initial scour adjacent to wall with lose of approximately 2 to 3 feet of soil. The wall has remained relative vertical with only minor misalignment. Soil boring 9BU-CHBD (Figure 30) is the closest boring to the wall in Figures 43. It shows the top 1.5 ft of the levee was composed of medium stiff lean clay (CL). The underlying layers are mostly fat clay (CH) with interbedded lean clay layers. At a depth of 9.7 ft below the crown, a shear Q test indicated cohesion value 238 psf at 32% water content and 88 pcf dry density in a CH layer. Figure 31 shows the approximate location on the LIDAR plot.



Figure 42. Sheetpile wall located south of the Bayou Bienvenue Control Structure

The sheetpile wall in Figure 43 shows greater degree of scour adjacent to wall with lose of approximately 4 to 6 feet of soil. The wall has rotated from vertical and has significant misalignment.



Figure 43. Sheetpile wall located south of the Bayou Bienvenue Control Structure

The sheetpile wall in Figure 44 suffered sufficient scour adjacent to the wall to allow it to collapse. Soil boring 11BU-CHBD (Figure 32) is the closest boring to wall show in Figure . It shows that the top 2 ft of levee was composed of soft fat clay (CH), with a 1-ft thick layer of poorly graded sand (SP) underneath. At a depth of 15.4 ft below the crown, a shear Q test indicated cohesion value 238 psf at 56% water content and 64 pcf dry density in a CH layer. Figure 33 shows the approximate location on the LIDAR plot.



Figure 44. Sheetpile wall located south of the Bayou Bienvenue Control Structure

c. Transitions

Figure 45 shows a sheetpile / levee transition along the MRGO southeast of Dupre at B/L Sta 980+58. Note that scour occurred behind the sheetpile wall and minimally beyond the levee transition. Approximate sheetpile elevation was 17 ft and levee crown elevation was 13 ft. Beyond the transition, the levee crown elevation was approximately 17 ft. The approximate surge and wave overtopping drop was 7 ft above the soil at the sheetpile base and 4 ft over the transition levee, thus the overtopping water velocities were different.

Nearest soil boring 10-CUHA (Figure 46) from 1991 at Sta 976+00 in the sheetpile reach shows the top 4 ft of levee (elevation 13) was composed of lean silt and clay (ML and CL) with CH layers underneath. Figure 47 shows the LIDAR plot. An earlier (1985) boring at Sta 989+00 (about 800 ft beyond the sheetpile/levee transition) showed the levee section was composed of fat clay (CH) with interbedded silt lenses (Figure 48). Figure 49 indicates minimal erosion occurred beyond the sheetpile transition.



Figure 45. Sheetpile-to-levee transition showing significant scour behind the sheetpile and minimal erosion on the levee southeast of Dupre.

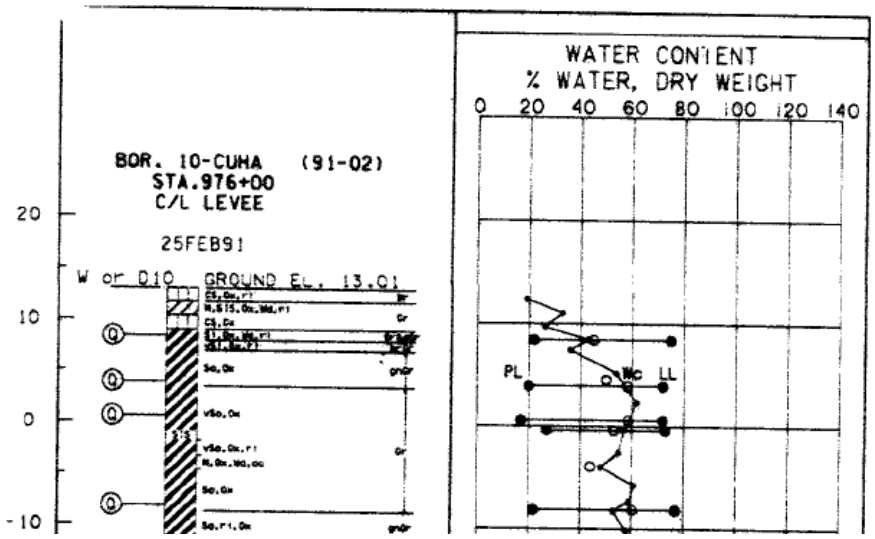


Figure 46. Boring 10-CUHA in the sheetpile reach. Note the soil layering typical of hydraulic fill – Location 7.

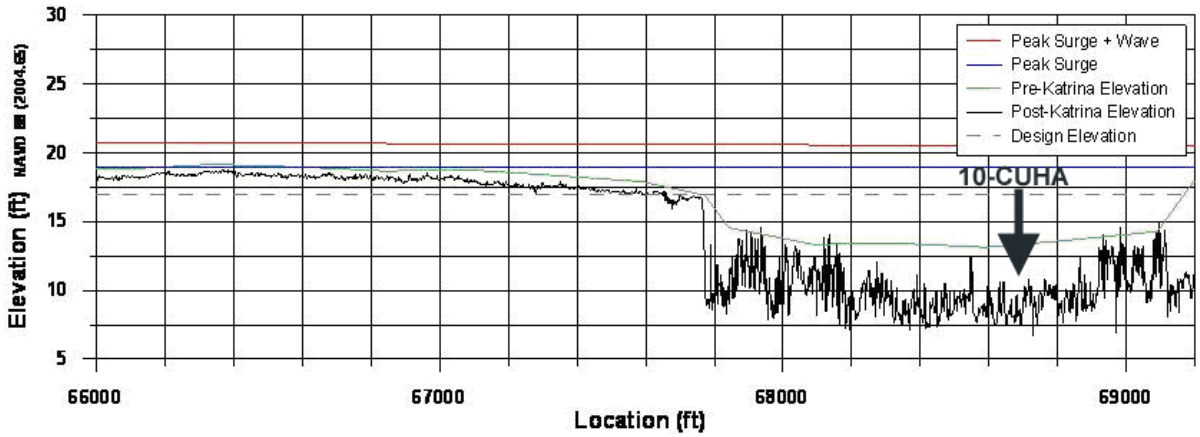


Figure 47. LIDAR plot of approximate location and scour depth - .

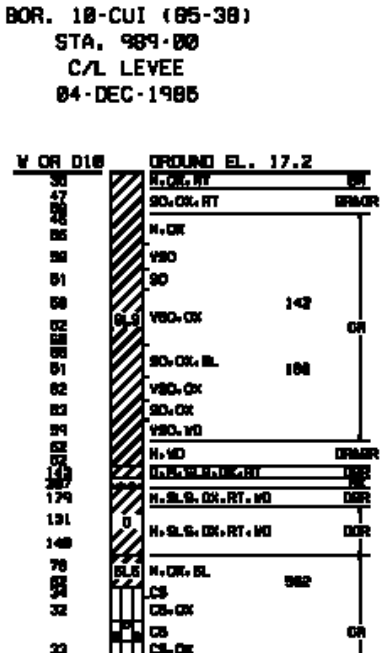


Figure 48. Boring 10-CUI beyond the sheetpile transition to levee. Top layer is fat clay – Location 8.

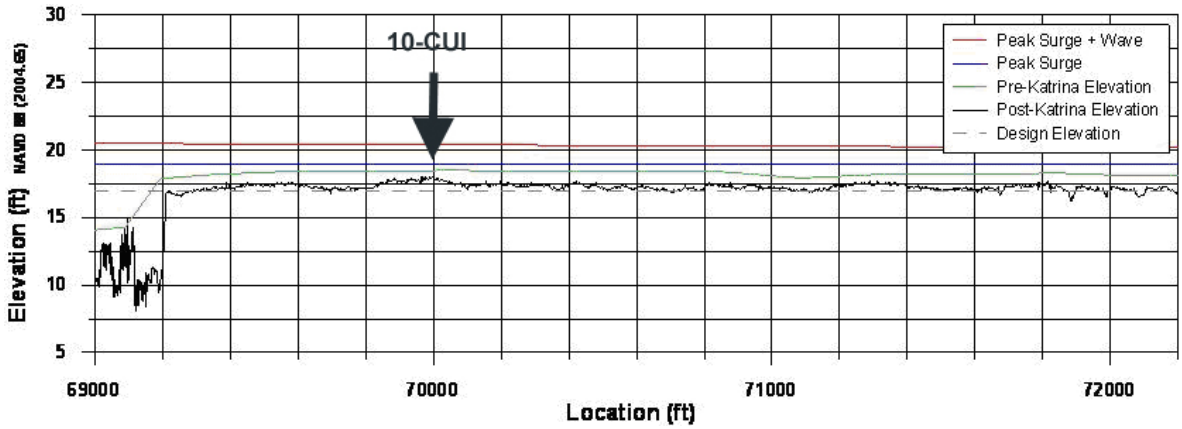


Figure 49. LIDAR plot showing minimal erosion at 10-CUI location.

Along Reach 2, the most severe scour and erosion occurring at transitions was at the two control structures (Bayou Bienvenue and Bayou Dupre). Figures 50 and 51 shows the scour and erosion Bayou Bienvenue and Bayou Dupre, respectively. The scour and erosion at the transition between the walls of control structures and the levees was so severe that the walls collapse allowing large hole to develop.


Figure 50. Bayou Bienvenue Control Structure



Figure 51. Bayou Dupre Control Structure

d. Soil Quality and Erosion

Figure 52 is a graph of scour depths versus surge/wave loading at selected points along the levee reaches, plotted from the data in Table 1. The soil borings and LIDAR data were compiled by levee crown soil type (SM = silty sand, CL = lean clay, and CH = fat clay); soil consistency (soft, medium, and stiff); erosion depth; and maximum water height (ft) above crown elevation. Figure 52 indicates a lack of correlation between water height and erosion depth, but it does show that fat clays with medium consistency (strength) fared better than soils having lower plasticity and strength.

Boring	Surface soil type	Scour depth, ft	Overtop crest, ft
9BU	med CL	5	2
11BU	soft CH	10	5
12BU	med CL	6	7
18UBD	SM	6.2	7

13BU	med CH	1	7
ERDCM3	med CH	0.7	7
10-CUI	med CH	0.5	6
9-CUA	stiff CL	7	5
44-U	med CH	0.5	1
45-U	med CL	8	2
5A-CAU	stiff CL	0	1

Table 1. Surface soil and scour versus hydraulic loading. Strengths (consistencies) are soft, medium (med) and stiff. Soils are lean clay (CL), fat clay (CH), and sandy silt (SM).

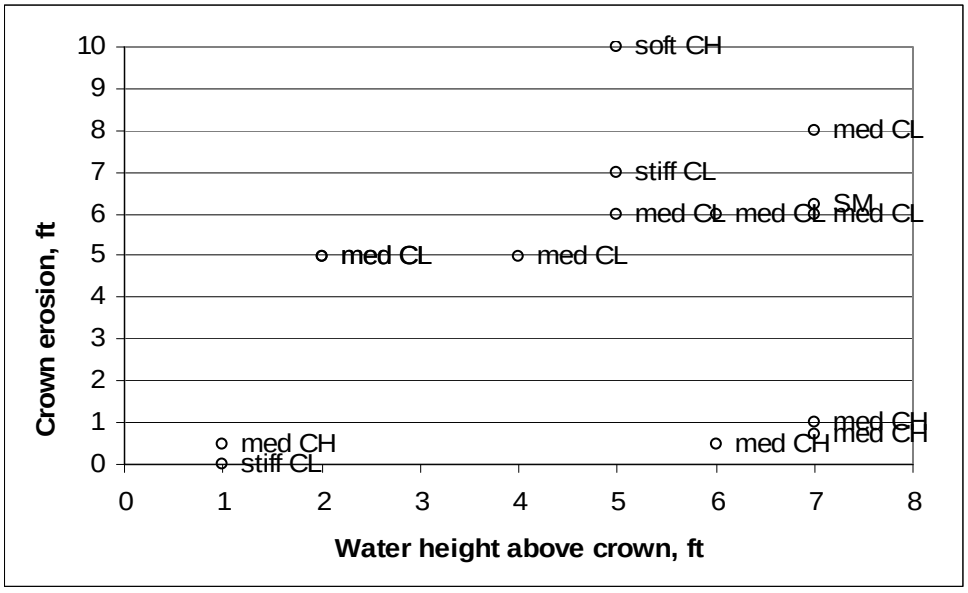


Figure 52. Scour depths versus surge/wave loading from soil borings and LIDAR data plotted from Table 1. Levee surface soil stiffness (strength) and soil type are labeled. Note that medium strength fat clay (med CH) had the least amount of erosion as the hydraulic loading increased.

4. Summary

Most erosion appeared to have occurred on the backside (landside or protected side) of both levees and floodwalls. The minor erosion / scour patterns (A) were the most geographically widespread. The most serious patterns (C and D) were confined to lengthy levee reaches generally the south bank of the MRGO (Bayou Bienvenue to Bayou Dupre and southeast of Bayou Dupre). Evidence of front-side erosion caused by wave damage suggests that wave damage occurred on levees with higher elevations which were exposed to waves for a longer duration, as a result of these levees proximity to Lake Borgne.

Erosion was initiated on soil surfaces ranging from sandy silts to fat clays. In general, the eroded soil surface contained sand / silt / lean clay layers, which are known to be more erodible than compacted fat clay generally specified as a levee "cap". The least amount of erosion from overtopping of the levees along Reach 2 of the MRGO occurred in locations where there was 10 ft or more of medium fat clay without any lenses of other soil types in the stratum. The two soil borings that show this relationship are 13BU-CHBD, Figure and 10-CUI, Figure. Therefore, the evidence suggests that levees which breached were constructed with more erodible soils, such as hydraulic fill with non-clay, variable soil type cross-sections along Reach 2 of the MRGO.

References

Hanson, G.J., K.R. Cook, W. Hahn, and S.L. Britton. 2003. "Evaluating erosion widening and headcut migration rates for embankment overtopping tests," American Society of Agricultural Engineers Paper no. 032067.

Hanson, G.J. and A. Simon. 2001. "Erodibility of cohesive streambeds in the loess area of the midwestern USA," *Hydrological Processes*, Vol 15, pp 23 - 38.

Hanson, G.J., K.M. Robinson, and K.R. Cook. 2001. "Prediction of headcut migration using a deterministic approach," *Transactions of the American Society of Agricultural Engineers*, Vol 44(3), pp 525 - 531.

Hughes, S.A. 2006. "Protection for backside levee slopes," draft report to the New Orleans District Corps of Engineers.

Hunt, S.L., G.J. Hanson, K.R. Cook, and K.C. Kadavy. 2005. "Breach widening observations from earthen embankment tests," *Transactions of the American Society of Agricultural Engineers*, Vol 48(3), pp 1115 - 1120.

Venard, J.K. and R.L. Street. 1975. *Elementary fluid mechanics*, 5th Ed., John Wiley and Sons, New York.

II. Assessment of Breaches along the Inner Harbor Navigation Canal

Introduction

Four breaches occurred on the Inner Harbor Navigation Canal (IHNC) during Hurricane Katrina, on the morning of August 29th. Two of the breaches occurred on the east bank between the Florida Avenue Bridge and the North Claiborne Avenue Bridge adjacent to the Lower 9th Ward, and two on the west bank just north of the intersection of France Road and Florida Avenue (Figure 53). Three of the breaches involved failures of floodwalls on levees, and one involved failure of a levee. For purposes of this report, only the two breaches occurring adjacent to the Lower Ninth Ward will be discussed.

All of the IHNC floodwalls and levees were overtopped on August 29th. The peak storm surge elevation in the IHNC was 14.2 ft[1] at 9:00 AM, about 1.7 ft above the tops of the floodwalls and levees. My review of available data shows that the water flowing over the I-walls when they were overtopped eroded trenches on the protected side of the walls as it cascaded onto the levee fill. The soil that was providing support for the walls eroded away, making the walls less stable. This loss of stability as a result of overtopping caused a floodwall failure on the southernmost breach of the floodwall protecting the Lower Ninth Ward, hereinafter referred to as the "south breach."

Although it is clear that the walls were overtopped, and that erosion on the protected side compromised their stability, their stability was compromised by the erosion that occurred, it is my opinion to a reasonable degree of scientific certainty that one of the east side breaches occurred before the wall was overtopped. Eyewitness reports indicate that the water level in the Lower 9th Ward near Florida Avenue was rising as early as 5:00 AM, when the water level in the IHNC was still below the top of the floodwall. In order to have this increase in the water level in the Lower 9th Ward, a large quantity of water would be required to be flowing into the Lower 9th Ward from the IHNC, which could only occur if the floodwall was breached. Stability analyses indicate that foundation instability would occur before overtopping at the "north breach" on the east side of the IHNC.

The soil immediately beneath the levees and floodwalls at these two all four breach locations included marsh, beneath which was clay, and beneath the clay, sand. Through most of their lengths, the critical potential failure surfaces passed through the marsh and clay. The stability analyses show that the critical potential failure surfaces did not extend to the sand layer beneath the clay.

Stability analyses of the north breach on the east side resulted in a computed factor of safety equal to 1.0 with a crack or gap on the canal side of the wall and water in the IHNC at elevation 11.2 ft. This is about 1.0 ft higher than the average IHNC water level

[1] All elevations refer to NAVD88(2004.65) datum.

at the time flood water was observed in the Lower 9th Ward. Considering that the effective water level could have been one foot higher due to wave effects, this result is consistent with the observed IHNC water level when flood water was first reported in the Lower 9th Ward. With a reasonable degree of scientific certainty, the north breach occurred before overtopping from foundation in stability, and this breach was the source of the first influx of water into the Lower 9th Ward.

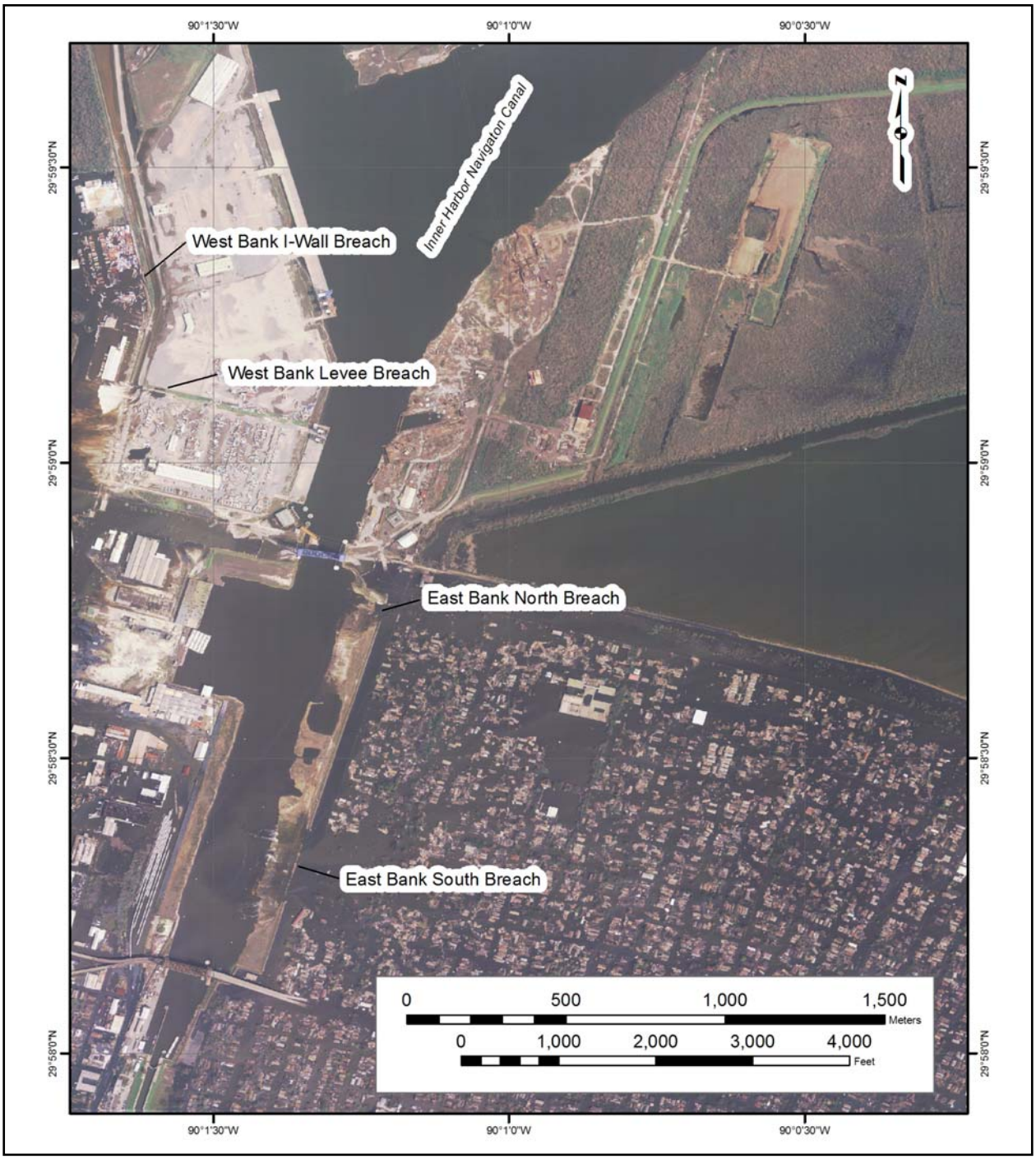


Figure 53. Four Breach Locations on the Inner Harbor Navigation Canal. The two breaches addressed in this report are the East Bank North Breach and East Bank South Breach

Stability analyses of the south breach on the east side, and the north breach on the west side, resulted in computed factors of safety larger than 1.0 with the water level at the top of the wall and a gap behind the wall, indicating that the walls at those locations would have remained stable if erosion did not remove the soil supporting the wall. none of the soil supporting the wall had been removed by erosion. Stability analysis of the south breach on the west side, where there was no I-wall, showed that the factor of safety there was also high, and the failure was due to overtopping erosion.

The lower computed factor of safety at the north breach on the east side relative to the south breach on the east side is attributable to the fact that the ground elevation on the protected side is lower at that location, and as a result there was less soil on the protected side of the wall that was able to provide support for the wall.

In summary, the failure that resulted in the north breach on the east side of the IHNC resulted from two differences between the stability analyses that were used as the basis for design and those described in this report: (1) the ground surface beyond the toe of the levee at the north breach location was lower than the landside ground surface in the design cross section, and (2) the floodwall was not designed to withstand prolonged overtopping and gap formation behind the wall design analyses did not consider the possibility of a gap forming behind the wall, allowing water to run into the gap and increase the load on the wall. The south breach on the IHNC was caused by overtopping and erosion.

1. Observations and Possible Modes of Failure

As shown by the hydrograph in Figure 54, the water level in the IHNC rose from elevation 1.0 ft. at 12:00 AM on August 28th to 14.2 ft. at 9:00 AM on August 29th. The peak water level was 1.7 ft. above the tops of the floodwalls and levees which were at elevation 12.5 ft. The hydrograph in Figure 55 shows that the water level in the Lower 9th Ward was rising at 5:00 AM on August 29th, when the water level in the IHNC was at elevation 10.2 ft., about 2.3 ft. below the tops of the floodwalls and levees. With ground surface elevations approximately -4.0 ft., water at elevation +2.0 ft. indicates that the water was 6.0 ft. deep in the Lower 9th Ward at 5:00 AM on August 29th.

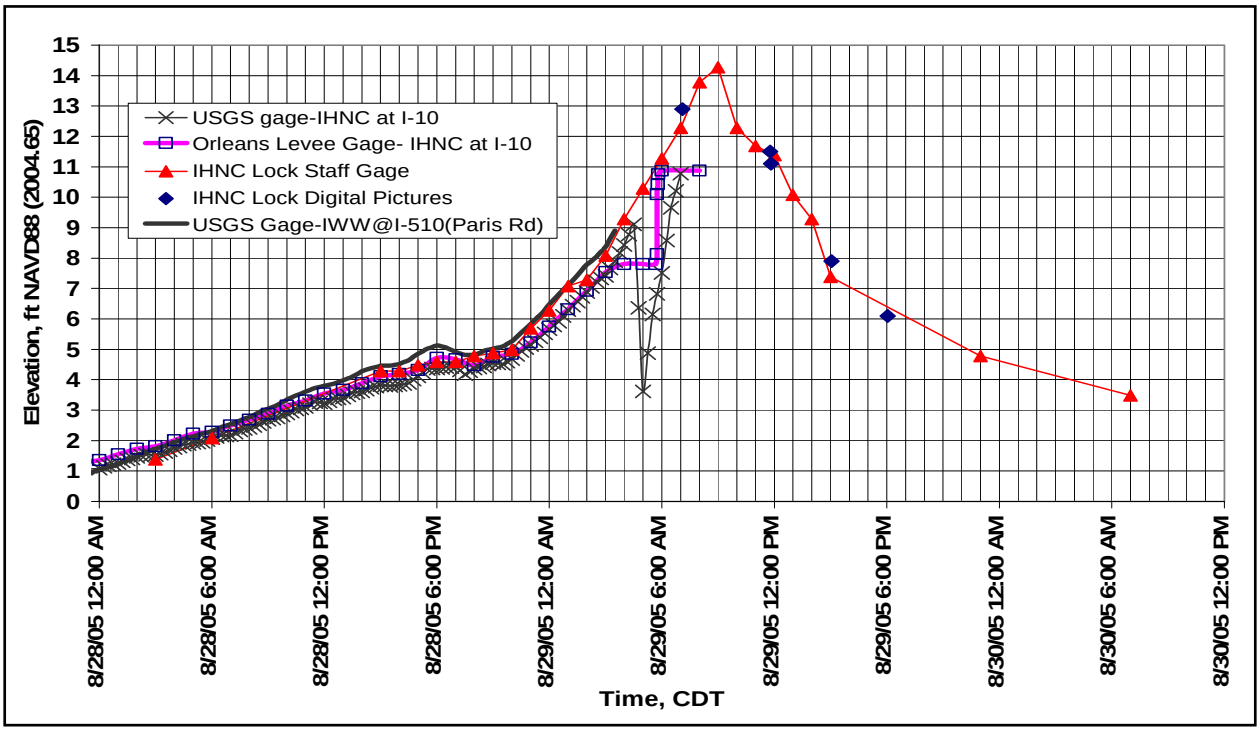


Figure 54. Katrina Hydrograph for the Inner Harbor Navigation Canal

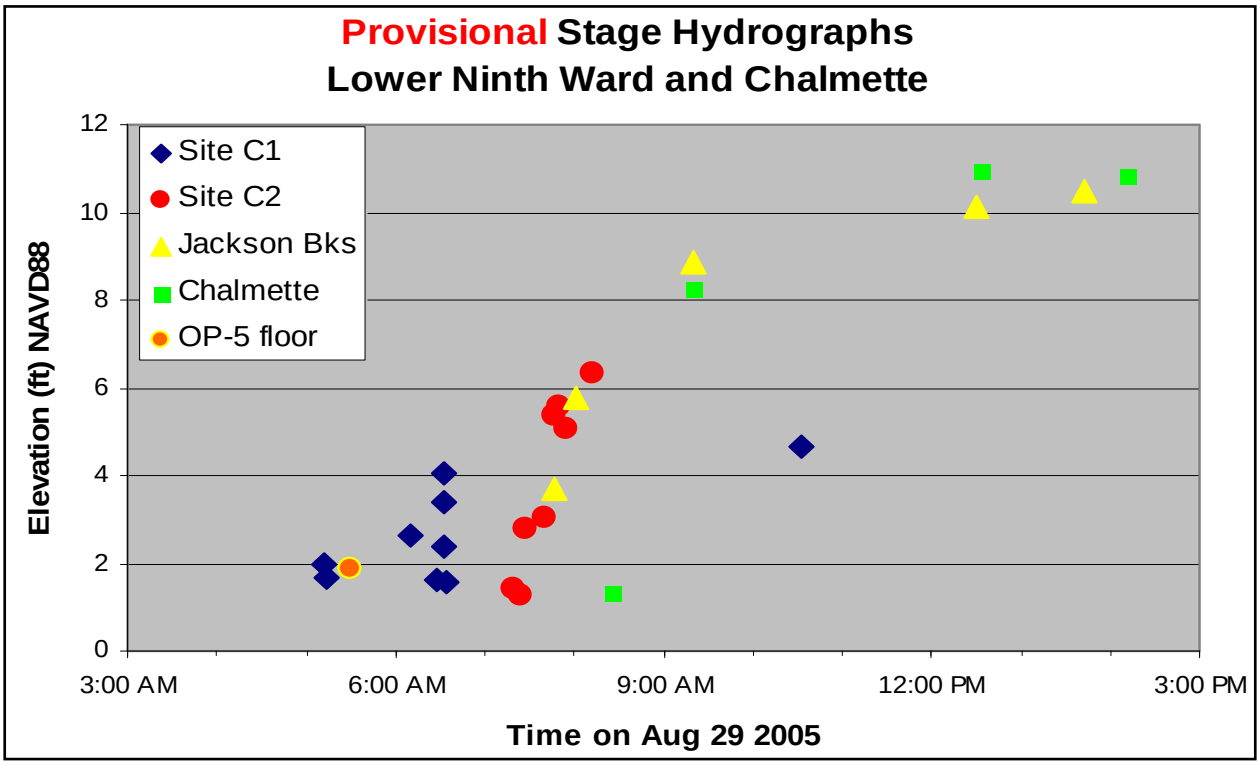


Figure 55. Hydrograph for the Lower 9th Ward Inundation

Initial observations after the hurricane revealed that overtopping had eroded at least one section of levee along the west bank and had eroded the soil adjacent to the wall on the protected side along the east and west bank. It appeared that water flowing over the floodwall scoured and eroded the levee on the protected side of the I-wall, exposing the supporting sheet piles and reducing the passive resistance (Figure 56). The erosion appeared to be so severe in the breach locations that the sheet piles may have lost all of their foundation support, resulting in failure (Figure 57). Perhaps the best evidence of this scour can be seen along the unbreached reaches of the east bank I-walls on the Inner Harbor Navigation Canal where U-shaped scour trenches could be found adjacent to the I-walls. As the scour increased, the I-wall may have moved laterally and leaned to the protected side, causing the scour trench to grow as the water began cascading farther down the slope until sufficient soil resistance was lost and the wall was carried landward.



Figure 56. Scour and Erosion on the Protected Side of the IHNC Adjacent to the Ninth Ward in the Vicinity of the South Breach



Figure 57. Scour and Erosion Leading to the Failure of the I-Wall on the IHNC Adjacent the South Breach (Lower 9th Ward)

Other possible modes of failure are sliding instability and piping and erosion from underseepage. Piping and erosion from underseepage is unlikely because the I-walls were founded in a clay levee fill, a marsh layer made up of organics, clay and silt, and a clay layer. Because of the thickness, the low permeabilities of these materials, and the relatively short duration of the storm, this failure mode was considered not likely based on a series of seepage analyses that were was performed for this area and presented in

Appendix B of this report. Based on these analyses, piping and erosion from underseepage was eliminated as a possible mode of failure.

It is necessary to investigate the possibility of sliding instability to determine if the I-walls could breach as a result of shear through the foundation. The foundation conditions are similar to the 17th Street Canal. As shown in Figure 58, no significant wall movement was found in the wall sections adjacent the south breach. However, Figure 59 shows significant wall movement did occur in the wall sections adjacent to the north breach.



Figure 58. IHNC East Bank – South Breach – Wall Movement



Figure 59. IHNC East Bank – North Breach – Wall Movement (View looking south)

2. Stratigraphy

a. IHNC East Bank – Lower 9th Ward

The data available to assess the stratigraphy of the area includes borings from the General Design Memorandum No. 3, "Chalmette Area Plan," hereinafter "GDM," (GDM), borings taken after the failure, and cone penetration tests taken after the failure. The locations of these borings and cone penetration tests are shown in Figure 60. Note that all borings taken after the failure were at the levee toe. The GDM contains 10 borings on the levee centerline (2-U, 3, 4, 5, 6-U and 7 in the vicinity of the breach, and four at the levee toe (2-UT, 3T, 4T and 6UT). A centerline profile under the levee is represented in Figure 61 and is based on both pre-Katrina and post-Katrina borings. This section shows 60 to 70 ft of predominantly fine-grained Holocene (i.e., less than 10,000 years old) shallow water and terrestrial sediments overlying the Pleistocene surface (i.e., older than 10,000 years). Holocene sediments are separated into various depositional environments in Figure 61, based on soil texture, organic content, and other physical and engineering properties. Engineering properties of these layers are described in greater detail below.

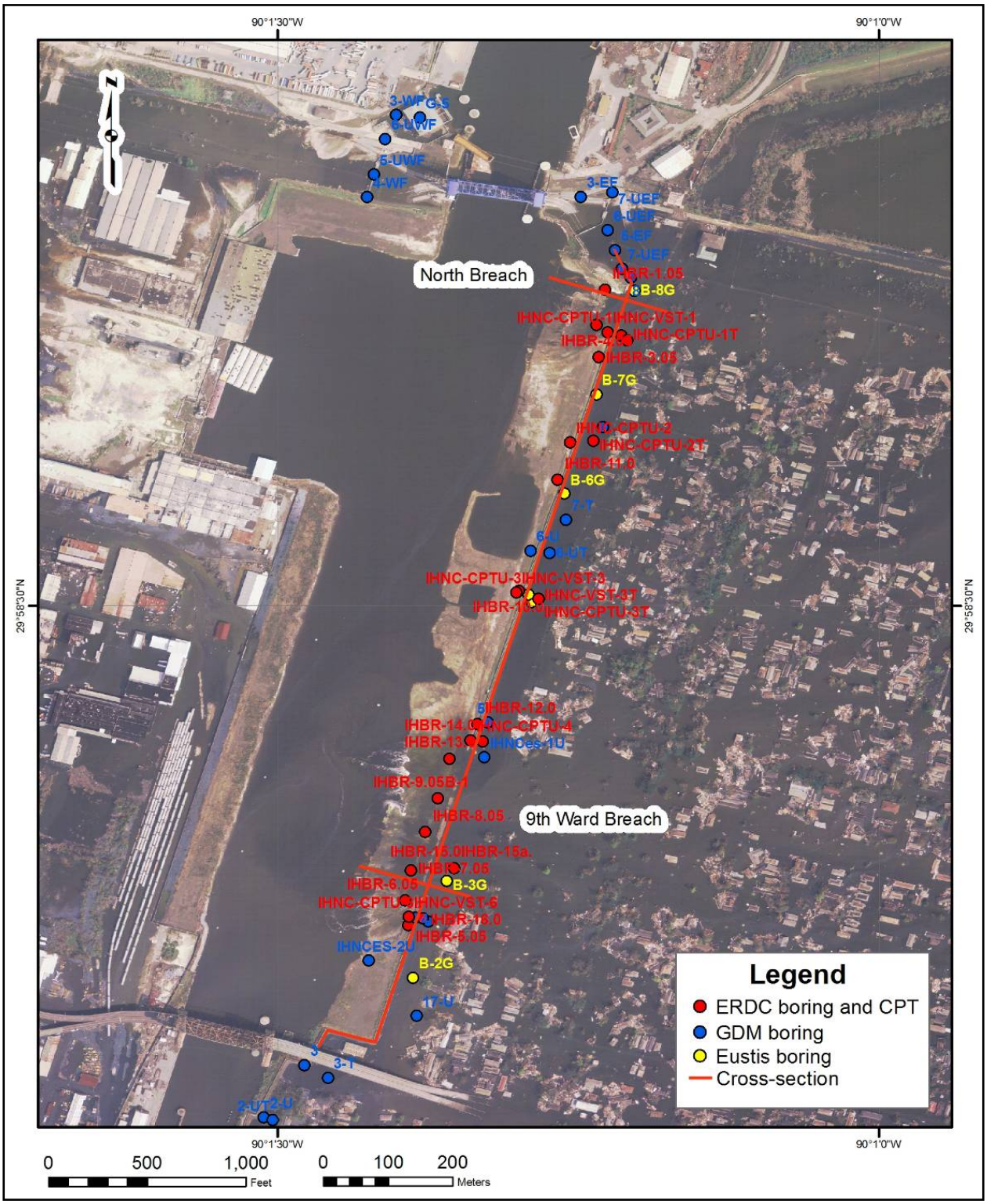


Figure 60. IHNC – East Bank (Between Florida Ave. and North Claiborne Ave.), Boring and CPTU Location Map

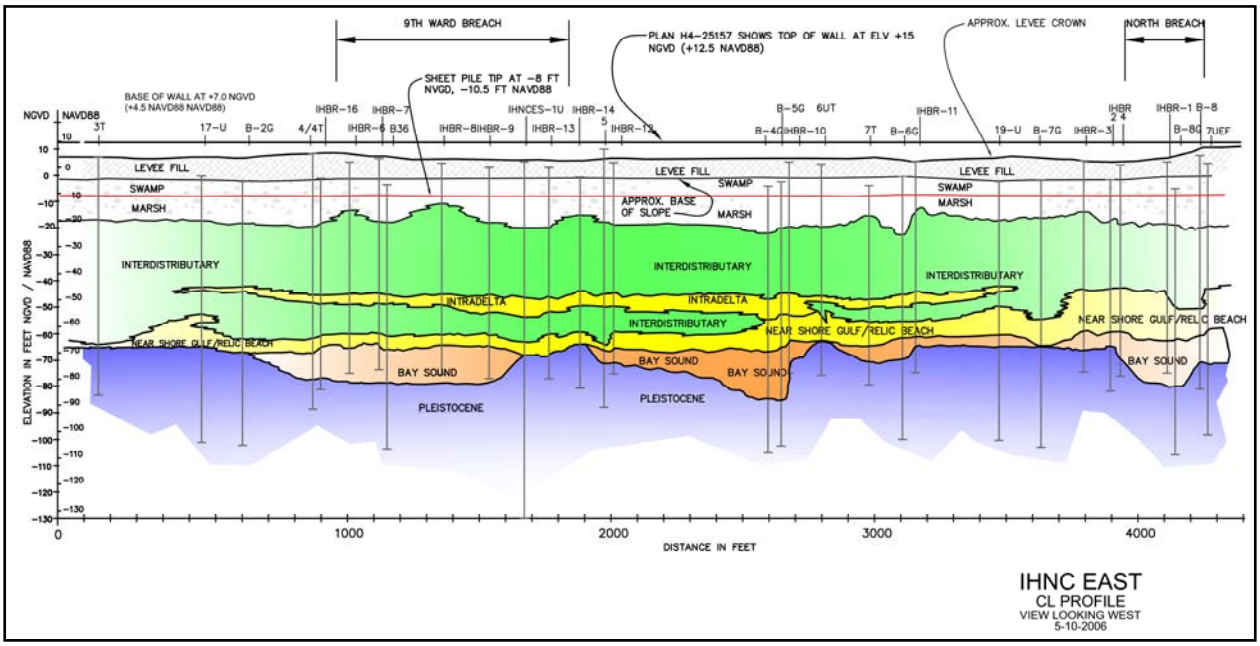


Figure 61. IHNC East Bank, Centerline Geologic Section Showing South (Lower 9th Ward) and North Breaches

The sections of the IHNC east bank where the north and south breaches occurred encompass Stations 54+00 to 56+00 and 22+00 to 31+00, respectively. These breaches occurred between Florida Avenue and North Claiborne Avenue. The strength evaluation focused primarily on these areas.

The GDM borings indicate the levee fill properties for the north and south breach areas are similar, consisting of compacted lean clay (CL) and heavy clay (CH) CL and CH materials. The average moist unit weight of the fill was estimated to be 109 pcf.

Beneath the fill is a marsh unit about 17 ft thick. The marsh layer is composed of organic material from the cypress swamp that occupied the area, together with silt and clay deposited in the marsh. Because the upper 8 to 9 ft of this unit has different material properties than the lower portion, it was divided into two layers, Marsh 1 and Marsh 2. Water contents and saturated unit weights determined from samples of marsh material taken from the toe are shown in Figures 62 and 63, respectively. These figures clearly depict the differences in the marsh layers.

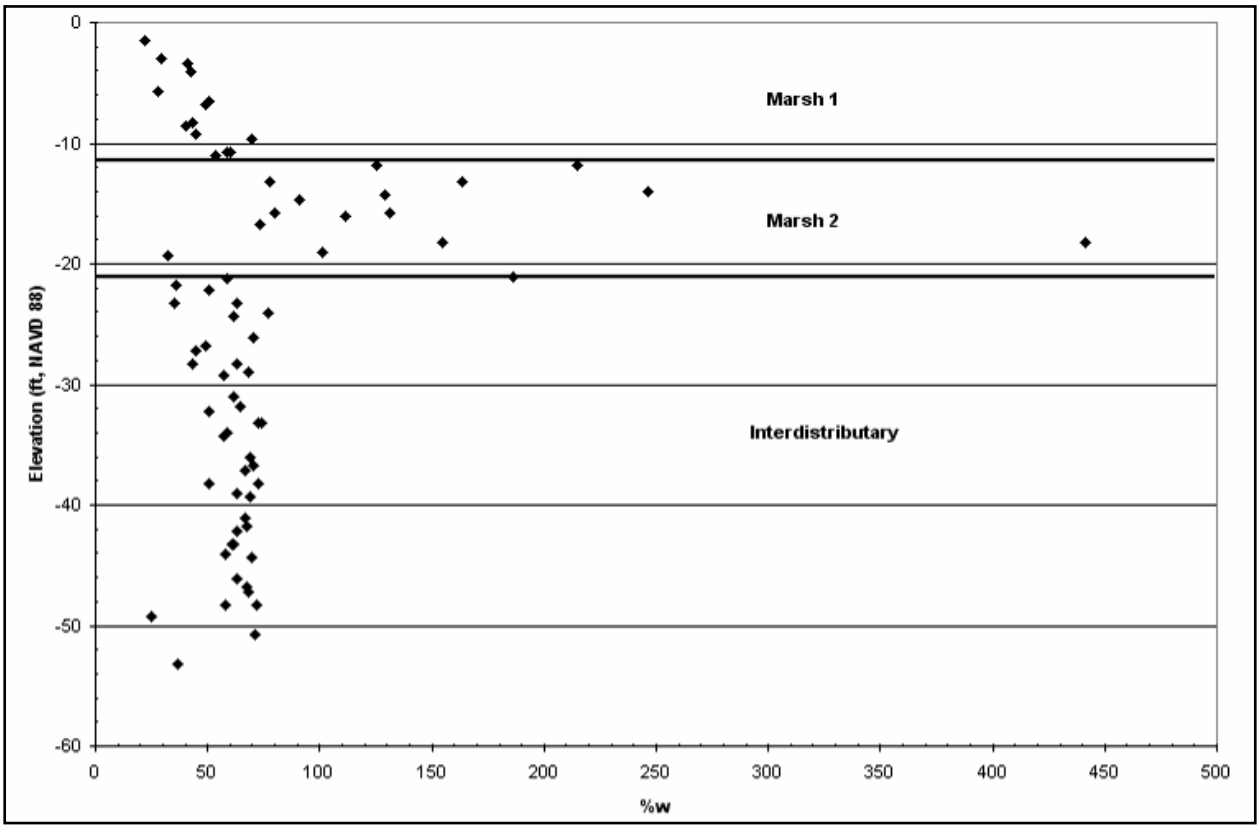


Figure 62. IHNC – East Bank (Between Florida Ave. and North Claiborne Ave.), % w Versus Elevation (ft, NAVD 88) from Toe Borings

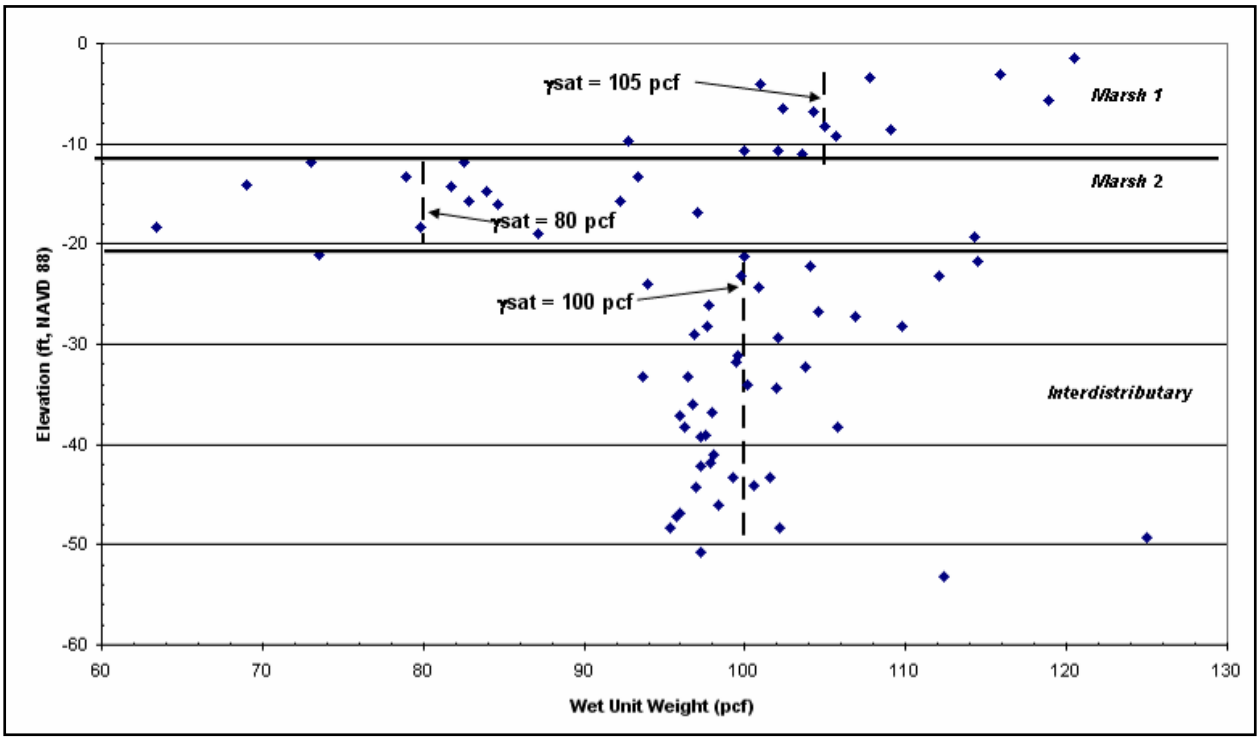


Figure 62. IHNC – East Bank (Between Florida Ave. and North Claiborne Ave.), Wet Unit Weight versus Elevation (ft, NAVD 88) from Post-Katrina Borings

Water contents, unit weights and undrained shear strengths are shown in Table 2, and these properties for the Marsh 2 layer are shown in Table 3. These properties are based on samples from post-Katrina borings at the levee toe. The average saturated unit weight of the Marsh 1 layer is about 105 pounds per cubic foot (pcf) pcf. Water contents of the Marsh 1 layer are as high as 80%. The average water content is approximately 49%. The average saturated unit weight of the Marsh 2 layer is about 80 pcf. Water contents of the marsh 2 layer are as high as 442%. The average water content is approximately 175%. The marsh 1 layer is mostly CH material. The Marsh 2 layer is fibrous at the top, and more amorphous near the bottom, indicating more advanced decomposition of the older organic materials at depth.

Beneath the marsh layers is a layer of interdistributary clay with an average Liquid Limit of about 79% and an average Plastic Limit of 26%. Based on consolidation test results presented in the GDM, the clay is normally consolidated throughout its depth. The average saturated unit weight of the clay is about 100 pcf, and the average water content is approximately 60%. Water content and unit weights are summarized in Table 4.

Beneath the clay is a layer of Beach Sand. This layer is not involved in the observed or calculated mechanisms of instability, and its strength is therefore of little importance in stability analyses, except as a more resistant layer beneath the clay.

The unit weights measured for individual laboratory test specimens and the values used in subsequent analyses are shown in Figure 62.

Table 2
Properties of Marsh 1 Layer from Post-Katrina Borings at Toe

Marsh 1 Layer					
Number of Samples = 16					
	Mean	Standard Deviation	COV	Max	Min
%w	49	17	0.342	80.2	21.9
Saturated Unit Weight (pcf)	104	9	0.081	120.5	92.2
S_u (psf)	550	214	0.389	3195	90.0

Table 3
Properties of Marsh 2 Layer from Post-Katrina Borings at Toe

Marsh 2 Layer					
Number of Samples = 12					
	Mean	Standard Deviation	COV	Max	Min
%w	175	96	0.549	441.6	90.9
Saturated Unit Weight (pcf)	78.4	7	0.091	87.1	63.4
S_u (psf)	195.3	116	0.595	336	64.6

Table 4
Properties of Interdistributary Clay from Post-Katrina Borings at Toe

Interdistributary Clay					
Number of Samples = 45					
	Mean	Standard Deviation	COV	Max	Min
%w	60	12	0.208	77.2	25
Saturated Unit Weight (pcf)	101.1	6	0.063	125	93.6

b. Shear Strength - IHNC – East Bank

The sources of shear strength data include borings from the General Design Memorandum (GDM), and borings, cone penetration tests, and vane shear tests performed as part of the failure investigation. From the available sources, two GDM borings, four cone penetration tests, and three vane shear tests provide information beneath the centerline of levee. From the GDM borings (2-U and 6-U), the results of 11 Q test envelopes and 26 unconfined compression tests were available. All laboratory tests were performed on specimens trimmed from 5-in diameter undisturbed tube samples.

Beneath the toe of the levee, the GDM contained the results of over 70 unconfined compression tests. In addition, about 100 unconfined compression tests have been conducted on test specimens obtained since Katrina. Tests were performed on 1.4-inch diameter specimens trimmed from 5-in.-diameter tube samples. Statistical analyses have been performed on the data from the post-Katrina tests to compute minimum, maximum, and average values of strength for the levee fill, the marsh layers, and the clay. The results of the statistical analyses are shown in Tables 1 through 3. Also, one cone

penetration test with pore pressure measurements (CPTU) and one series of vane shear tests were performed near the area of the breaches after the failure.

Shown in Figure 63 are the available laboratory and vane shear test results for samples obtained beneath the crest of the levee, as well as values of undrained shear strength determined from CPTU-1 using Mayne's method.[2]. Figure 64 presents the data available for undrained shear strength from the toe of the levee and areas beyond the toe. Plotted with these data are the results from CPTU-1T, which was performed at the toe of the levee.

[2] Mayne, P. W. (2003). "Class 'A' Footing Response Prediction from Seismic Cone Tests," Proceedings, Deformation Characteristics of Geomaterials, Vol. 1, Lyon, France.

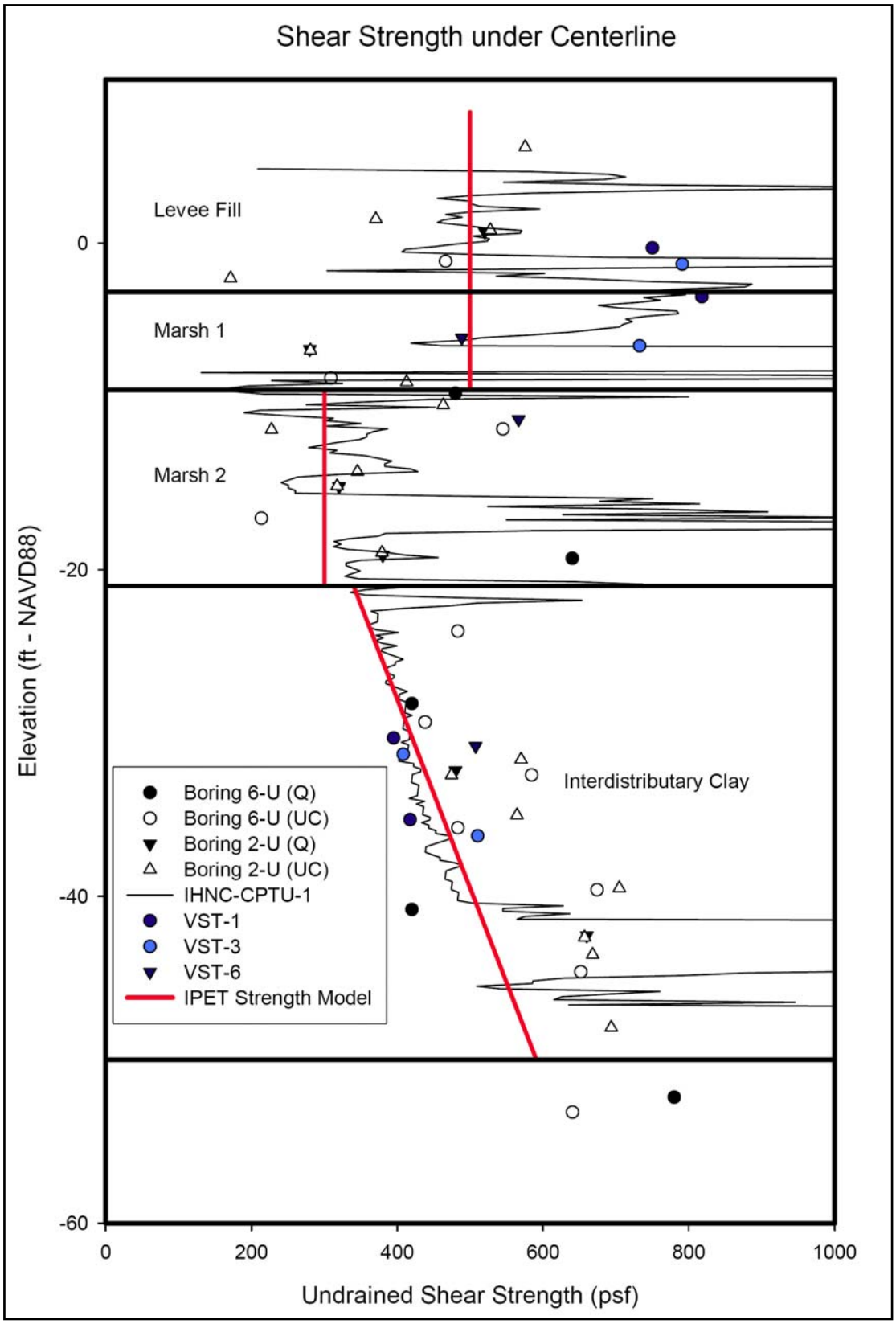


Figure 63. IHNC – East Bank Laboratory and Field Shear Strength Results for the Centerline of the Levee

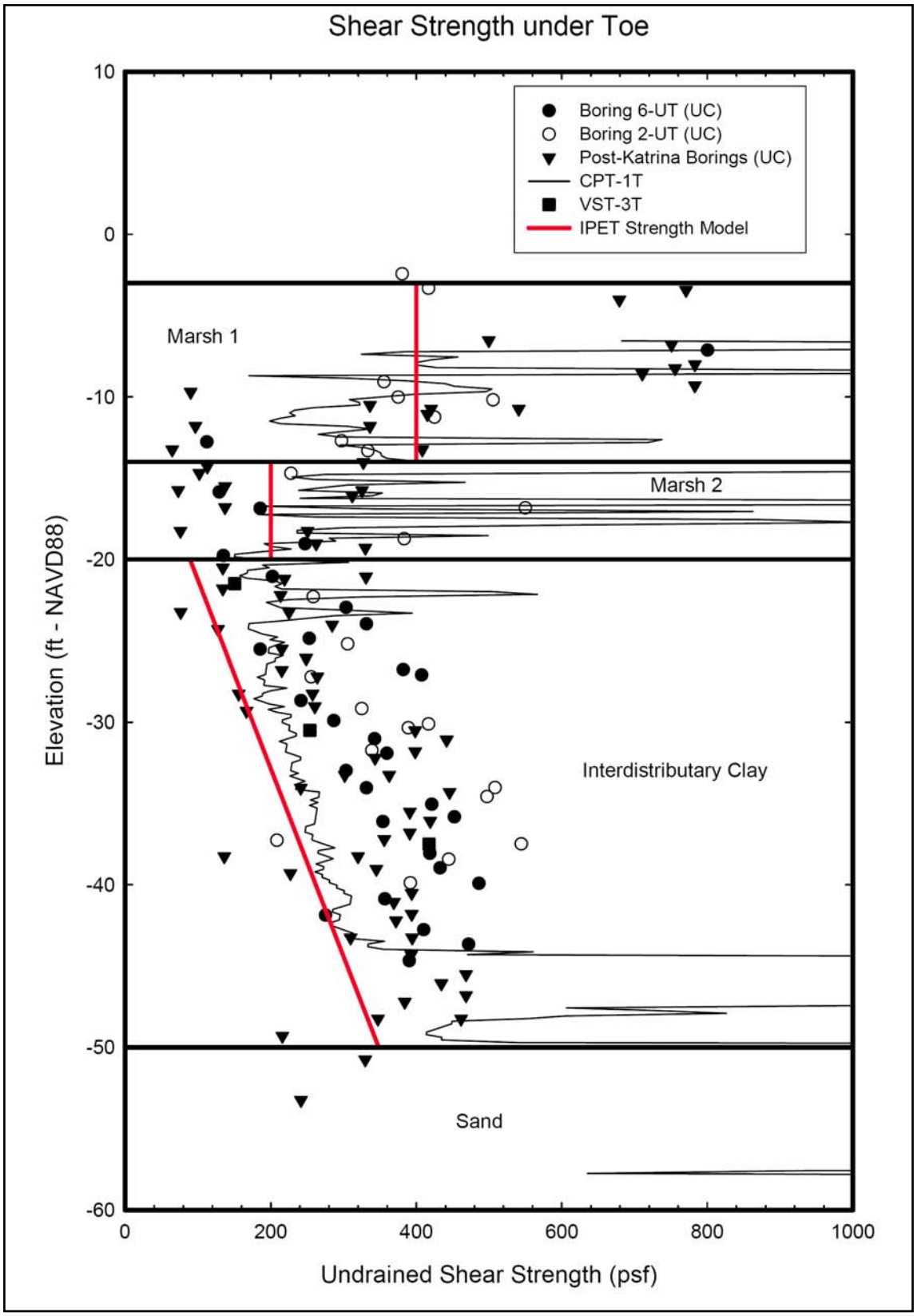


Figure 64. IHNC – East Bank Laboratory and Field Shear Strength Results for Toe of Levee and Beyond

Only a few strength tests for the levee fill are available from GDM borings in the breach area. The shear strength used for design (s_u =500 psf) was assumed for the levee-fill strength in the IPET strength model. As can be seen in Figure 61-62, a value of s_u = 500 psf for the levee fill seems reasonable based on the results of the CPTU tests, vane shear tests, and laboratory tests. However, the strength of the levee is not much involved in the calculated mechanisms of instability and therefore has limited importance in the stability analyses.

The marsh material is stronger beneath the levee crest where it has been compressed under the weight of the levee, and weaker at the toe of the levee and beyond, where it has not been compressed so heavily. CPTU data, vane shear tests, and unconfined compression tests conducted on test specimens trimmed from 5-in. samples were used to measure the Marsh 1 layer strengths at the toe. The measured shear strengths from the unconfined compression tests in the Marsh 1 layer scatter very widely from about 90 psf to over 800 psf, as shown in Figures 63 and 64. The vane shear test results summarized in Table 5 were conducted under the levee; they indicate shear strengths (corrected for strain rate effects and plasticity) ranging from 490 psf to 820 psf. Values of s_u = 650 psf beneath the levee crest, and s_u = 550 psf beneath the levee toe appear to be reasonably representative of the measured strengths for Marsh 1 layer, and these values are shown by the solid lines on Figures 63 and 64.

Table 5
IHNC East Bank - Results of Vane Shear Tests in Marsh 1 Layer, Beneath Levee

Vane Shear Tests	Elev. ft NAVD88	%w	PI	Corrected Peak Strength (psf)
IHNC-VST-3	-6.3	--	--	732
IHNC-VST-6	-5.8	73	56	489
IHNC-VST-6	-10.8	--	--	566
IHNC-VST-1	-3.3	--	--	818
Average				**651**

The shear strength characterization of the Marsh 2 layer was difficult because of large scatter in the data. Data obtained from post-Katrina toe borings taken between Florida Avenue and North Claiborne Avenue are presented in Table 3. Noting Figures 12 and 13, which include both pre-Katrina and post-Katrina strength results, the undrained shear strength of the Marsh 2 layer ranges from about 200 to 620 psf under the levee centerline, and from 90 to 500 psf beneath the levee toe. Values of s_u = 300 psf beneath the levee crest, and s_u = 200 psf beneath the levee toe appear to be reasonably representative of the measured values; these values are shown on Figures 63 and 64. These strengths are the same as were used in the GDM design analyses.

Interpretation of the undrained shear strength of the interdistributary clays was developed considering the results of all laboratory and field tests. The pore pressure results from the CPTU tests were questionable, and for this reason, less emphasis was placed on determining undrained shear strengths from the cone penetration test results.

The CPTU tests did indicate that the clay deposit was normally consolidated, and that the undrained shear strength increased linearly with depth. Figure 63 shows the undrained shear strength with depth determined using Mayne's method[3] for CPTU-1, which was conducted under the centerline of the levee. Figure 64 presents the results of CPTU-1T, which was conducted at the toe of the levee.

The straight line shown in Figure 63, representing the average undrained shear strength in the clay, has a slope of 8.6 psf per foot of depth. This rate of strength increase with depth appears to compare reasonably well to the laboratory strength test results.

The rate of increase of strength with depth is directly related to the s_u/p' ratio for the clay and its buoyant unit weight as follows:

$$\frac{s_u}{p'} = \frac{\text{rate of increase of } s_u \text{ with depth}}{\text{rate of increase of } p' \text{ with depth}} = \frac{\Delta s_u / \Delta z}{\gamma_{buoyant}} \quad \text{.....(1)}$$

The value of $\gamma_{bouyant}$ for the clay is 100 pcf – 62.4 pcf = 37.6 pcf. Thus, the value of s_u/p' is:

$$\frac{s_u}{p'} = \frac{8.6 \;\; psf \;\; per \;\; ft}{37.6 \, pcf} = 0.23 \quad \text{.....(2)}$$

which is a reasonable value for this normally consolidated clay.

These values provide a good basis for establishing undrained strength profiles in the clay. The undrained strength at the top of the clay is equal to 0.23 times the effective overburden pressure at the top of the clay, and the undrained strength increases with depth in the clay at a rate of 8.6 psf per foot.

In the IPET strength model, the undrained shear strength of the clay is equal to 0.23 times the effective overburden pressure. The clay strength thus varies with lateral position, being greatest beneath the levee crest where the effective overburden pressure is greatest, and varying with depth, increasing at a rate of 8.6 psf per foot at all locations. Figure 13 shows the calculated undrained shear strength variation in the interdistributary clay at the toe of the levee and beyond. Based on the available test data, the IPET strength model appears to be an adequate, albeit conservative, representation of the strength beneath the toe.

The IPET strength model does not consider details of the stress distribution beneath the levee, which would result in "load spread" effects. These effects would result in rotation of principal stresses beneath the levee, and in the added stress due to the levee load that would decrease with depth. The model described in the previous paragraphs uses a simple stress distribution beneath the levee that satisfies vertical equilibrium. The

[3] Mayne, P. W. (2003). "Class 'A' Footing Response Prediction from Seismic Cone Tests," Proceedings, Deformation Characteristics of Geomaterials, Vol. 1, Lyon, France.

consequences of this assumption are that the vertical effective stresses in the clay layer beneath the toe, and thus the undrained shear strength distribution, is underestimated. Likewise, the undrained strength distribution in the clay layer beneath the crest is overestimated using the vertical equilibrium assumption. These two effects tend to balance out, and the average shear strength on the failure plane is approximately the same as would be obtained from more complex methods of calculating the vertical effective stress in the clay layer.

It is also important to note that the ground elevation of the toe of the levee is not constant; therefore it is not possible to use the same strength versus elevation relationship for the south breach and the north breach. The decrease in elevation of the toe from the south breach to the north breach is shown in the LIDAR survey of the area in the year 2000, which is plotted in Figure 65. The elevation of the protected side levee toe decreases about 4 ft from the south breach to the north breach.

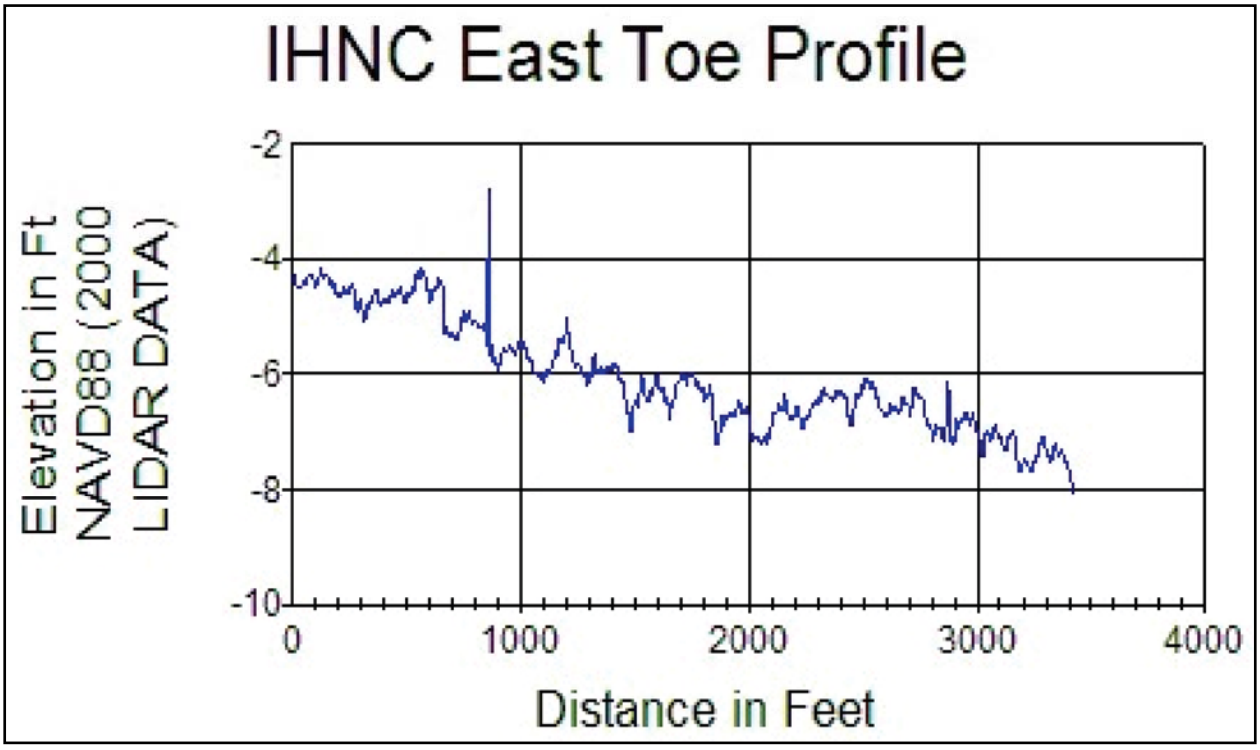


Figure 65. LIDAR Data at Toe of Levee

The drained friction angle of the sand beneath the clay was estimated to be 30 degrees for the stability analysis. As noted previously, the sand layer is not involved in observed or computed failure mechanisms, and the value of ϕ' assigned to it, therefore, has no influence on computed factors of safety.

c. Original Design Strengths - East Bank

The design analyses in GDM No. 3 the Chalmette Area Plan General Design Memorandum (GDM)[4] used undrained strengths for the levee fill, the marsh layers, and the clay, and a drained friction angle to characterize the strength of the sand layer beneath the clay, as does the IPET strength model described above. However, there are four marsh layers in the GDM interpretation compared to only two marsh layers for the IPET strength model. The design strengths are comparable to the IPET strengths discussed here and shown in Table 6 and Figure 66.

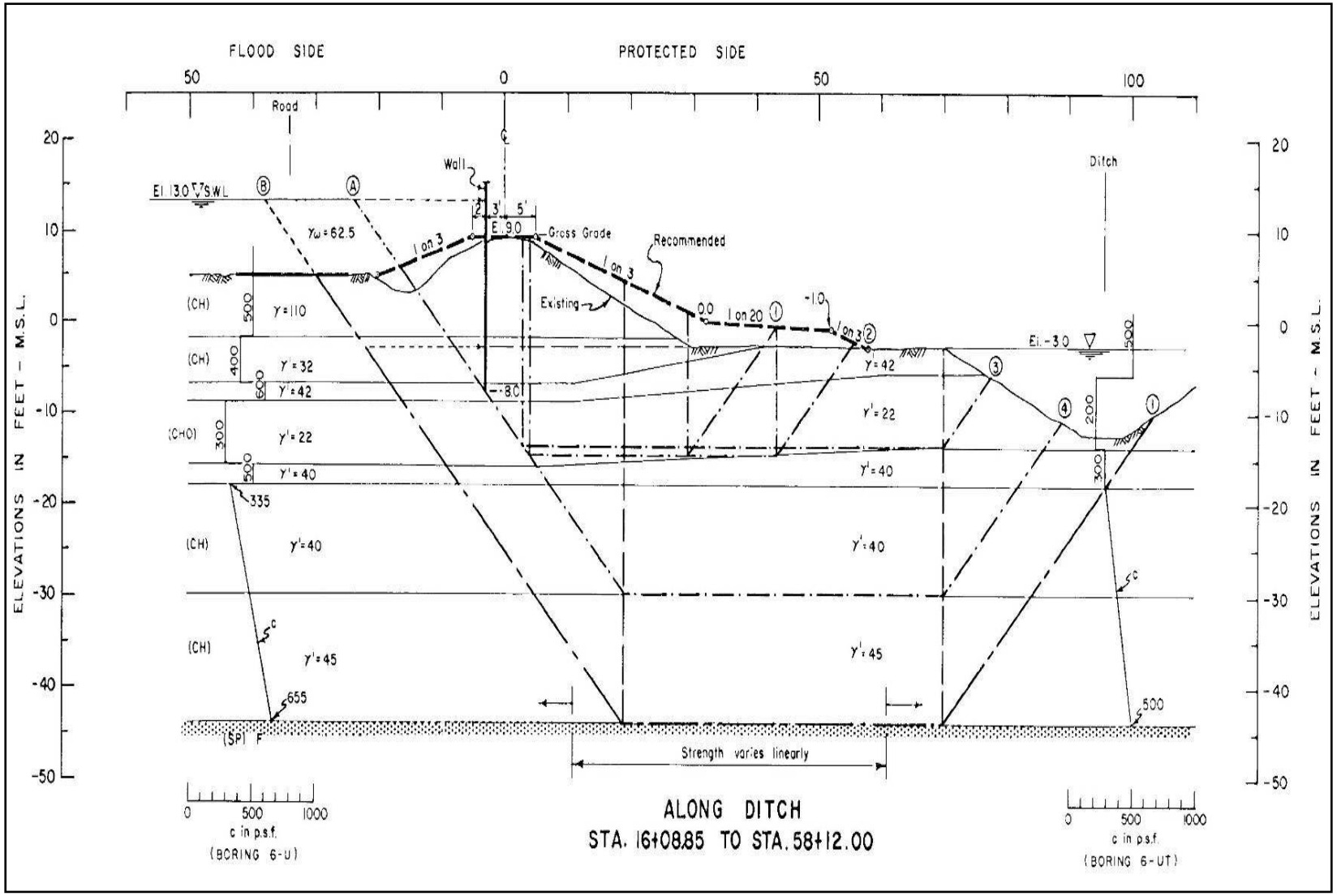


Figure 66. Cross Section Used for Design for Stations 16+09 to 58+12. Both East Bank Breaches Occurred Between These Two Stations

The values of strength for the levee fill, the marsh layers, and the clay layer that were used in the design analyses for the IHNC I-wall, Station 16+08.85 to Station 58+12.00, are shown in Table 5. This reach includes both breach areas on the east bank, which extends approximately from Stations 54+00 to 56+00 for the north breach and 22+00 to 31+00 for the south breach.

Table 6
Comparison of Strengths of Levee Fill, Marsh Layers, and Interdistributary Clay Used in Design for Stations 16+08.85 to 58+12.00 with the IPET Strengths

Material	Strengths used for design	IPET strength model
Levee fill	s_u = 500 psf, ϕ = 0	s_u = 500 psf, ϕ = 0
Marsh 1a layer (uppermost marsh layer)	s_u = 400 psf, ϕ = 0 beneath the levee and toe	s_u = 650 psf, ϕ = 0 beneath levee s_u = 550 psf, ϕ = 0 beneath toe
Marsh 1b layer (directly below uppermost marsh layer)	s_u = 600 psf, ϕ = 0 beneath levee s_u = 500 psf, ϕ = 0 beneath toe	
Marsh 2a layer (highly organic layer)	s_u = 300 psf, ϕ = 0 beneath levee s_u = 200 psf, ϕ = 0 beneath toe	s_u = 300 psf, ϕ = 0 beneath levee s_u = 200 psf, ϕ = 0 beneath toe
Marsh 2b layer (directly below marsh 2a layer)	s_u = 500 psf, ϕ = 0 beneath levee s_u = 300 psf, ϕ = 0 beneath toe	
Interdistributary Clay	12.3 psf/ft increase beneath levee (starting at 355 psf) 8 psf/ft increase beneath toe (starting at 300 psf)	Su/p' = 0.23; 8.6 psf/ft increase both beneath levee and toe (starting value depends on depth of overburden)

A comparison between the GDM and IPET strength models is presented in Figures 67 and 68 for the GDM design cross section. Shown in Figure 67 is the shear strength profile under the crest of the levee (horizontal coordinate of 0 ft) used in the original design, and the shear strength profile calculated using the IPET model. The IPET strength model has higher shear strengths in the Marsh 1 layer, and the GDM strength model has higher strengths in the lower portion of the Marsh 2 layer. Both models show a linear increase in undrained shear strength in the interdistributary clay layer, with the rate of increase greater for the GDM model than the IPET model. The difference in the rate of increase can be partially attributed to the difference in unit weights used in each model. The GDM strength model assumes a unit weight of the clay of 102.4 pcf for the upper portion of the clay and 107 pcf for the lower portion of the clay. The IPET model uses a unit weight of 100 pcf for the clay. The higher unit weights used in the GDM strength model would produce a larger increase in undrained shear strength per foot than the IPET model for the same undrained strength ratio. In addition, based on the assumed unit weights and the rate of strength increase, the GDM model corresponds to a greater undrained strength ratio, from about 0.28 to 0.31.

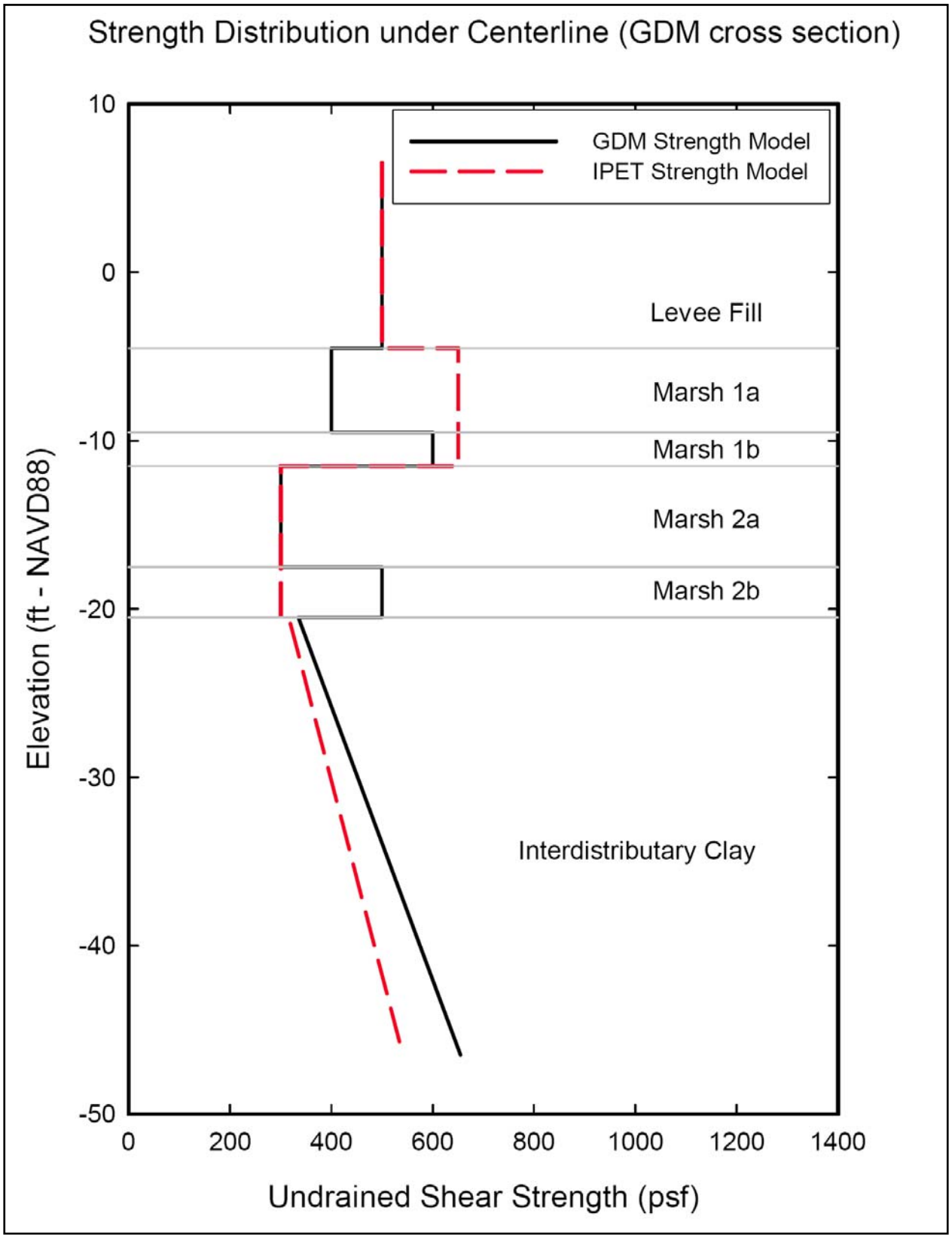


Figure 67. Comparison of GDM and IPET Shear Strength Models for GDM Design Cross Section at the Centerline (Horizontal Coordinate of 0 ft in Figure 66)

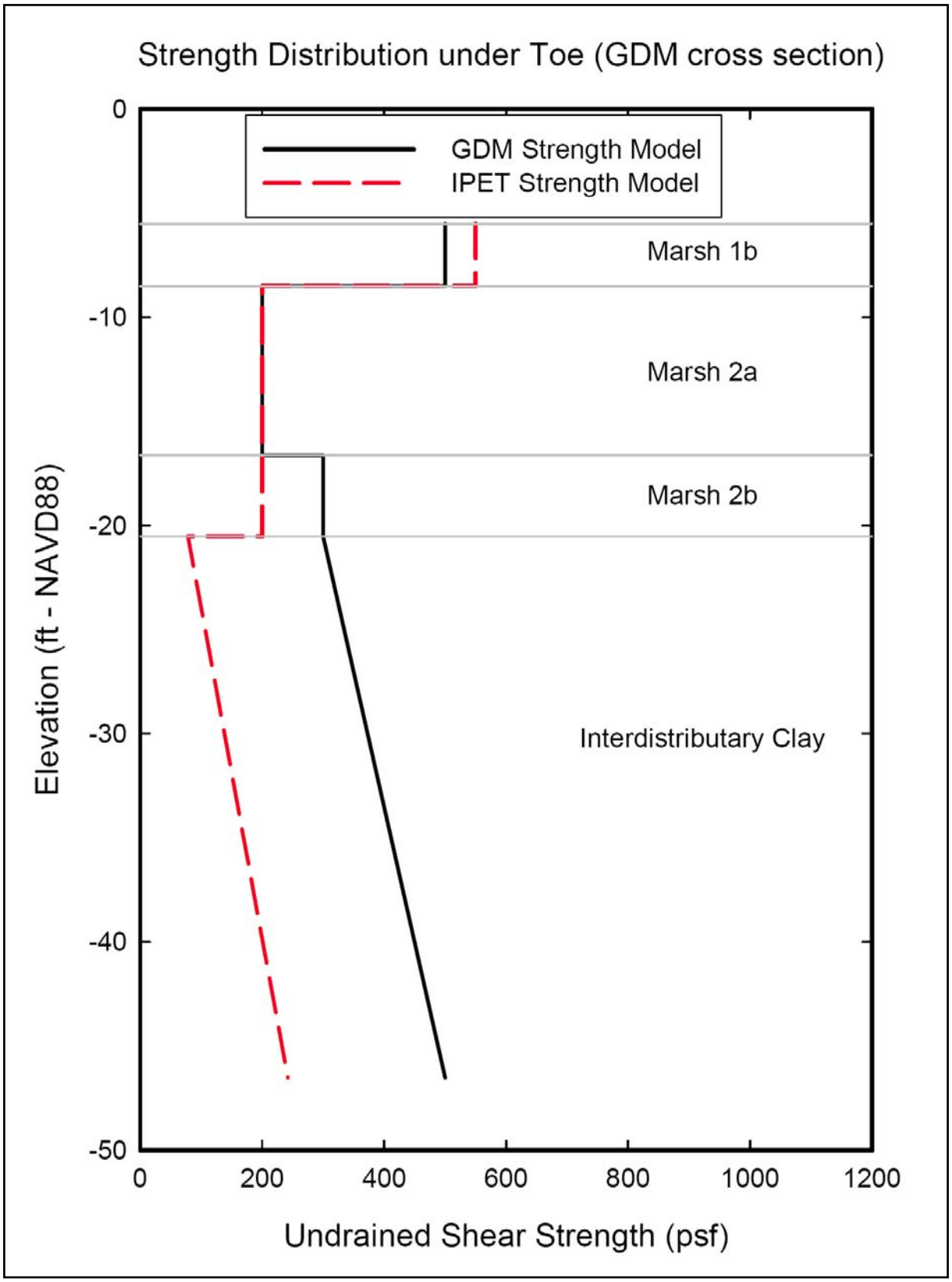


Figure 68. Comparison of GDM and IPET Shear Strength Models for GDM Design Cross Section at the Toe (Horizontal Coordinate of 60 ft in Figure 66)

The difference between the GDM and IPET strength model is more pronounced for undrained strengths below the toe of the levee. Shown in Figure 68 is the shear strength profile under the toe of the levee (horizontal coordinate of 60 ft) used in the original design, and the shear strength profile calculated using the IPET model. The undrained shear strengths are comparable in the marsh layers, but there is about a 200 psf difference in undrained shear strength in the interdistibutary clay. The rate of increase for both models is essentially the same, but the IPET strength model produces a lower shear strength at the marsh/clay interface. As stated earlier, the IPET strength model would tend to underestimate the undrained shear strengths beneath the toe when compared to available test data.

It is interesting to note the similarity of the two strength models, particularly since the GDM strength model was developed about 40 years ago. Both models share the essential characteristics of using different strengths under the levee crest and toe, and a lateral variation of shear strengths between these points.

2. IHNC East Bank North and South Failures

Eighteen slope stability analyses (Cases 1 through 5, 5a, and 6 through 17 in Table 7) were performed for the cross section at Station 55+00 at the north breach. The cross section used for these analyses is shown in Figure 69. Also, 17 slope stability analyses (Cases 1 through 17 in Table 8) were performed for a cross section developed for Station 26+00 at the south breach. The cross section used for these analyses is shown in Figure 70.

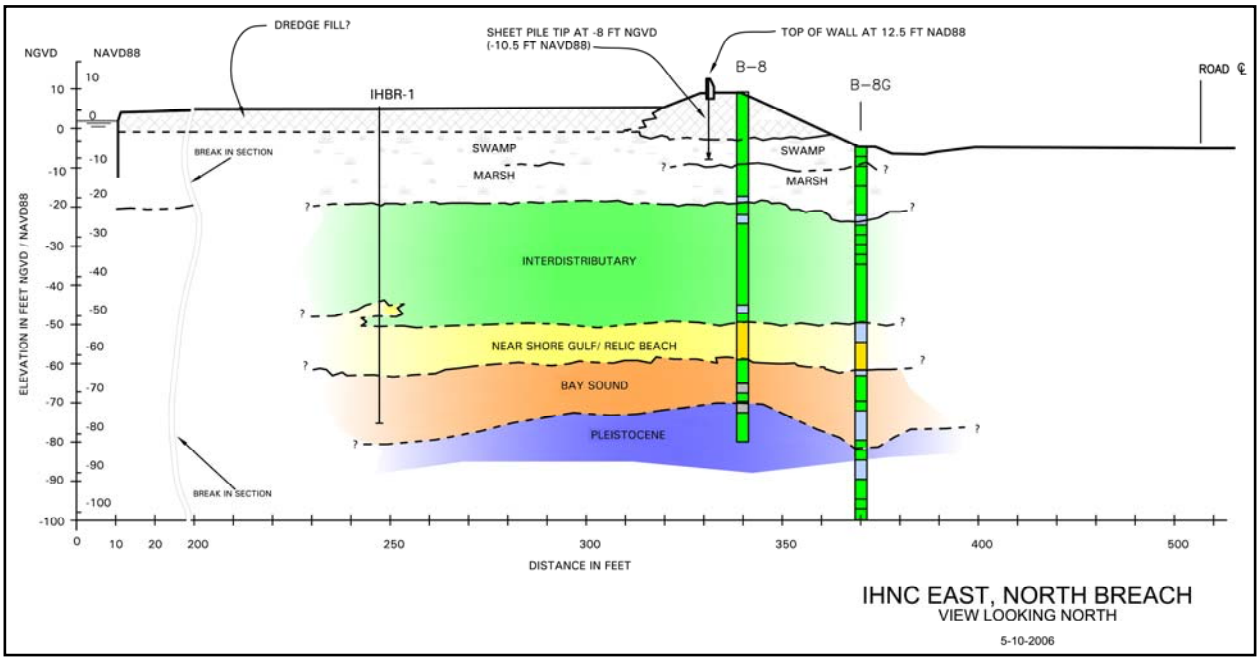


Figure 69. Profile of the North Breach at IHNC East bank, View Looking North

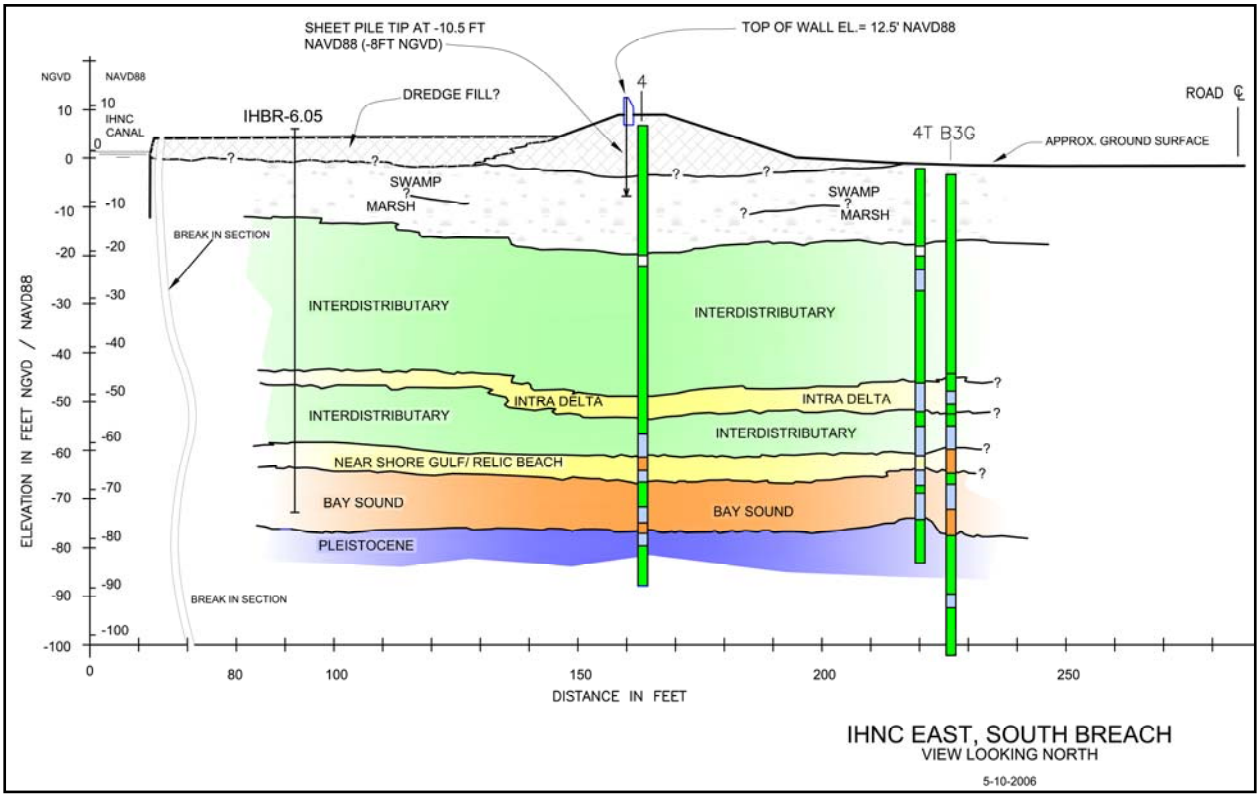


Figure 70. Profile of the South (Lower 9th Ward) Breach at IHNC East Bank, View Looking North

In addition, four slope stability analyses (Cases 1 through 4 in Table 9) were performed using the cross section and strength profile shown in the GDM, and presented in this report as Figure 66.

Average values of saturated unit weight were used in the analyses: γ_{sat} = 109 pcf for the levee fill, γ_{sat} = 105 pcf for the Marsh 1 layer, γ_{sat} = 80 pcf for the Marsh 2 layer, and γ_{sat} = 100 pcf for the interdistributary clay beneath the marsh layers. These values are based on values measured in laboratory tests on undisturbed samples.

The critical slip surfaces found in the analyses did not extend down to the sand beneath the clay, and the sand strength and unit weight therefore did not influence the results of the analyses.

The analyses were performed for undrained conditions in the levee fill, the marsh layer, and the clay beneath the marsh layer. Based on available information, it appears that the values of permeability of all three of these materials were low enough so that dissipation of excess pore pressures during the rise of the water level in the canal would have been negligible, and would have had, at most, a minor influence on stability.

Analyses were performed for two conditions regarding contact between the I-wall and the adjacent soil on the canal side of the wall. These are indicated by "yes" or "no" in the column labeled "Crack" in Tables 7, 8 and 9.

- For the "no crack" analyses, it was assumed that the soil on the canal side of the wall was in intimate contact with the wall. Water pressures were applied to the surface of the levee fill, and to the I-wall where it projected above the crown of the levee, but were not applied to the face of the wall below the crown of the levee.

- For the "crack" analyses, it was assumed that the I-wall was separated from the levee fill on the canal side of the wall as the water level in the canal rose and caused the wall to deflect away from the canal. Full hydrostatic water pressures were applied to the I-wall, from the water level in the canal to the bottom of the wall.

For the north breach, stability analyses were performed for canal water elevations of 10.0, 10.5, 11.2, and 12.5 ft. Analyses were performed with water elevations of 10.0, 10.5, and 12.5 for the south breach. The elevation of the top of the wall is 12.5 ft for both the north and south cross sections.

The analyses described here were performed using the computer program UTEXAS4[5]. Critical circular slip surfaces were located for each case using the search routines available in UTEXAS4. The analyses were verified using the computer program SLIDE[6]. The analyses were performed using Spencer's method[7], which satisfies all

[5] Available from Shinoak Software, 3406 Shinoak Drive, Austin, TX 78731
[6] Available from Rocscience Inc., 31 Balsam Avenue, Toronto, Ontario, Canada M4E 3B5

conditions of equilibrium. Methods that satisfy all conditions of equilibrium have been shown to result in values of factor of safety that are not influenced appreciably by the details of the assumptions they involve[8].

Table 7
Results of Slope Stability Analyses for IHNC East Bank, North Breach. Note all Analyses Use Spencer's Method and Circular Slip Surfaces

Case	Water Elev. ft NAVD88	Strength Model	Crack (Yes or No)	Factor of Safety
1	10.0	IPET	Yes	1.04
2	10.5	IPET	Yes	1.03
3	10.5	IPET	No	1.22
4	11.2	IPET	Yes	1.00
5	12.5	IPET	Yes	0.96
5a	12.5	IPET	No	1.13
6	10.0	Marsh 1 + 25%	Yes	1.12
7	10.0	Marsh 1 – 25%	Yes	0.96
8	10.0	Marsh 2 + 25%	Yes	1.12
9	10.0	Marsh 2 – 25%	Yes	0.95
10	10.0	Interdistributary + 25%	Yes	1.12
11	10.0	Interdistributary – 25%	Yes	0.94
12	12.5	Marsh 1 + 25%	Yes	1.04
13	12.5	Marsh 1 – 25%	Yes	0.88
14	12.5	Marsh 2 + 25%	Yes	1.05
15	12.5	Marsh 2 – 25%	Yes	0.88
16	12.5	Interdistributary + 25%	Yes	1.03
17	12.5	Interdistributary – 25%	Yes	0.88

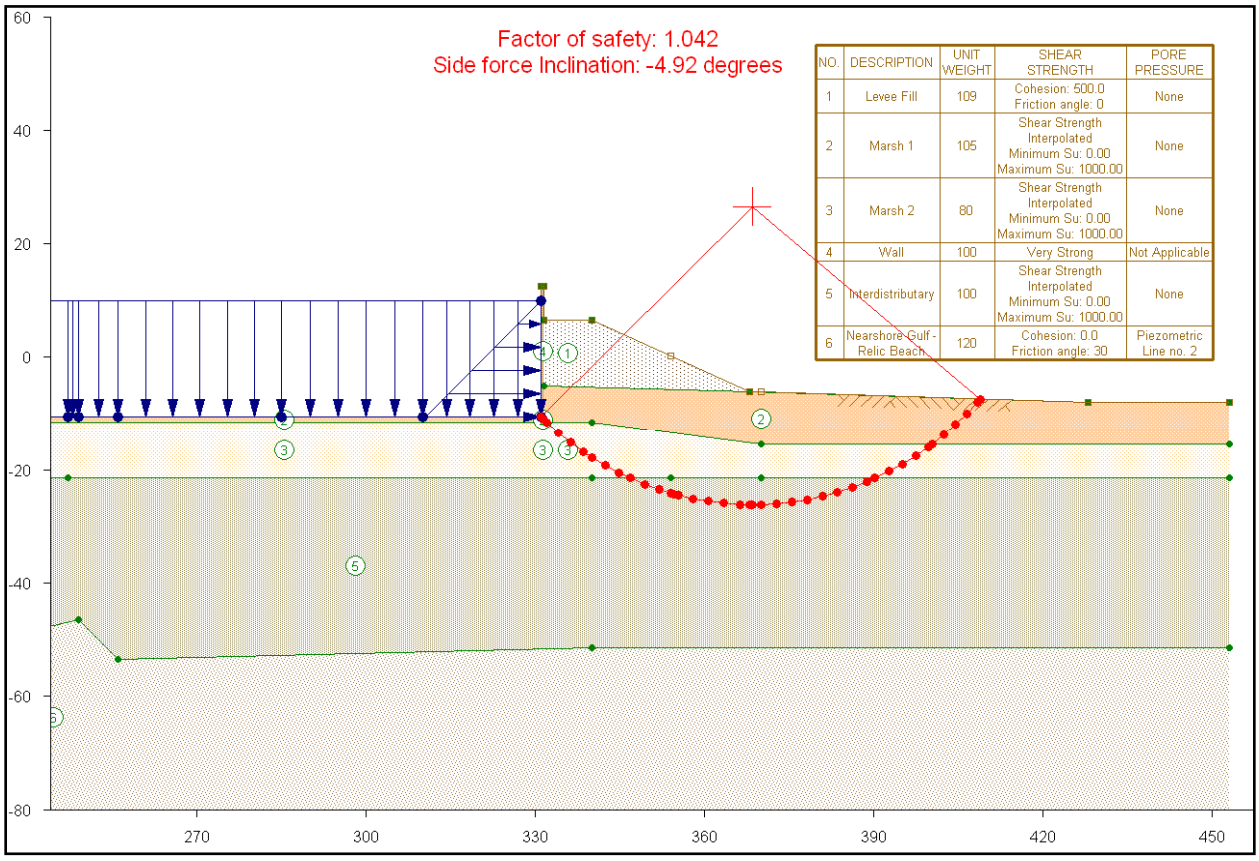
[7] Spencer, E. (1967) "A Method of Analysis of the Stability of Embankments Assuming Parallel Inter-Slice Forces," *Geotechnique*, Institution of Civil Engineers, Great Britain, Vol. 17, No. 1, March, pp. 11-26.
[8] Duncan, J. M., and Wright, S. G. (2005), *Soil Strength and Slope Stability*, John Wiley and Sons, New York, 293 pp.

Table 8
Results of Slope Stability Analyses for IHNC East Bank, South Breach. Note all Analyses Use Spencer's Method and Circular Slip Surfaces

Case	Water Elev. ft NAVD88	Strength Model	Crack (Yes or No)	Factor of Safety
1	10.0	IPET	Yes	1.20
2	10.5	IPET	Yes	1.18
3	10.5	IPET	No	1.34
4	12.5	IPET	Yes	1.10
5	12.5	IPET	No	1.25
6	10.5	Marsh 1 + 25%	Yes	1.29
7	10.5	Marsh 1 – 25%	Yes	1.07
8	10.5	Marsh 2 + 25%	Yes	1.27
9	10.5	Marsh 2 – 25%	Yes	1.09
10	10.5	Interdistributary + 25%	Yes	1.27
11	10.5	Interdistributary – 25%	Yes	1.07
12	12.5	Marsh 1 + 25%	Yes	1.21
13	12.5	Marsh 1 – 25%	Yes	1.00
14	12.5	Marsh 2 + 25%	Yes	1.18
15	12.5	Marsh 2 – 25%	Yes	1.02
16	12.5	Interdistributary + 25%	Yes	1.18
17	12.5	Interdistributary – 25%	Yes	1.01

Formation of a crack on the canal side of the wall, allowing hydrostatic water pressure acting through the full depth of the crack, causes a very significant reduction in the value of the calculated factor of safety. Evidence that a crack did form behind the wall near the breaches can be seen in Figures 6 and 7.

For the north breach (Station 55+00), with the canal water level at elevation 12.5 ft (top of the wall), the calculated factor of safety for the cracked condition is 0.96, as compared to 1.13 for the uncracked condition (Cases 5 and 5a). A canal water elevation of 11.2 ft produces a factor of safety of unity for the cracked condition (Case 4). Figures 71 through 76 show the critical circles from UTEXAS4 analyses for the north breach for Cases 1 through 5 and Case 5a.



NO.	DESCRIPTION	UNIT WEIGHT	SHEAR STRENGTH	PORE PRESSURE
1	Levee Fill	109	Cohesion: 500.0 Friction angle: 0	None
2	Marsh 1	105	Shear Strength Interpolated Minimum Su: 0.00 Maximum Su: 1000.00	None
3	Marsh 2	80	Shear Strength Interpolated Minimum Su: 0.00 Maximum Su: 1000.00	None
4	Wall	100	Very Strong	Not Applicable
5	Interdistributary	100	Shear Strength Interpolated Minimum Su: 0.00 Maximum Su: 1000.00	None
6	Nearshore Gulf - Relic Beach	120	Cohesion: 0.0 Friction angle: 30	Piezometric Line no. 2

Figure 71. IHNC – East Bank (North Breach), Case 1, Canal Water Level = 10.0 ft (NAVD 88), with Crack

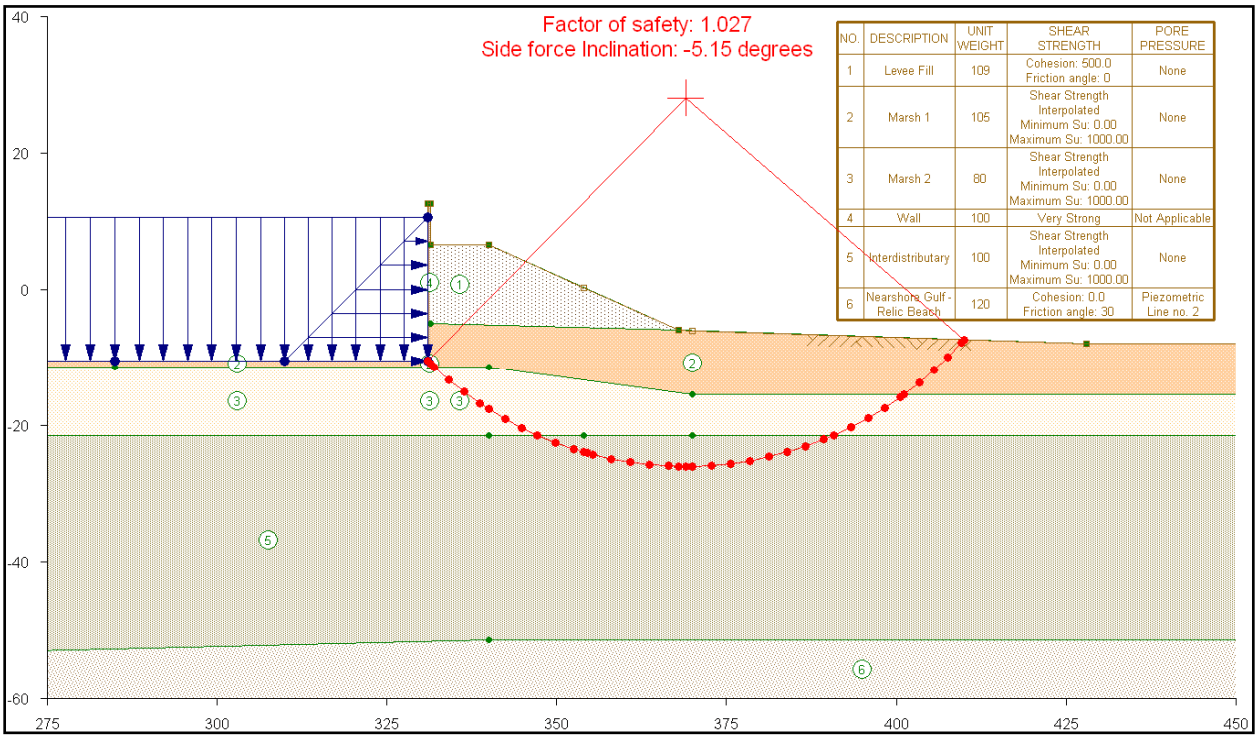


Figure 72. IHNC – East Bank (North Breach), Case 2, Design Canal Water Level = 10.5 ft (NAVD 88), with Crack

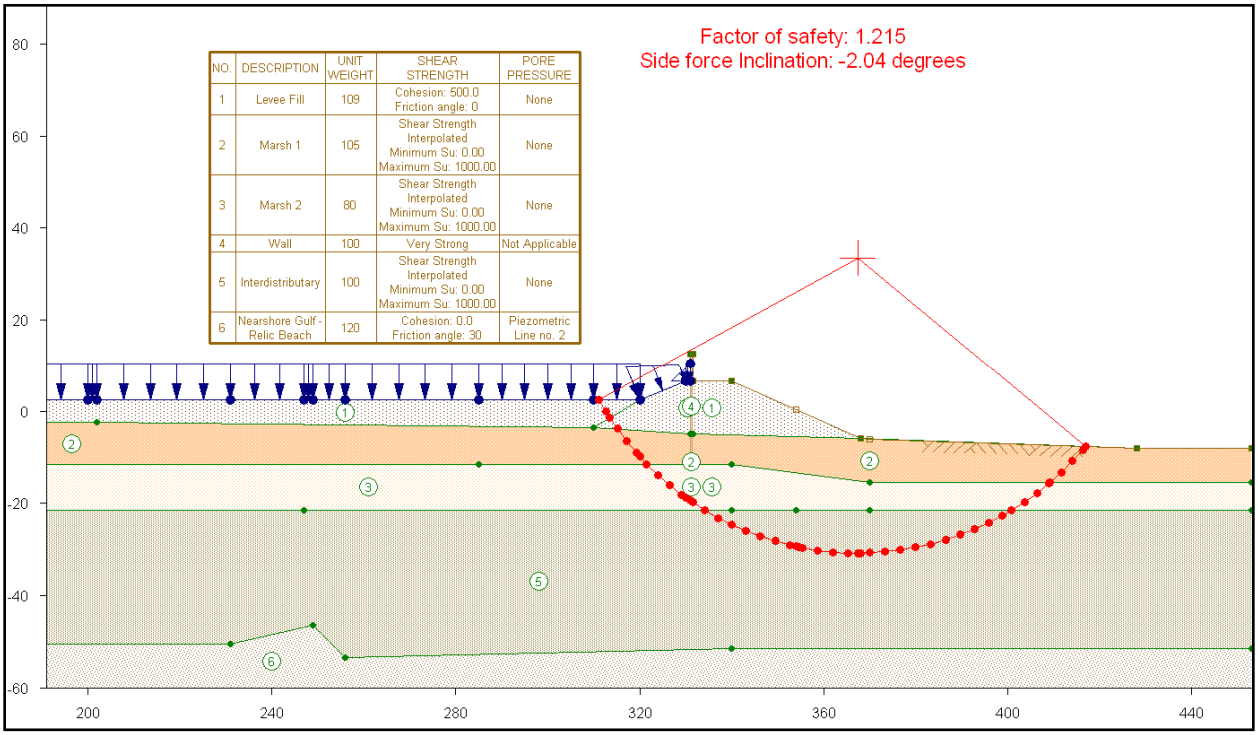


Figure 73. IHNC – East Bank (North Breach), Case 3, Design Canal Water Level = 10.5 ft (NAVD 88), without Crack

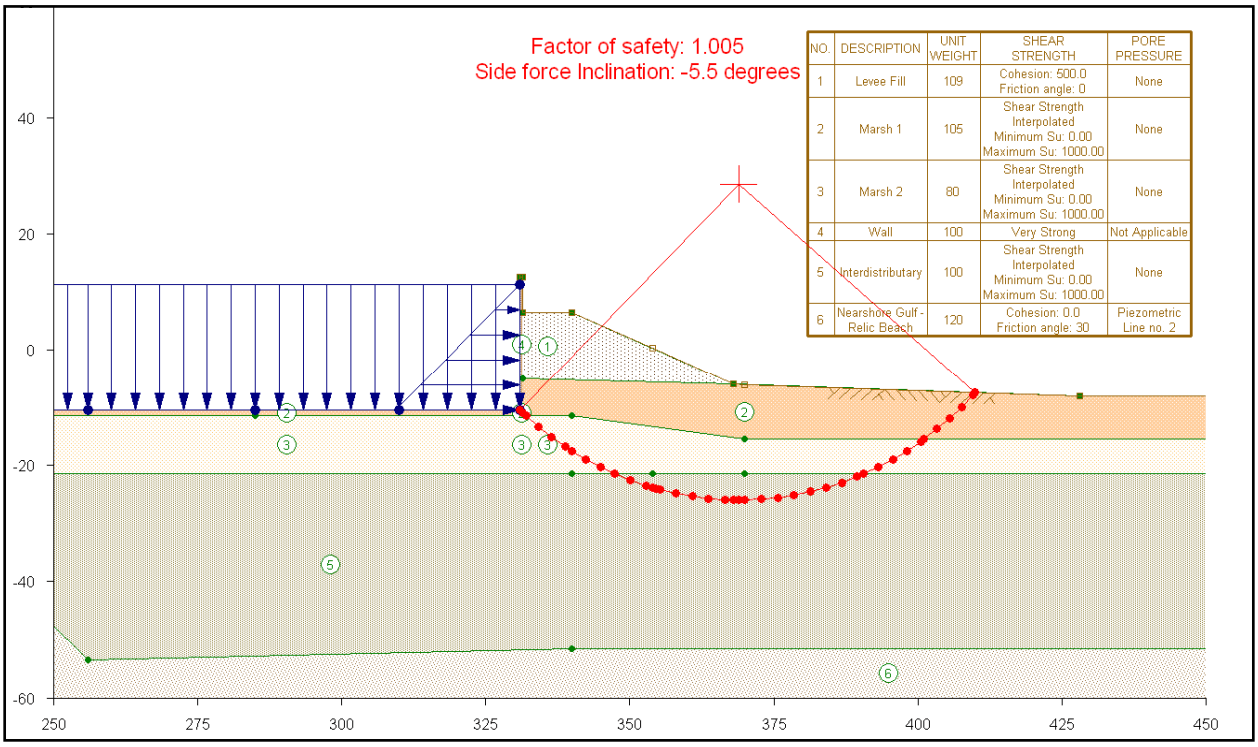


Figure 74. IHNC – East Bank (North Breach), Case 4, Canal Water Level = 11.2 ft (NAVD 88), with Crack

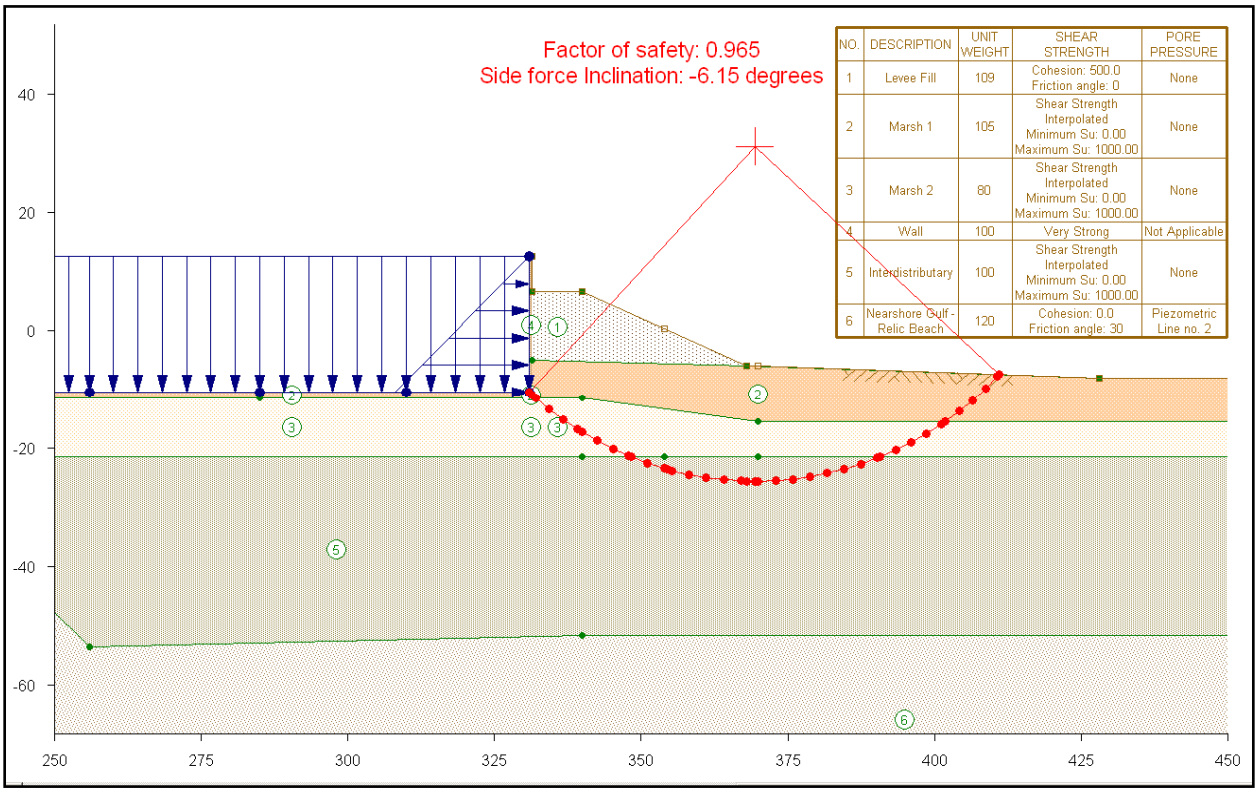
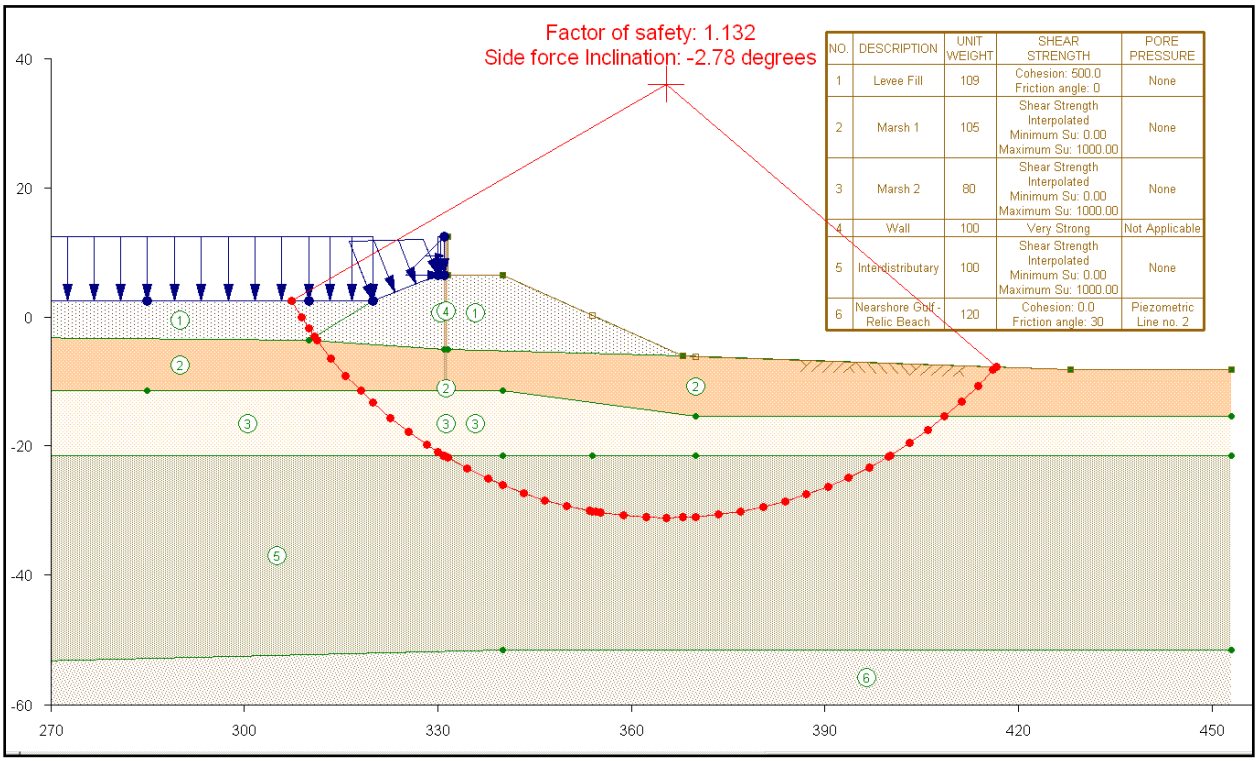


Figure 75. IHNC – East Bank (North Breach), Case 5, Canal Water Level = Top of Wall = 12.5 ft (NAVD 88), with Crack



NO.	DESCRIPTION	UNIT WEIGHT	SHEAR STRENGTH	PORE PRESSURE
1	Levee Fill	109	Cohesion: 500.0 Friction angle: 0	None
2	Marsh 1	105	Shear Strength Interpolated Minimum Su: 0.00 Maximum Su: 1000.00	None
3	Marsh 2	80	Shear Strength Interpolated Minimum Su: 0.00 Maximum Su: 1000.00	None
4	Wall	100	Very Strong	Not Applicable
5	Interdistributary	100	Shear Strength Interpolated Minimum Su: 0.00 Maximum Su: 1000.00	None
6	Nearshore Gulf - Relic Beach	120	Cohesion: 0.0 Friction angle: 30	Piezometric Line no. 2

Figure 76. IHNC – East Bank (North Breach), Case 5a, Canal Water Level = Top of Wall = 12.5 ft (NAVD 88), without Crack

For the south breach (Station 26+00), the factor of safety was greater than unity for all canal water elevations analyzed using the IPET strength model. For the most extreme case of the canal water level at elevation 12.5 ft (top of the wall), the calculated factor of safety for the cracked condition is 1.10. The critical circles for the stability analyses performed on the south breach for Cases 1 through 5 are shown in Figures 77 through 81.

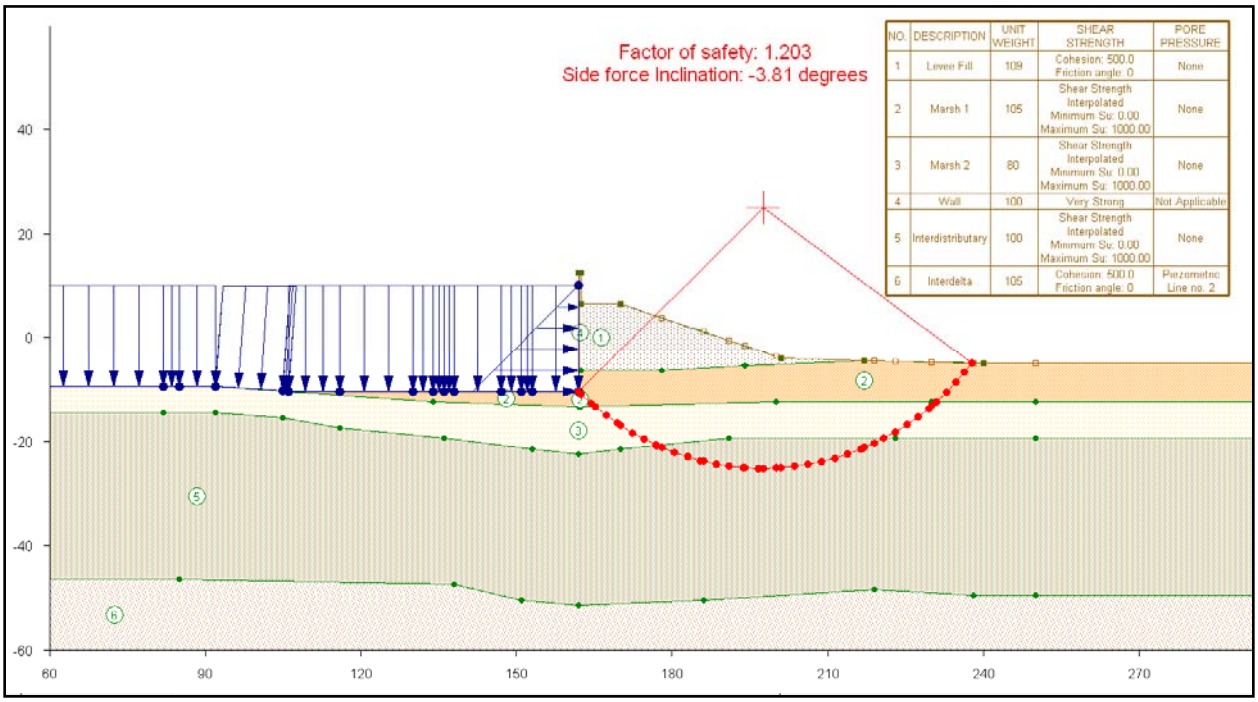


Figure 77. IHNC – East Bank (South Breach), Case 1, Canal Water Level = 10.0 ft (NAVD 88), with Crack

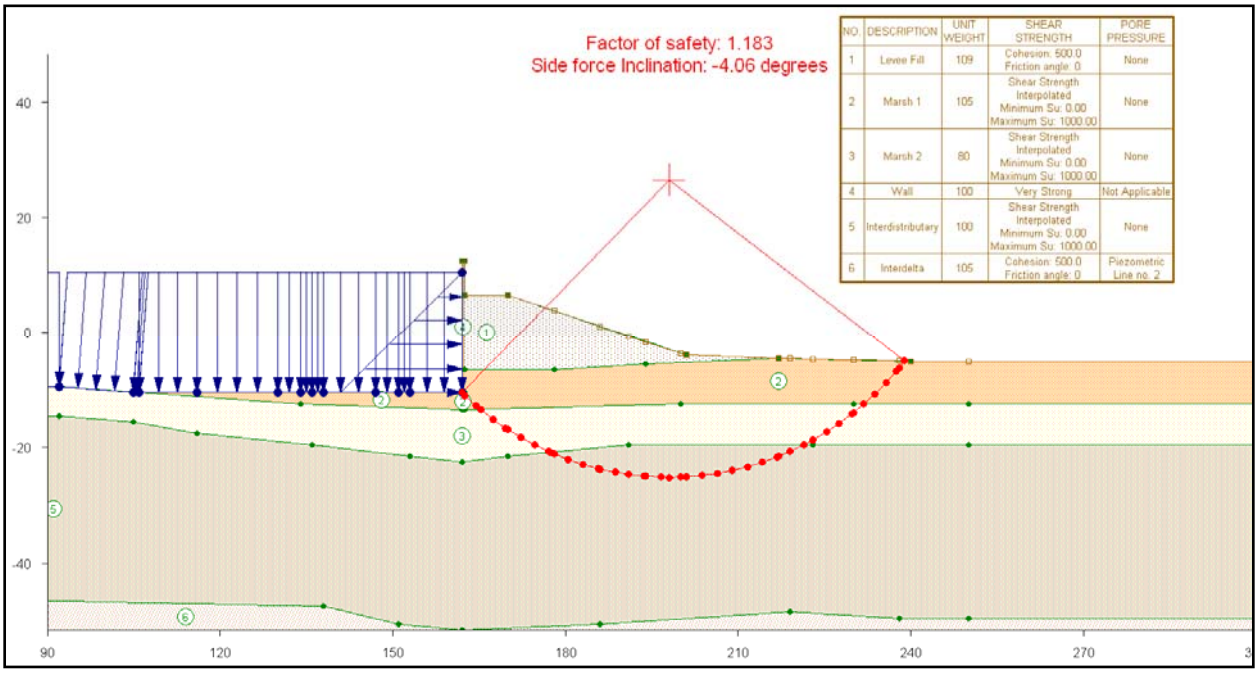


Figure 78. IHNC – East Bank (South Breach), Case 2, Design Canal Water Level = 10.5 ft (NAVD 88), with Crack

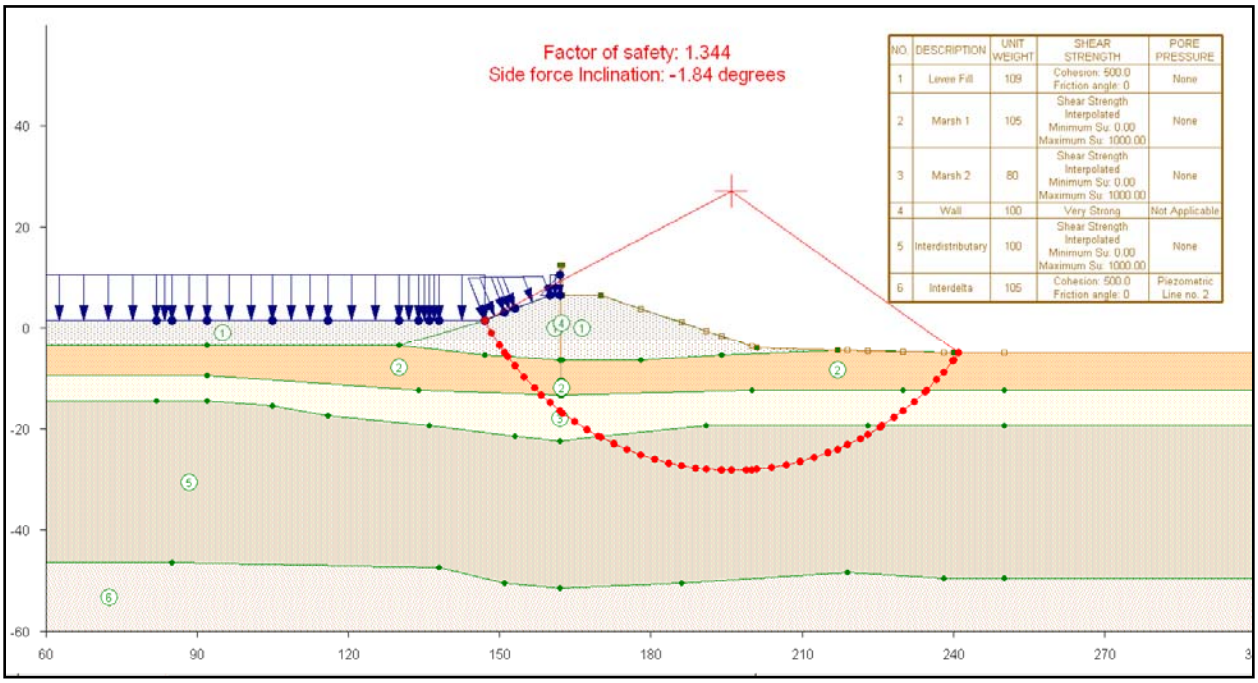


Figure 79. IHNC – East Bank (South Breach), Case 3, Design Canal Water Level = 10.5 ft (NAVD 88), without Crack

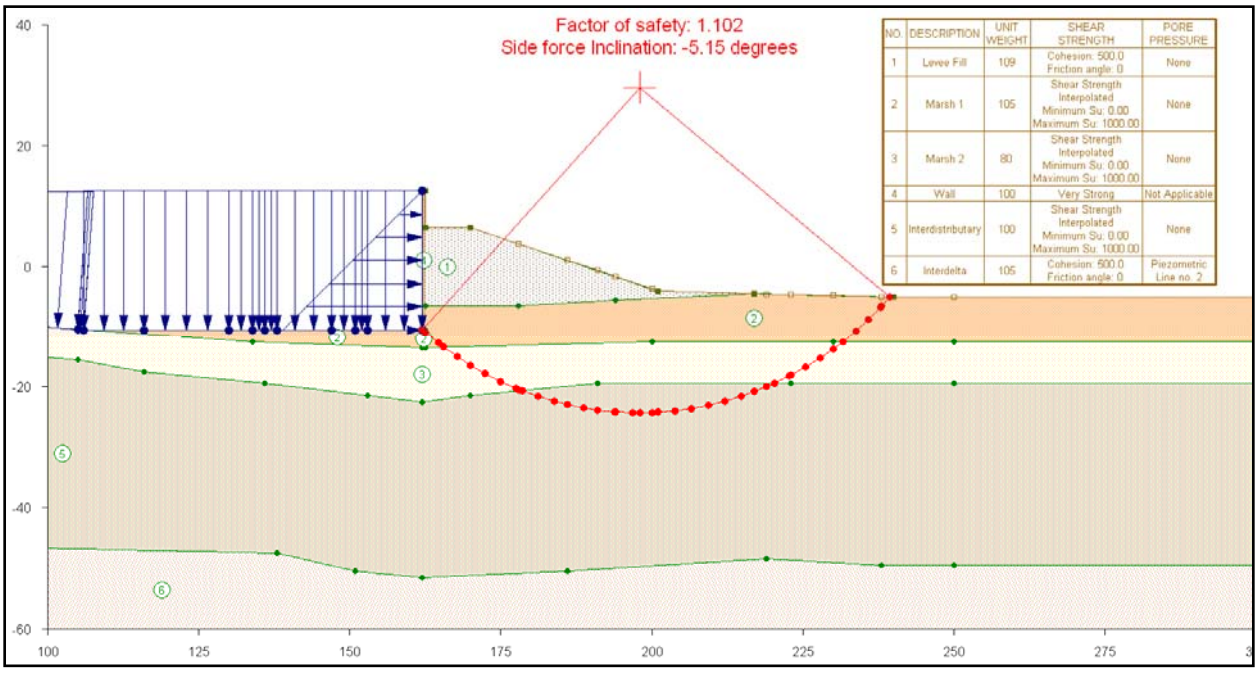


Figure 80. IHNC – East Bank (South Breach), Case 4, Canal Water Level = Top of Wall - 12.5 ft (NAVD 88), with Crack

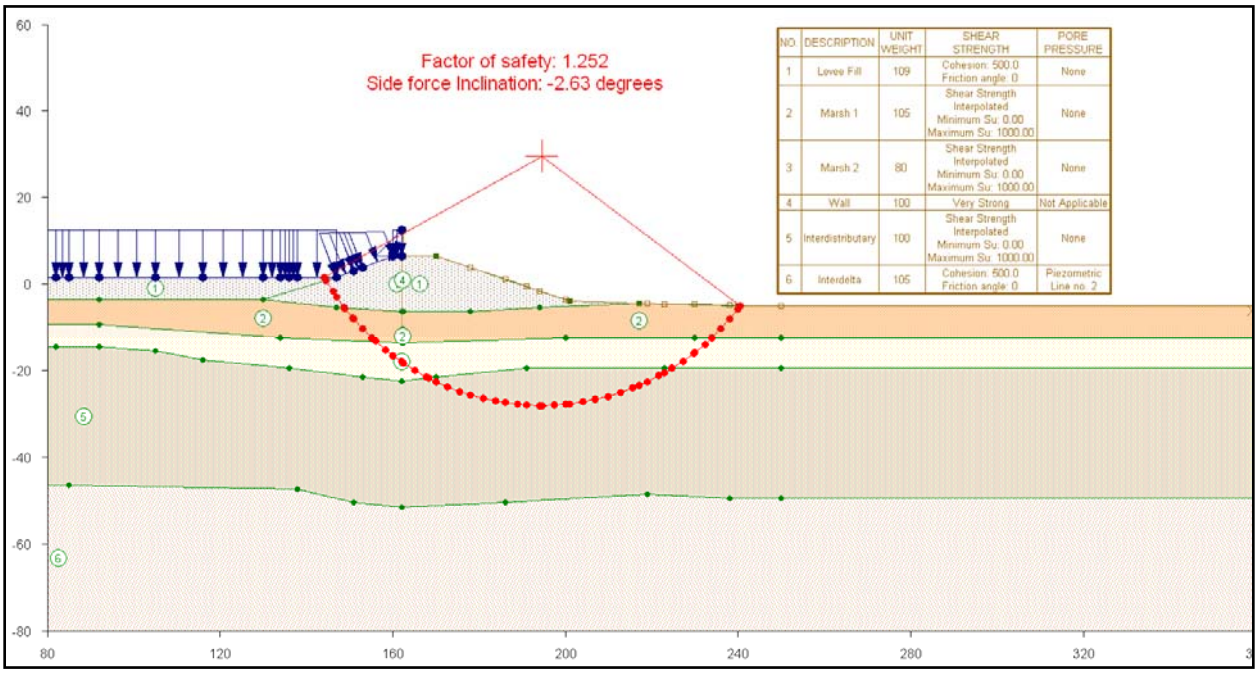


Figure 81. IHNC – East Bank (South Breach), Case 5, Canal Water Level = Top of Wall - 12.5 ft (NAVD 88), without Crack

3. Analysis of GDM Cross section

An analysis of the design cross section was performed using the GDM strength model discussed earlier. This analysis allows a comparison of the Method of Planes, used in the original design, with Spencer's method using circular failure surfaces.

In the original design, a canal water level of 10.5 ft NAVD88 (13.0 ft NGVD29) was used as the design water level load condition. The Method of Planes resulted in a minimum factor of safety of 1.25 for a horizontal failure plane located in the Marsh 2 layer. Using Spencer's method with the GDM strength model, a factor of safety of 1.45 was calculated for the same canal water level. Thus, the Method of Planes is conservative by about 14% in this case.

Three other variations of the design cross section were analyzed. Introducing a crack behind the wall for the design water level decreases the factor of safety to 1.19. For a canal water elevation at the top of the wall (12.5 ft NAVD88), the factor of safety is 1.35 for the uncracked condition and 1.05 for the cracked condition. The results of all analyses performed on the GDM cross section are presented in Table 9. Figures 82 through 85 show the critical circles for the UTEXAS4 analysis.

Table 9
Results of Slope Stability Analyses for IHNC East Bank, Using GDM No. 3, Plate 38. Note All Analyses Use Spencer's Method with Critical Circles

Case	Water Elev. ft. NAVD88	Strength Model	Crack (Yes or No)	Factor of Safety
1	10.5**	GDM	No	1.45
2	10.5**	GDM	Yes	1.19
3	12.5 – Top of Wall	GDM	No	1.35
4	12.5 – Top of Wall	GDM	Yes	1.05
Note: Design WL is 2.0 ft below top of wall				

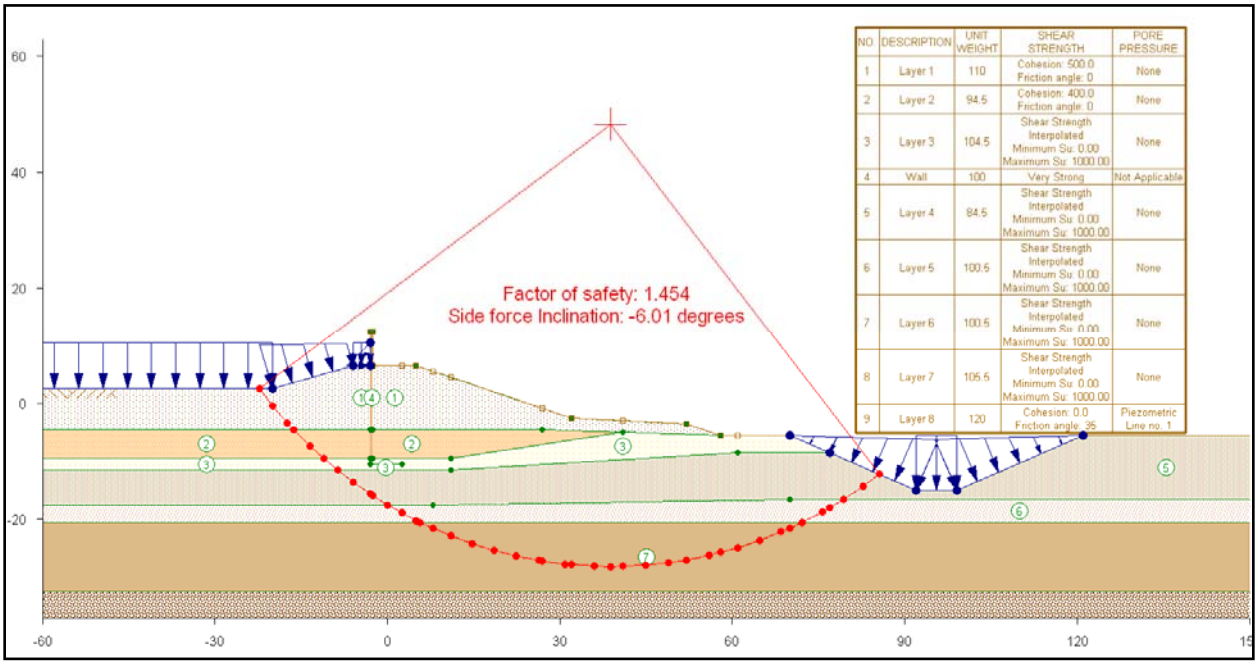
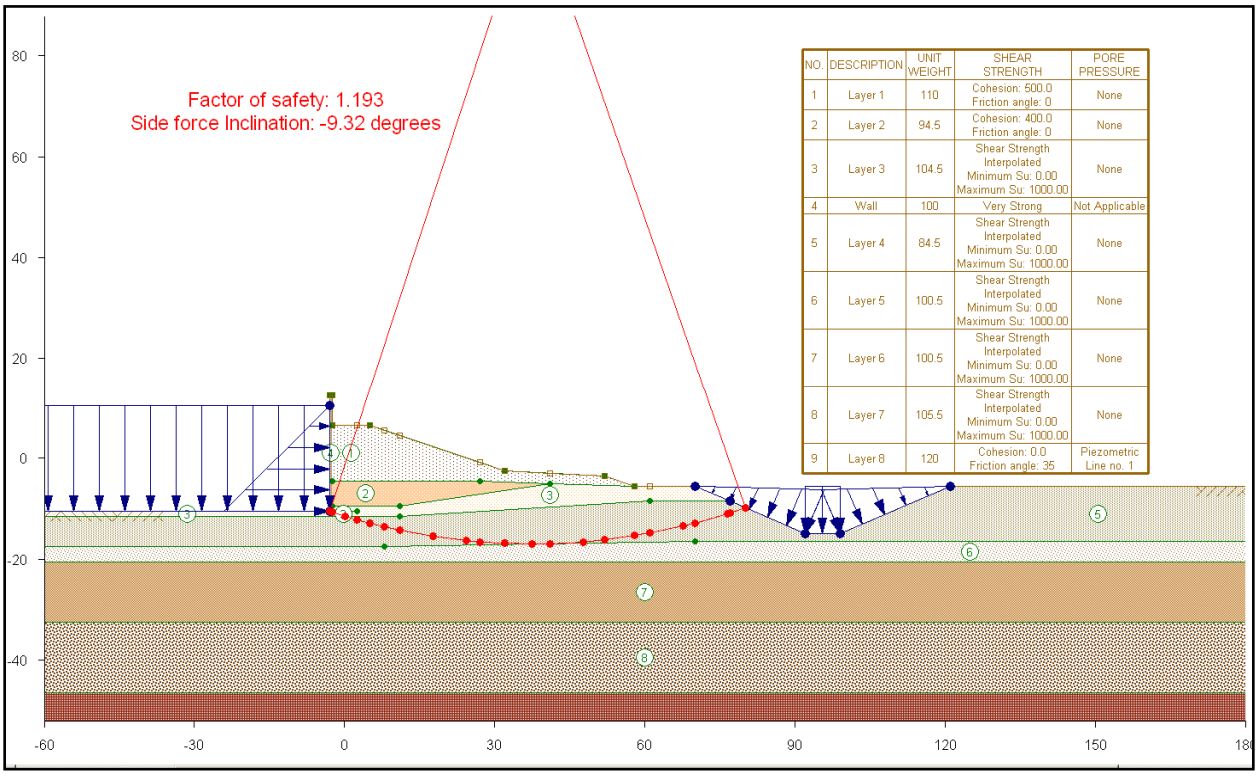
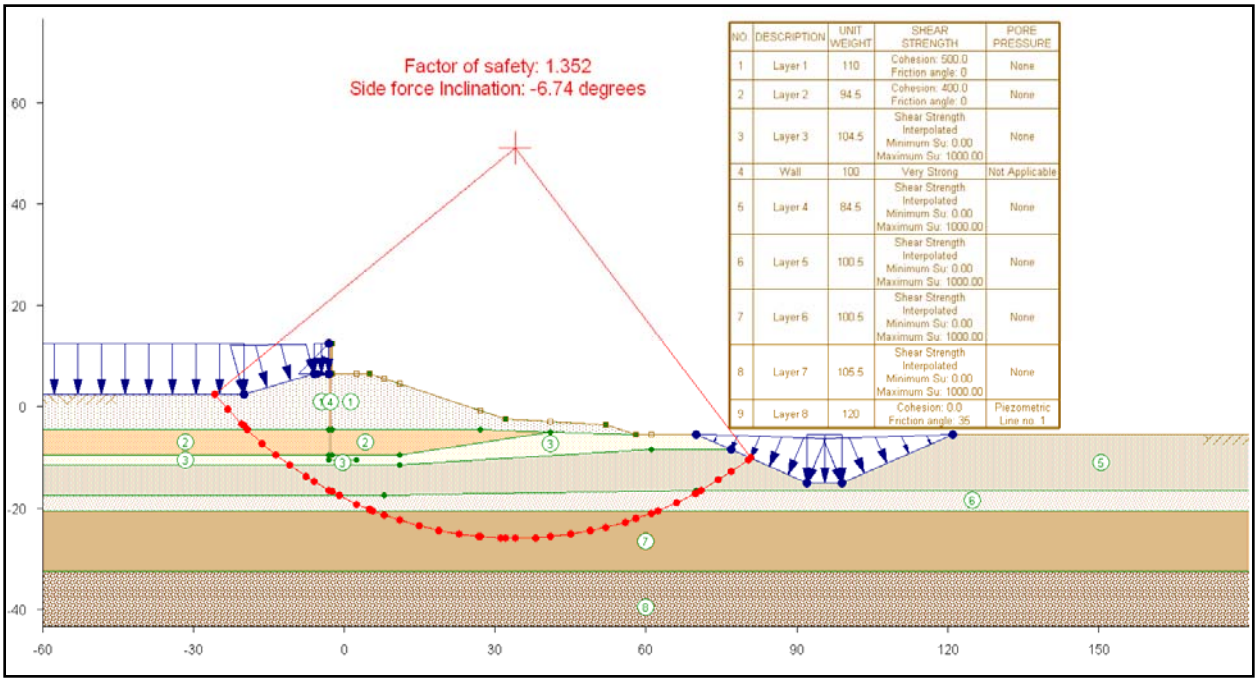


Figure 82. IHNC – East Bank (GDM Stability Plate), Case 1, Canal Water Level = Design - 10.5 ft (NAVD 88), without Crack



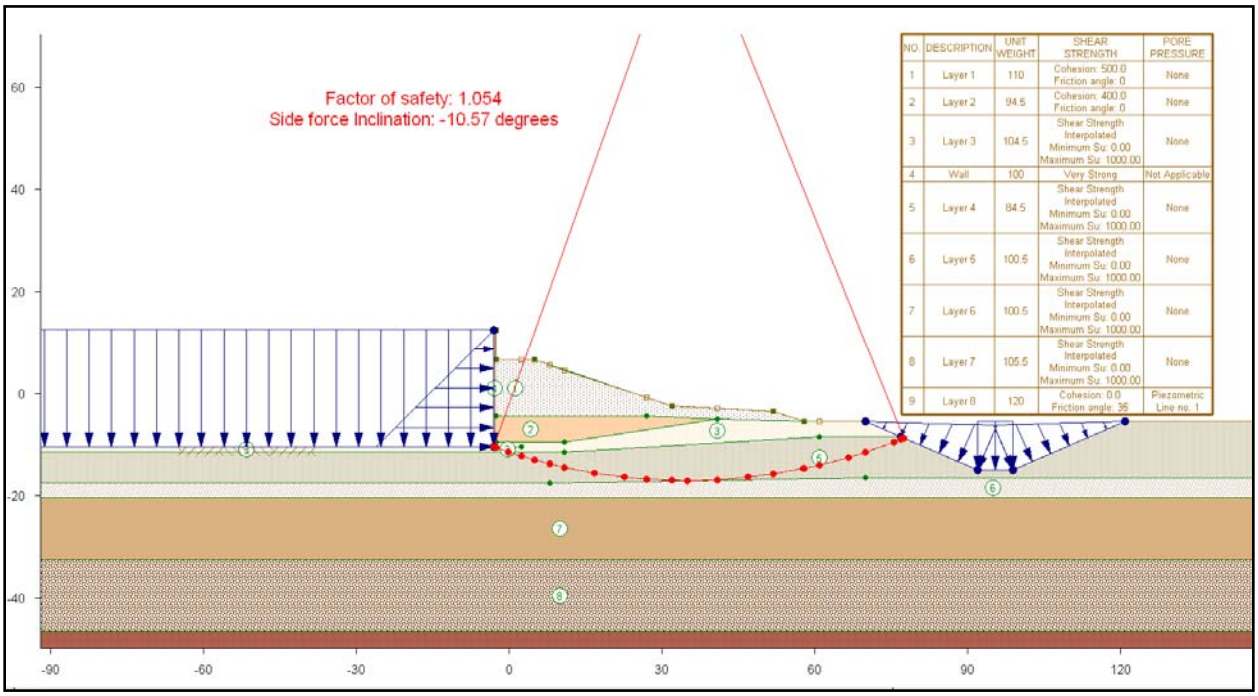
NO.	DESCRIPTION	UNIT WEIGHT	SHEAR STRENGTH	PORE PRESSURE
1	Layer 1	110	Cohesion: 500.0 Friction angle: 0	None
2	Layer 2	94.5	Cohesion: 400.0 Friction angle: 0	None
3	Layer 3	104.5	Shear Strength Interpolated Minimum Su: 0.00 Maximum Su: 1000.00	None
4	Wall	100	Very Strong	Not Applicable
5	Layer 4	84.5	Shear Strength Interpolated Minimum Su: 0.00 Maximum Su: 1000.00	None
6	Layer 5	100.5	Shear Strength Interpolated Minimum Su: 0.00 Maximum Su: 1000.00	None
7	Layer 6	100.5	Shear Strength Interpolated Minimum Su: 0.00 Maximum Su: 1000.00	None
8	Layer 7	105.5	Shear Strength Interpolated Minimum Su: 0.00 Maximum Su: 1000.00	None
9	Layer 8	120	Cohesion: 0.0 Friction angle: 35	Piezometric Line no. 1

Figure 83. IHNC – East Bank (GDM Stability Plate), Case 2, Canal Water Level = Design - 10.5 ft (NAVD 88), with Crack



NO.	DESCRIPTION	UNIT WEIGHT	SHEAR STRENGTH	PORE PRESSURE
1	Layer 1	110	Cohesion: 500.0 Friction angle: 0	None
2	Layer 2	94.5	Cohesion: 400.0 Friction angle: 0	None
3	Layer 3	104.5	Shear Strength Interpolated Minimum Su: 0.00 Maximum Su: 1000.00	None
4	Wall	100	Very Strong	Not Applicable
5	Layer 4	84.5	Shear Strength Interpolated Minimum Su: 0.00 Maximum Su: 1000.00	None
6	Layer 5	100.5	Shear Strength Interpolated Minimum Su: 0.00 Maximum Su: 1000.00	None
7	Layer 6	100.5	Shear Strength Interpolated Minimum Su: 0.00 Maximum Su: 1000.00	None
8	Layer 7	105.5	Shear Strength Interpolated Minimum Su: 0.00 Maximum Su: 1000.00	None
9	Layer 8	120	Cohesion: 0.0 Friction angle: 35	Piezometric Line no. 1

Figure 84. IHNC – East Bank (GDM Stability Plate), Case 3, Canal Water Level = Top of Wall - 12.5 ft (NAVD 88), without Crack



NO.	DESCRIPTION	UNIT WEIGHT	SHEAR STRENGTH	PORE PRESSURE
1	Layer 1	110	Cohesion: 500.0 Friction angle: 0	None
2	Layer 2	94.5	Cohesion: 400.0 Friction angle: 0	None
3	Layer 3	104.5	Shear Strength Interpolated Minimum Su: 0.00 Maximum Su: 1000.00	None
4	Wall	100	Very Strong	Not Applicable
5	Layer 4	84.5	Shear Strength Interpolated Minimum Su: 0.00 Maximum Su: 1000.00	None
6	Layer 5	100.5	Shear Strength Interpolated Minimum Su: 0.00 Maximum Su: 1000.00	None
7	Layer 6	100.5	Shear Strength Interpolated Minimum Su: 0.00 Maximum Su: 1000.00	None
8	Layer 7	105.5	Shear Strength Interpolated Minimum Su: 0.00 Maximum Su: 1000.00	None
9	Layer 8	120	Cohesion: 0.0 Friction angle: 35	Piezometric Line no. 1

Figure 85. IHNC – East Bank (GDM Stability Plate), Case 4, Canal Water Level = Top of Wall - 12.5 ft (NAVD 88), with Crack.

Summary

The peak storm surge elevation in the IHNC was 14.2 ft at 9:00 AM on August 29, about 1.7 ft above the tops of the floodwalls and levees. Water flowing over the walls when they were overtopped eroded trenches on the protected side of the walls as it cascaded onto the levee fill, and soil that was providing support for the walls was removed by this erosion, making the walls less stable.

It is clear that one of the east side breaches occurred before the wall was overtopped, because eyewitness reports indicate that the water level in the Lower 9th Ward near Florida Avenue was rising when the water level in the IHNC was still below the top of the floodwall. Stability analyses indicate that foundation failure would occur before overtopping at the north breach on the east side of the IHNC. This breach location is thus the likely source of the early flooding in the Lower 9th Ward. Stability analyses indicate that the other three breach locations would not have failed before they were overtopped. The failure at the north breach on the east side of the IHNC resulted from two differences in the stability analyses that were used as the basis for design and those described in this report: (1) the ground surface beyond the toe of the levee at the north breach location was lower than the landside ground surface in the design cross section, and (2) the design analyses did not consider the possibility of a crack forming behind the wall, allowing water to run into the gap and increase the load on the wall.

References

Mayne, P. W. (2003). “Class ‘A’ Footing Response Prediction from Seismic Cone Tests,” Proceedings, Deformation Characteristics of Geomaterials, Vol. 1, Lyon, France

Spencer, E. (1967) "A Method of Analysis of the Stability of Embankments Assuming Parallel Inter-Slice Forces," *Geotechnique*, Institution of Civil Engineers, Great Britain, Vol. 17, No. 1, March, pp. 11-26.

Duncan, J. M., and Wright, S. G. (2005), *Soil Strength and Slope Stability*, John Wiley and Sons, New York, 293 pp.

III. Assessment of Erosion Potential for MRGO Hypothetical Alternative Conditions

The Plaintiffs have proposed a series of hypothetical alternative conditions for the MRGO to try to demonstrate effects of the construction and maintenance of the MRGO on the hydrodynamic loading conditions, water levels, wave conditions, velocities and overtopping rates, on the levees along Reach 2 of the MRGO and the eastern side IHNC floodwall adjacent to the Lower 9th Ward from Hurricane Katrina. The analysis was done using numerical storm surge and wave models, applied to various hypothetical conditions for alternatives for the MRGO, to make the assessment of changes to hydrodynamic loading conditions. The following base conditions and hypothetical alternative conditions were analyzed:

1) Case H1 (Base Case): occurrence of Katrina for the actual levee and MRGO channel and wetland conditions that existing at the time the hurricane struck on August 29, 2005.

2) Case H2: occurrence of Katrina for a hypothetical condition that assumes the MRGO navigation channel did not exist; wetlands are in their 2005 condition, with the LPV levees/walls at their pre-Katrina locations and actual elevations. This case designed to examine any direct effect of the MRGO channel itself.

3 Case H3: occurrence of Katrina for a hypothetical condition that assumes the MRGO navigation channel did not exist; wetlands are in their pre-MRGO condition (1958), with the LPV levees/walls at their pre-Katrina locations and actual elevations. This case is designed to examine both the direct effects of the MRGO channel and effects of changes to wetlands that have occurred since MRGO construction. It is left for others to debate and decide how much of the wetland change that has occurred since MRGO construction is due to the channel itself or to regional and local subsidence.

4) Case H5: occurrence of Katrina for a hypothetical condition that assumes the MRGO navigation channel is at its authorized dimensions (eliminating effects of side bank erosion and changes to cross-sectional area that have occurred), wetlands are in their 2005 condition, with the LPV levees/walls at their pre-Katrina locations and actual elevations. Purpose was to examine the effect of not maintaining the channel at its design cross-section.

5) Case H6: occurrence of Katrina for a hypothetical condition that assumes the MRGO navigation channel is at its authorized dimensions (eliminating effects of side bank erosion and changes to cross-sectional area that have occurred), wetlands are in their pre-MRGO condition (1958), with the LPV levees/walls at their pre-Katrina locations and actual elevations. Designed to be an ideal case in

which the MRGO was present at its design dimensions and there were no changes to the wetlands surrounding the channel since its construction.

The damage due to Hurricane Katrina to the levees along Reach 2 of the MRGO and to the floodwall along the eastern side of the IHNC adjacent to the Lower 9th Ward has been presented earlier in this report. Based on the available data, it has been shown to a reasonable degree of scientific certainty that the levee sections along Reach 2 of the MRGO were eroded and breached as a result of overtopping from the waves and surge generated by Hurricane Katrina. It has also been shown that the north breach of the floodwall along the eastern side of the IHNC adjacent to the Lower 9th Ward failed prior to the overtopping of the floodwall, and the south breach of the floodwall failed after only 30 minutes of overtopping.

The only way the hypothetical alternative conditions would result in differences in the damage that occurred during Hurricane Katrina, is if the hydrodynamic loading conditions, water levels, wave conditions, velocities and overtopping rates, were different that those that occurred during the actual event. Ebersole's analyses have shown that the most important hydrodynamic variables influencing backside levee erosion is overtopping/overflow as related to the duration of waves breaking over the crest and the maximum mean water level above the levee crest. While waves breaking over the levee crest will develop sufficient flow velocities down the backside of the levee to cause erosion, Ebersole has shown that once the mean water level rises above the crest, the backside of the levee is subjected to very damaging overflow conditions, irrespective of any wave effects. The presence of waves will just make the onset of breaching occur sooner. Figure 86 shows the variation in maximum water level along the levee, for the Base Case, H1, and the alternatives.

Figure 86 shows that complete removal of the MRGO channel (cases H2 and H3) had a negligble effect on peak water levels along the entire MRGO Reach 2 levee, and a negligible effect in the critical Bayou Bienvenue (location 3 in the Figure 86) to Bayou Dupre (location 11 in the Figure 86) reach, the reach that was most heavily damaged during Hurricane Katrina. The differences in maximum water level between the Base Case and cases H2 and H3 ranged from zero to 0.2 ft. In the vicinity of Bayou Dupre, differences were slightly larger, 0.3 to 0.5 ft. South of Bayou Dupre, differences were 0.3 to 0.4 ft. To put these small water level changes in perspective, differences of 0.3 ft are less than 4 inches of change to a maximum storm surge that reached 17.5 to 18.3 ft.

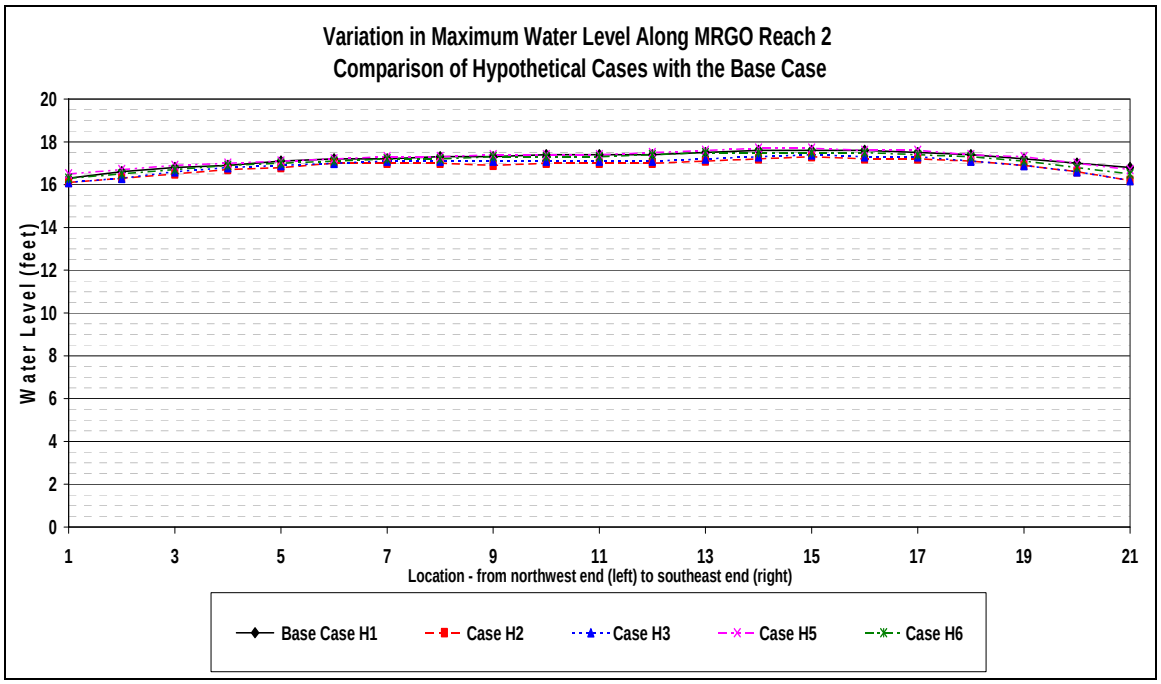


Figure 86. Along-levee variability in maximum water level for all cases

With little difference in the maximum water level between the actual conditions and hypothetical alternative conditions, the next characteristic of the hydrodynamic loading conditions is to compare the variation of water level with time, both the magnitude and duration of high water levels. These are important factors effecting the erosion and the subsequent degradation of the levees leading to breaching. Figures 87 (for Bayou Bienvenue), 88 (for Bayou Dupre) and 89 (for the southeastern end) show differences in hydrograph shape for points that span the MRGO Reach 2 levee. The figures show that there is little difference the magnitude and shape of the hydrographs of the hypothetical alternatives when compared the actual conditions.

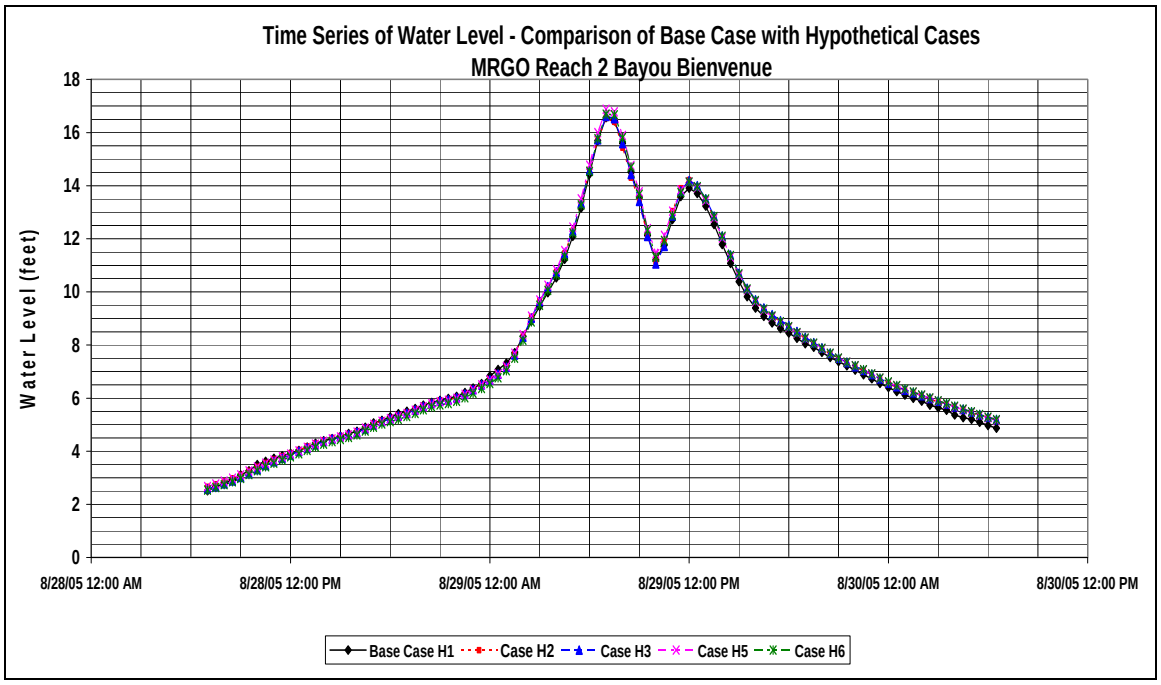


Figure 87. Comparison of temporal variation in water level for all cases, at Bayou Bienvenue

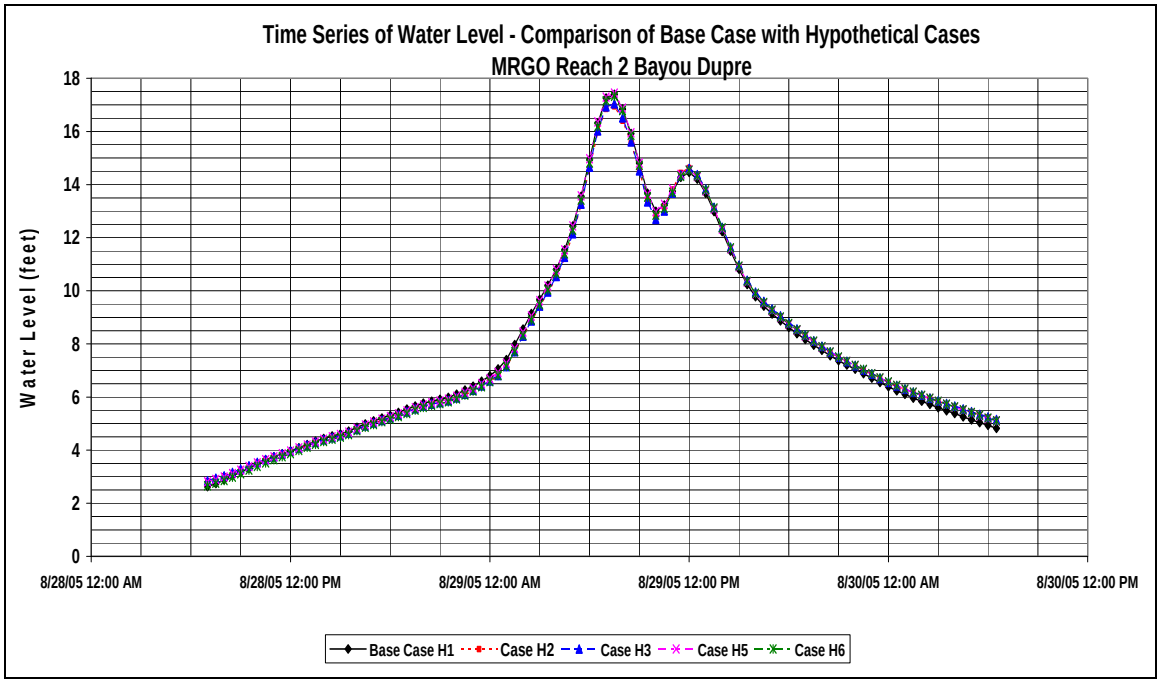


Figure 88. Comparison of temporal variation in water level for all cases, at Bayou Dupre

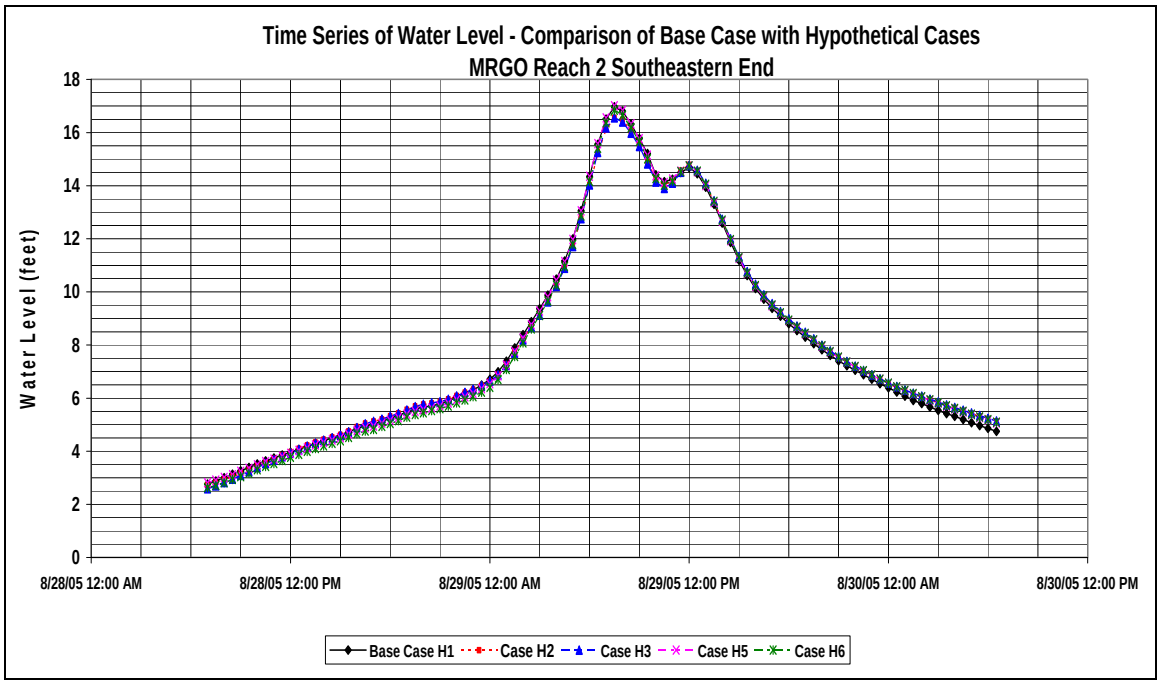


Figure 89. Comparison of temporal variation in water level for all cases, at southeastern end of the levee

Figure 90 shows the variation of maximum significant wave height along the MRGO Reach 2 levee for the actual conditions and hypothetical alternatives. Waves are generally higher between Bayou Bienvenue and Bayou Dupre for the actual conditions, while the variation along the levee is essentially the same for the actual conditions and all of hypothetical alternative conditions. These differences in maximum wave height would be expected to cause similar differences in the contribution of waves to overtopping. The peak waves arrive near the time of peak surge.

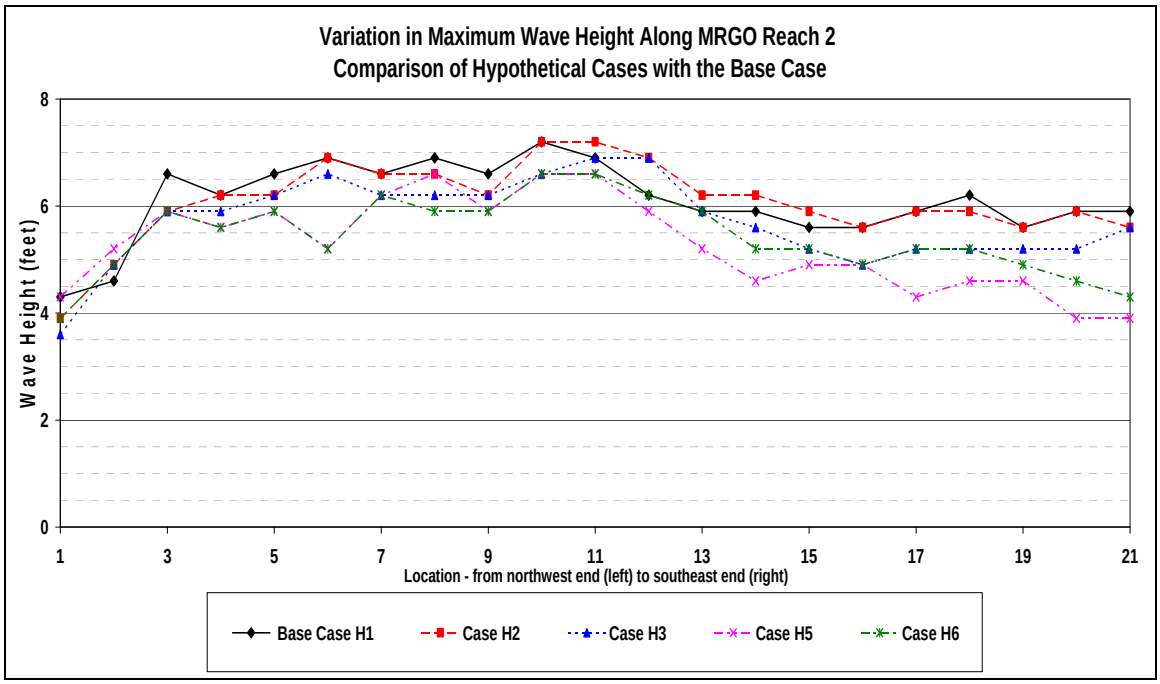


Figure 90. Comparison of along-levee variability in maximum significant wave height, for Base Case and all Cases

The most important factor influencing the erosion and breaching along the MRGO Reach 2 levee is overtopping and overflow conditions. Overtopping and overflow was the primary cause for levee erosion and degradation, and damage to floodwalls. Extreme water levels were the most important factor that influenced overtopping/overflow as relates to the height above the crest. Aside from any wave effects, water levels were high enough to induce overflow for a long period of time along significant lengths of this levee, especially between Bayou Bienvenue and Bayou Dupre, which would have destroyed the levee with or without the presence of waves. While the waves were not necessary to destroy the levees, the waves from either actual conditions or the hypothetical alternatives would have contributed to overtopping rates and levee erosion. They would have triggered the onset of overtopping and early damage for the more erodable sections of levee before the surge water level reached the crest.

Based on my review of the available data and analyses that have been performed, it is my opinion to a reasonable degree of scientific certainty, that the erosion and breaching which occurred along the levees adjacent to Reach 2 of the MRGO during Hurricane Katrina would also have occurred if the hypothetical alternative conditions had been in place during Hurricane Katrina. With breaching of the levees adjacent to Reach 2 of the MRGO being essentially the same for all of the hypothetical alternative conditions as the actual conditions, their contribution to flooding along Reach 2 would be the same as the actual event. Fitzgerald (2008) analysis of the volume of flooding from the breaching shows that 85 percent of the volume of flooding is due to breaches along Reach 2.

Therefore, even under hypothetical alternative conditions along Reach 2 alone, the flooding in St. Bernard Parish would have been severe.

The floodwall running along the eastern side of the IHNC adjacent to the Lower 9th Ward had two breaches, a north and south breach. It has been shown in this report that the north breach occurred before the surge waters from Hurricane Katrina reached the top of the floodwall, and the south breach occurred due to overtopping and the subsequent removal of the foundation supporting the wall by scour and erosion.

The elevations of the top of the floodwall along the eastern side of the IHNC adjacent to the Lower 9th Ward were between 12.0 and 12.5 ft. Ebersole's assessment of the maximum peak water level for the actual conditions and hypothetical alternative conditions show that the water levels would have been greater than the top of the floodwall. Even Kok et al (2008) and de Wit et al (2008) report that the water level at breach site was 4.4 m (14.4 ft) for their ideal scenario (Scenario 2C – similar to H3) which removes the MRGO completely. This water level would be approximately 2 ft above the top the floodwall. Ebersole's (2008) analysis of the stop clock data shows that it only took about 30 minutes for the south breach to form once it was overtopped. Results in de Wit et al (2008) suggest the water level would have stayed above the wall crest elevation for 1.5 to 2 hours, sufficent time to have form the breach.

Based on my review of the available data and analyses that have been performed, it is my opinion to a reasonable degree of scientific certainty, that breaching of floodwall running along the eastern side of the IHNC adjacent to the Lower 9th Ward which occurred during Hurricane Katrina would also have occurred if the hypothetical alternative conditions had been in place during Hurricane Katrina. The north breach occurred when the water level reached between 9.5 and 10.5 ft which are well below the maximum peak water level for the hypothetical alternative conditions. Plaintiff's experts, Kok et al (2008) and de Wit et al (2008), have shown that the hypothetical alternative conditions would yield sufficient overtopping of the floodwall to result in causing the south breach occur in a similar fashion as it occurred during Hurricane Katrina.

References

Bea, R., 2008. "Declaration No. 1 – Engineering Forensic Studies of Performance of the Man-Made Features Bordering the Reach 2 of the Mississippi River-Gulf Outlet (MR-GO) During Hurricane Katrina," July 11, 2008.

Bea, R. and Storesund, R., 2008. "Technical Report No. 1 – Analysis of Breaching of MR-GO Reach 2 EBSBs During Hurricane Katrina & The 'Neutral' MR-GO Hurricane Katrina Conditions," July 11, 2008.

CivilTech Engineering, 2008. "Expert Opinion Report – Analysis of Flooding of the Lower Ninth Ward and St. Bernard Parish Hurricane Katrina August 2005 New Orleans, Louisiana," June 27, 2008. Prepared for Ingram Barge PSLC.

Interagency Performance Evaluation Task Force, 2006. “Performance Evaluation of the New Orleans and Southeast Louisiana Hurricane Protection System, Volume IV, The Storm.” (https://ipet.wes.army.mil/)

Interagency Performance Evaluation Task Force, 2007. “Performance Evaluation of the New Orleans and Southeast Louisiana Hurricane Protection System, Volume V, The Performance – Levees and Floodwalls.” (https://ipet.wes.army.mil/)

Independent Levee Investigation Team, 2006, “New Orleans Systems, Hurricane Katrina, 2005, Chapter Nine: Erosion Tests on New Orleans Levee Samples.” May 26, 2006.

Kok M., Aalberts M., Maaskant B., and de Wit, L., “Polder Flood Simulations for Greater New Orleans: the neutral MRGO scenario,” July 9, 2008.

Seijffert, J.W., Verheij, H., Grass covers and reinforcement measures, Dike and revetments; design, maintenance and safety assessment. Edited by K.W. Pilarczyk, RWS-DWW, 1998.

de Wit, L., Maaskant B., Kok M., and Vrjiling, J.K., “Flow Modeling New Orleans – Mississippi River Gulf Outlet Hurricane Katrina August 2005: Final Report, Scenario 1, 2A, 2B, 2C, 2D, 3,” June 2008.

Appendix A: Oblique Photos - MRGO Reach 2 Levees and Floodwalls

This series of oblique aerial photos was taken of the MRGO Reach 2 Levee following Hurricane Katrina. Photos were taken during a north-to-south flight inspection along the levee, so the MRGO navigation channel is always on the left hand side of the photos. An interpretation of what is seen in each photo is provided.



Figure A1. Bayou Bienvenue Gate Structure. Breaching and flanking of flood wall at transition from concrete wall to steel sheet-pile wall. Sediment deposits evident on both sides of the breach, indicating flow both into and out of the polder. Scour trench on the protected (back) side caused by overtopping of the steel sheet-pile wall in the adjacent levee. Deposits of sediment washed out from the scour trench are evident on the back side. No indication of significant erosion on the front (exposed) side of the levee face.



Figure A2. Embedded steel sheet-pile wall in the levee. Wall misalinement is evident at a section in upper part of the photo. Wide scour trench caused by overtopping on the backside of the wall. Deposits of sediment washed out from the scour trench are evident on the back side. Some traces of surface erosion due to waves on exposed side along the wall are evident; isolated occurrence of more surface erosion near top of photos suggests more erodable sediments there. Much greater erosion signtaure and levee degradation on the back side due to overtopping compared to wave-induced erosion on the front side.



Figure A3. Embedded steel sheet-pile wall in the levee. Wall rotated and misalinement. Wide scour trench on the protected side caused by overtopping. Large deposits of sediment washed out from the scour trench reflect considerable scour. Some slight erosion evident higher up on the levee face in front of the wall, probably due to wave action. Much greater erosion and degradation on the back side due to overtopping compared to degree of wave-induced erosion on the front side. Wall appears to be breached at top of photo.



Figure A4. Severely degraded levee. Evidence of overtopping indicated by overwash sediment deposits on back side. Channel present just to south (top edge) of the barge. Backside elongated sediment deposit suggests high overflow. Traces of deposited sediment at front of the channel mouth also suggest outflowing water. Channel likley fomed on outflow. Lowest spots on the degraded levee likely served as outflow channels for water exiting the polder following storm's passage. Situation in lower half of photo is less clear. Overwashed sediment evident, erosion pattern at bottom could be due to entering or exiting flow. Predominance of sediment deposits on the back side in the upper part of the photo suggests degradation caused by overtopping/head-cutting.



Figure A5. Severely degraded levee; entire levee gone in foreground; crest gone in background. Evidence of overtopping indicated by numerous overwash sediment deposits on back side. In upper portion of photo, deradation seems dominated by headcutting with traces of surface erosion higher up on the levee front face. Lower half of photo is less clear. Significant sediment deposts on back side indicating overtopping. Erosion pattern on front side in foreground could be due to entering or exiting flow; cleanness of curved erosion line at southern edge of this breached area suggests a flow line marking edge of a channelized region of exiting water.



Figure A6. Rotational wall failure and breaching induced by overtopping and scour trench formation. Localized extremely wide scour trench probably induced by rotating wall sending overtopping jet further landward. Narrower scour trench evident along upright wall sections to either side. At top of photo, failure at transition from wall to levee is evident. Length of fan-shaped sediment deposits are evidence of strong flow through the breach. Surface erosion and loss of vegetation on front side evident higher up on the levee near base of the wall, due to breaking wave action. Erosion and degradation is dominated by overtopping processes.



Figure A7. Levee entirely eroded in many places. Evidence of overtopping and strong landward flows indicated by numerous elongated overwash sediment deposits on back side, some reaching considerable distances from the levee. Back-side head-cutting evident in center of the photo, as are several small wave-induced bench-cuts lower on the front face. Hour-glass shaped channel in the foreground and sediment fans on front side indicatechannelized exiting water; head-cut evident on back side of this channel likley due to flow exiting the basin. Evidence of channelized exiting flow (channel and/or sedimetn deposits on the front side) also seen at two other locations.



Figure A8. Levee cross section in foreground is intact; no loss of crest elevation. Some traces of surface erosion evident on the front face, including beginning stages of front side bench cutting probably due to wave action, but no significant erosion of bench cuts into or through the levee crest. Overwash sediment deposits on the backside are evident at the top of the photo; they extend for considerable distances behind the most advanced breaches indicating high flows through the breah. Head-cutting associated with overtopping appears to be the dominant erosion mode; several stages are evident in the center of the photo, including advanced states that have cut completely through the levee crest.



Figure A9. Intermittent areas of levee degradation and loss of the crest, separated by fully intact cross-sections. Head-cut has migrated completely through the crest and well into the front levee face in numerous places. Elongated sediment overwash deposits on the backside are pronounced and they reflect high flow through the breaches. It is impossible to determine if wave-induced bench-cut on front-side leading to overtopping occurred along this section. Immediately south of the first bench cut (bottom of the photo) is an area of more advanced head-cutting on the back side which appears to be unconnected to the presence of any possible wave-induced bench cut. Also, there is no evidence of significant wave-induced erosion anywhere else on the front face.



Figure A10. Most of the levee intact. Vegetation appears to be healthier and denser. Breach in center of the photo due to head-cutting; head cut has migrated completely through the crest and well into the front levee face. Overwashed sediment deposits on the backside are evident and they extend considerable distances. Head-cutting associated with overtopping appears to be the dominant erosion mode. Slight traces (an along-levee band) of wave-induced erosion higher up on the levee face seems are evident. No significant erosion due to waves on the front side in areas where head-cuts are not present.



Figure A11. Most of the levee crest degraded. Deep scour holes evident near the base of the levee on backside, probably due to high turbulence where flow regime changes from supercritical to subcritical. Traces of wave-induced erosion are evident on the levee front face, especially at top of the photo. Predominant erosion signature induced by back-side head-cutting. Head cuts have migrated completely through the crest and well into the front levee face. Overwash sediment deposits on the backside are evident and they extend considerable distances indicating very high water velocities due to overtopping on the backside.



Figure A12. Levee crest is degraded in places; intact along much of this reach. Scour holes evident near the base of the levee on backside. Predominant erosion signature induced by head-cutting on the back side. Several stages of head-cutting are evident; head cut has migrated completely through the crest and well into the front levee face in places. Overwash sediment deposits on the backside are evident. Only traces of wave-induced erosion evident on the levee front face at the intact sections at the center of the photos where there is extensive erosion on the back side. Erosion on back side at base of levee.

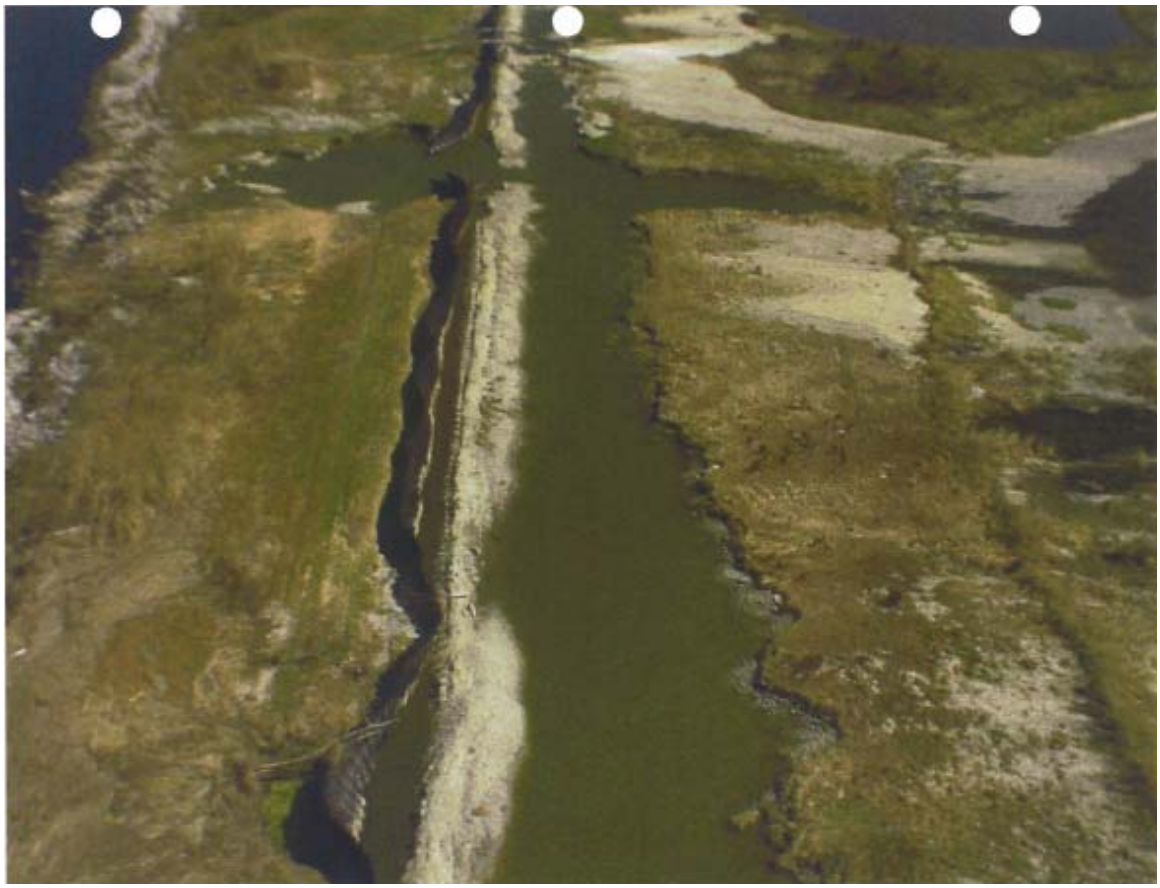


Figure A13. Severe rotational failure and misalinement of steel sheet pile wall embedded in the levee. Two scour trenches evident; a narrow straight trench close to the wall perhaps indicating early overflow with low wave action and much wider more irregular trench. Larger trench seems too wide for overtopping-induced scour; may be due to water flowing along the wall to exit the through breach after the storm. Breach through the wall is seen in the background. Wider trench on back side could have been formed initially due to wave overtopping and steady overflow and widened after wall rotated and failed, then widened later with exiting flow moving toward the breach. Evidence of flow in both directions through the breach (sediment deposits on both sides).



Figure A14. Levee crest degraded in a few places; intact elsewhere. Scour trench evident on backside of the floodwall in the background, with evidence of sediments carried away out of the trench and deposited further landward. Scour at transition from wall to levee. No significant erosion on the front side away from areas where head-cutting is evident. No along-levee band of wave-induced surface erosion is evident on the front face, only traces. Predominant erosion signature induced by head-cutting. Overwash sediment deposits on the backside are evident behind the levee and floodwall. Erosion at the levee base on the backside.



Figure A15. Sheet pile wall embedded in levee. Wide irregular scour trench due to overtopping evident on the backside along the entire length of wall, with evidence of considerable amount of sediment eroded and carried away out of the trench and deposited further landward. No erosion on the front side, except traces in the foreground. Predominant erosion signature induced by overtopping.



Figure A16. Most of the levee crest degraded. Deep scour holes evident in the degraded levee, probably due to high turbulence and high speed flows though the head-cuts and breaches. Traces of surface wave-induced erosion on the levee front face in the foreground, but not in the upper half of the photo. Predominant erosion signature induced by overtopping and head-cutting. Several stages of headcutting are evident; head cut has migrated completely through the crest and well into the front levee face along much of this levee reach. Overwash sediment deposits on the backside are evident. No evidence of sediment deposition on the front side.



Figure A17. Short sheet pile wall embedded in levee. Wide scour trench due to overtopping evident on the backside along the entire length of wall, with evidence of sediments carried away out of the trench and deposited further landward. Erosion due to flow concentration is evident at transitions from wall to levee at both ends of the wall. Traces of wave-induced erosion evident on the front side, as are a few small erosion benches in the foreground (they not extend to or through the levee crest). No along-levee band of wave-induced surface erosion is evident on the front face, only traces. Erosion caused by overtopping is predominant.



Figure A18. Levee crest in foreground is degraded; mostly intact elsewhere. Overwash sediment deposits on the backside are evident behind the levee. Predominant erosion signature induced by overtopping and backside head-cutting. Upper part of the photo shows two locations were front-side bench cutting occurred high on the levee face and lead to overtopping and overwash of sediment. In middle of the photo there is a backside head cut evident near the levee crest, in an early stage of formation, which could also lead to the type of cut seen at one of the other two locations. Minor front side erosion is seen at the toe of the front-side. No clear along-levee band of wave-induced surface erosion. Erosion at base of levee on backside.



Figure A19. Levee crest intact throughout this reach, except at one spot where back-side headcut is near levee center. Predominant erosion signature induced by backside head-cutting. Only early stages are evident. Overwash sediment deposit evident at the more advanced headcut. Traces of erosion on front and back sides near the base of the levee and on front face. No evidence of significant erosion on the front side, even in areas where back-side head-cuts are evident. Overtopping at this location appears to be less, or levees here are highly resistant to erosion.



Figure A20. Levee crest is intact throughout this reach.Traces of erosion on backside near the base of the levee. Evidence of minor wave-induced surface erosion band on the levee front face. Overtopping at this location appears to be minimal, or levees are highly resistant to erosion.



Figure A21. Levee crest mostly intact, except at a few locations. Severe levee degradation is evident in the background. Some traces of erosion on the backside near the base of the levee. Traces of wave-induced surface erosion are seen on front face. Erosion signature is dominated by bench-cutting (wave induced) higher up on the front levee face near the crest, without evidence of strong back-side head-cutting. Front side bench has progressed through the levee crest, and some sediment is deposited on the backside due to overtopping. Overtopping at this location appears to be minimal, or levees highly resistant to erosion.



Figure A22. Levee crest is completely degraded in center of the photo; intact to either side. Vegetation cover on the levee faces appears dense where the levee remains. Only a few traces of erosion on the front side anywhere else. Predominant erosion signature is head-cutting that has reached an advanced stage with a deep channel scoured through the levee. Overwash sediment deposits on the backside are evident behind the levee and breach channel. At the deep scour hole located on the levee front side, there is evidence of exiting water (fan-shaped deposit of sediment caused by water exiting from the polder).



Figure A23. Bayou Dupre Gate Structure. Section of the flood wall failed. Flanking and breaching of the flood wall at the transition from wall to levee. Deep scour hole formed on back side of the transition erosion Sediment fan evident at breach. Levee in foreground completely degraded. Surficial erosion on the levee front face is evident in the foreground, as is the vertical face of a head cut that has advanced completely though the levee crest to the surface wave erosion zone.



Figure A24. Bayou Dupre Gate Structure. Flanking and breaching of the flood wall at the transition from concrete wall to levee. Deep scour hole formed on back side of the transition erosion Sediment fan evident behind the breach. Levees in the background completely degraded. On front side, no evidence of wave-induced erosion seaward of the head-cuts or accumulation of sediment on the frotn side of the levee.



Figure A25. Predominant erosion signature is advanced stages of head-cutting on the backside due to overtopping and overwash of sediment. Where the levee is severely degraded, erosion pattern shows sharp nearly vertical leading edge of head-cuts which have advanced completely through the levee crest to and through the band of wave-induced surface erosion on the front side. The sharpness and prevalence of this leading edge does not suggest that this degree of degradation is initiated as wave-induced erosion that starts at the base of this surface erosion zone and works toward the crest. There is evidence of small front side erosion bench that has not cut through the crest; however, there is even more extensive backside erosion by head-cutting at this samelocation.



Figure A26. Levee crest intact except at one spot. Predominant erosion signature is backside head-cutting. Early stages that have not advanced back through the levee crest are evident, as is a more advanced cut which has. Overwash sediment deposits evident behind the larger head-cuts. Slight wave-induced erosion on the front face is evident, in a band along the levee. No significant evidence of front-side erosion in several areas where back-side head-cutting is evident. Slight erosion evident at the backside base of the levee. Overtopping at this location appears to be minimal, or levees highly resistant to erosion.



Figure A27. Levee crest intact, except at two locations. Predominant erosion signature is backside head-cutting induced by overtopping. Early stages of backside surface erosion and cuts that have not advanced back through the levee crest are evident. Advanced head-cuts are also seen. Overwash sediment deposits evident behind the larger head-cuts. Band of slight surface erosion on the front face. No evidence of bench cuts higher up on the front face in areas where early stages of backside head-cutting are evident, or anywhere else. Slight erosion is evident at the levee base on the backside.



Figure A28 Intact levee crest interrupted by severe levee degradation and breaching. Predominant erosion signature is head-cutting induced by overtopping. Sharp leading edge of head-cut has advanced completely through the levee crest to and through the front-side band of wave-induced surface erosion. Early stages of backside surface erosion and head-cutting are evident along much of the levee. Overwash sediment deposits evident behind advanced head-cuts. Possible evidence of a wave-induced bench cut higher up on the front side levee face(bottom of the breach) that lead to overtopping; if so overtopping became dominant erosion signature. No significant wave-induced erosion in areas where head-cutting is not evident. Slight erosion at the levee base on the backside.



Figure A29. Excellent example showing various stages of backside head-cut advance toward the levee crest, eventually cutting through the crest in the foreground and into the front-side zone of wave-induced surface erosion. Predominant erosion signature is head-cutting induced by overtopping and overwash sediment deposits on the backside. Overwash deposits evident behind the more advanced head-cuts; their inland extent, elongation and size correlate well with size of the head-cut. No front-side wave-induced erosion through the levee crest is evident in any area where the backside head-cut has not advanced through the crest. The entire area shows signs of erosion on the backside, and little erosion on the front side.



Figure A30. Levee crest degraded at many locations. Predominant erosion signature is head-cutting induced by overtopping. Overwash sediment deposits evident behind the more advanced headcuts. Continuous band of wave-induced surface erosion on the front face is evident. All major head-cuts have reached a similar state of advance through the levee crest and into the surface erosion band on the front side. Head-cuts in earlier stages of development are evident. No wave-induced erosion to or through the crest is evident in areas where head-cutting has not eroded the levee crest or in areas where the head-cutting is in an early stage of formation.



Figure A31. Levee crest intact, except in the background. Excellent example of early stages of backside surface erosion and head-cut formation caused by overtopping. Predominant erosion signature is backside erosion and head-cutting; also present is wave-induced surface erosion zone all along the levee front face. At one location in the foreground, a small bench formed higher on levee front face. Bu the levee crest is intact here. No significant wave-induced erosion into or through the levee crest from the front side is evident anywhere, particularly where erosion and overwash of sediment on the backside due to overtopping is evident.



Figure A32. Levee crest degraded at many locations in this reach. All major head-cuts have reached a similar state of advance through the levee crest; less advanced toward the top of the photo. Clear steeper leading edge along the head-cut is visible. Predominant erosion signature is head-cutting induced by overtopping. Large overwash sediment deposits evident behind the head-cuts. Surficial wave-induced erosion on the front face is evident all along the levee. No significant wave-induced erosion of the levee crest is evident in areas where head-cutting has not eroded to or through the levee crest or in areas where the head-cuts are forming on the backside.



Figure A33. Levee crest intact except at locations at top of the photo. Excellent example of early stages of backside surface erosion and head-cut development, and some later stages. Predominant erosion signature is minor surficial wave-induced erosion of the levee surface on the front side and more substantial head-cutting induced by overtopping on the backside. No significant wave-induced erosion of the levee crest is evident in areas where head-cutting has not eroded to the levee crest or in areas where the head-cutting is in an early stage of formation.



Figure A34. Levee crest is intact except at a few locations. Predominant erosion signature is head-cutting induced by overtopping; several stages are evident. Overwash sediment deposits evident behind the more advanced head-cuts. Band of surficial wave-induced erosion on the front face is evident all along the levee. No wave-induced erosion up to or through of the levee crest is evident in areas where head-cutting has not eroded the levee crest. Traces of erosion seen near toe of levee on both front and back sides



Figure A35 Predominant erosion signature is minor wave-induced erosion of the levee surface on the front side and more substantial head-cutting induced by overtopping on the backside. Example of early stages of backside erosion and head-cut development. More advanced cut completely through the levee crest and into the zone of wave-induced surface erosion on the front side is seen in foreground. The band of surficial erosion reaches a similar elevation and no higher toward the crest; this is seen in many other photos. No significant wave-induced erosion of the levee crest is evident in areas where headcutting has not advanced into the crest.



Figure A36 Example of early stages of backside head-cut development, and some later stages where cut is through the crest. Predominant erosion signature is minor wave-induced erosion of the levee surface on the front side and more substantial head-cutting induced by overtopping on the backside. No significant wave-induced erosion of the levee crest is evident in areas where head-cutting has not eroded to the levee crest or in areas where the head-cutting is in an early stage of formation. The band of surficial erosion reaches a similar elevation and no higher toward the crest, unlike headcuts on the back side which vary in distance from the crest.



Figure A37. Levee crest intact throughout this reach. Excellent example of early stages of head-cut development. Predominant erosion signature is minor surficial wave-induced erosion of the levee surface on the front side and more substantial head-cutting induced by overtopping on the backside. No significant wave-induced erosion of the levee crest is evident in areas where head-cutting has not eroded to the levee crest or in areas where the head-cutting is in an early stage of formation. The band of surficial erosion reaches a similar elevation and no higher toward the crest, unlike head-cuts on the back side which vary in distance from the crest.



Figure A38 Levee crest mostly intact, except at two locations. Example of early stage of head-cut development, and some later stages where cut is through the crest. Predominant erosion signature is minor surfical wave-induced erosion of the levee surface on the front side, only traces in places, and more substantial head-cutting induced by overtopping on the backside. Large overwash deposits on back side behind advanced head-cuts. No significant wave-induced erosion of the levee crest is evident in any areas where head-cutting has not eroded to the levee crest or in areas where the head-cutting is in an early stage of formation.



Figure A39 Levee crest intact throughout this reach, except in the foreground. Example of early stages of head-cut development, and a later stage (foreground) where cut is through the crest. Predominant erosion signature is minor wave-induced erosion of the levee surface on the front side and more substantial head-cutting induced by overtopping on the backside. Larger overwash sediment deposits evident behind the more advanced head-cuts. No significant wave-induced erosion of the levee crest is evident in areas where head-cutting has not eroded to the levee crest or in areas where the head-cutting is in an early stage of formation.



Figure A40. Prevalent pattern of surface erosion on the front side and bench-cutting due to wave action, without much evidence of overtopping. Two of the bench cuts extend just through the center of the crest. Crest elevations here were high, about 19 to 19.5 ft. Overtopping is minimized at this high crest elevation, so wave action is concentrated on the front face for the longest possible duration. Photo suggests how far wave-induced bench-cuts on the front side could develop in the absence of overtopping sufficient enough to cause head-cutting at this location. No severe front side levee degradation is evident.



Figure A41. Levee crest intact throughout this reach except at one location. Some localized surficial wave-induced erosion and bench cutting evident on front side. Bench-cutting high on the profile has completely cut through the levee crest at a high elevation to induce the overtopping which then lead to much more rapid erosion by head-cutting associated with overtopping. Sediment overwash deposit on backside due to overtopping. Overtopping and overflow appear to have been minimal along this reach, except at this one location. No severe front side levee degradation is evident outside the localized bench-cut.



Figure A42. Levee crest intact except at two locations. Traces of localized surficial wave-induced erosion evident on front side in places. Head-cutting formed by overtopping at two locations. Head-cutting has advanced just through the levee crest. At both locations bench-cutting due to breaking waves is not evident on the front side. Traces of erosion on the levee backside near the base. Overtopping and overflow appears to have been minimal along this reach.



Figure A43 Levee crest degraded at a number of locations. Different stages of head-cut advance toward the front side and through the levee crest are evident, some very advanced. Steep leading edge on head-cuts is pronounced. Predominant erosion signature is head-cutting induced by overtopping. Large overwash sediment deposits evident behind each of the head-cuts. Band of surficial breaking wave-induced erosion on the front face is evident, lower on the levee face. No wave-induced erosion of the levee crest is evident in areas where headcutting has not eroded through the levee crest. No evidence of sediment being deposited on front face.



Figure A44. Levee crest intact, except in background. Excellent example of early stages of head-cut development. Predominant erosion signature is minor surficial wave-induced erosion in a band along the levee surface on the front side and more substantial head-cutting induced by overtopping on the backside. No significant wave-induced erosion of the levee crest is evident in areas where head-cutting has not eroded to the levee crest or in areas where the head-cutting is in an early stage of formation. No severe erosion initiated from lower edge of surface erosion zone on the front face; no deposition of sediment on the levee front face.



Figure A45. Levee crest degraded along this reach. Different stages of head-cut advance toward the front side and through the levee crest are evident, many are very advanced. Steep leading edge along head-cut is evident. Predominant erosion signature is head-cutting induced by overtopping. Large overwash sediment deposits evident behind each of the head-cuts. No evidence of surface erosion on the front face or levee crest. Vegetation appears to be dense, apparently enough to resist wave-induced erosion on the front face but not enough to resist overtopping forces. Note the debris (water-borne) that appears to have been blown into the area.



Figure A46. Levee crest intact except for one location. Several small over-topping-induced head-cuts visible, including some very narrow ones. Traces of front-side local scour. No continuous band of wave-induced surface erosion. No significant wave-induced erosion of the levee crest is evident in areas where head-cutting has not eroded to the levee crest or in areas where the head-cutting is in an early stage of formation. Wide deep scour trench due to overtopping evident on the backside along the entire length of wall.



Figure A47. Rotational failure and misalinement of the sheet pile wall. Wide irregular scour trench due to overtopping evident on the backside along the entire length of wall, with evidence of sediments carried away out of the trench and deposited further landward. Some traces of surficial erosion induced by wave action on the front side. Predominant erosion signature induced by overtopping, not front side erosion due to waves.



Figure A48. Levee crest intact throughout this reach. Some localized wave-induced erosion evident at one isolated location. A few pockets of early stages of head-cut development evident on the bcakside. Predominant erosion signature is minor head-cutting induced by overtopping on the backside. Overwash sediment deposit evident behind the more advanced head-cut. Overtopping and overflow appears to have been minimal along this reach. No band of surficial wave-induced erosion along the front face.



Figure A49. Levee crest intact, except at one localized erosion area. Some traces of erosion caused by overtopping are evident on the back side. Traces of the band of surficial wave-induced erosion seen along the front face. Overtopping appears to have been minimal along this reach.



Figure A50. Southeastern end of the MRGO Reach 2 levee. Levee crest intact. Several small over-topping-induced head-cuts visible. Predominant erosion signature is traces of wave-induced erosion of the levee on the front side and localized head-cutting due to overtopping on the back side. Surface erosion evident at base of levee on the front side.

Appendix B: Inner Harbor Navigation Canal (IHNC) Seepage Analysis

In the IPET Final Draft Report (June 1, 2006), it noted that other possible modes of failure beside overtopping/erosion for the breaches of the IHNC I-wall along the Lower Ninth Ward included "sliding instability and piping and erosion from underseepage." The report goes on to say that "*Piping and erosion from underseepage is unlikely because the I-walls were founded in a clay levee fill, a marsh layer made up of organics, clay and silt, and a clay layer. Because of the thickness, the low permeabilities of these materials, and the relatively short duration of the storm, this failure mode was considered not likely and was eliminated as a possible mode of failure.*" In the NSF-Berkeley report (ILIT Final Report, July 31, 2006), they stated "*This greatly underestimates the permeability, and especially the laterally permeability of the marsh deposits. It also continues the very dangerous assumption that underseepage was not a serious problem for 'short duration' storm surge loading that plagued the original design of many sections of the New Orleans regional defense system, and led to use of sheetpile curtains that far too short to effectively (and safely) cut off underseepage flows.*" Plaintiffs' expert Dr. Robert Bea, a member of the ILIT team, adopts the findings and opinions of the ILIT report in his expert report dated July 11, 2008. For the following reasons, it is my opinion to a reasonable degree of scientific certainty that Dr. Bea and the ILIT team's analysis of seepage in the Lower Ninth Ward is the product of inaccurate data applied to a flawed and idiosyncratic methodology.

The value of coefficient of permeability assigned to the marsh layer in the NSF-Berkeley report and applied in Dr. Bea's report was 10^{-2} cm/sec. In Dr. Bea's expert witness report of July 2008, he states that a range of coefficient of permeabilities for the Marsh material in the cross-section of the levee founding the I-wall along the Lower Ninth Ward was used in the seepage analyses he performed, but he only uses the results for a coefficient of permeability of "10^{-3} cm/sec" when he discusses the effects of seepage that might lead to failures of the I-wall. Because the seepage is dominated by horizontal flow, the coefficient of permeability for the Marsh material of "10^{-3} cm/sec" used by Dr. Bea is really a coefficient of permeability for the Marsh material of 10^{-2} cm/sec because he used an anisotropic factor (ratio of vertical to horizontal) of) of 0.1. This is three orders of magnitude higher than the highest coefficient of permeability IPET determined from consolidation tests on undisturbed samples of the marsh layer, as shown in Figure B-1. Consolidation tests performed by IPET show that the coefficient of permeability of the marsh material decreases as consolidation pressure decreases, from a maximum of 10^{-5} cm/sec for low consolidation pressures, to values as low as 10^{-8} cm/sec for consolidation pressure equal to 4,000 psf.

Weber (1969) found a similar variation of permeability with effective overburden pressure using field permeability (piezometer) tests on peat in the California Delta, as shown in Figure B-1. Weber's peat coefficient of permeability values are roughly the same as the values determined from the IPET consolidation tests on marsh material from New Orleans, but the scatter of the values from consolidation tests is greater. The

difference may be due to the fact that the consolidation tests represent point values, whereas the field tests represent average values for a larger volume of soil. There may also be some inherent differences between the materials.

The permeability values for the marsh materials used by Dr. Bea in their seepage analyses were at least **1,000** times too high. These values are higher than the permeability values for the sand layer at the London Avenue Canal determined from field pump tests. The NSF-Berkeley report states, "*The values of lateral permeability used in these analyses were based on experience with similar geologic units from other regions, our own field observations, and the accumulated reports indicating high lateral permeability. A best-estimated coefficient of lateral permeability of* $k_h \sim 10^{-2}$ *cm/sec was modeled for the most open of the marsh sub-strata.*" Dr. Bea in his expert report selected permeability values from the literature for his analyses that did not have the same physical characteristics as the marsh soils at the IHNC. The extremely high permeability values he cites in his report are for fibrous marsh/peat soils. The fibrous content creates a more open structure which supports higher permeability than the marsh soils at the IHNC. These fibrous marsh/peat soils have very high void ratios and high water content. The water content values of these peats are 3 to 5 times the values found for the IHNC marsh soils. There is no possible or plausible explanation for Dr. Bea's choice of permeability values for the marsh material.

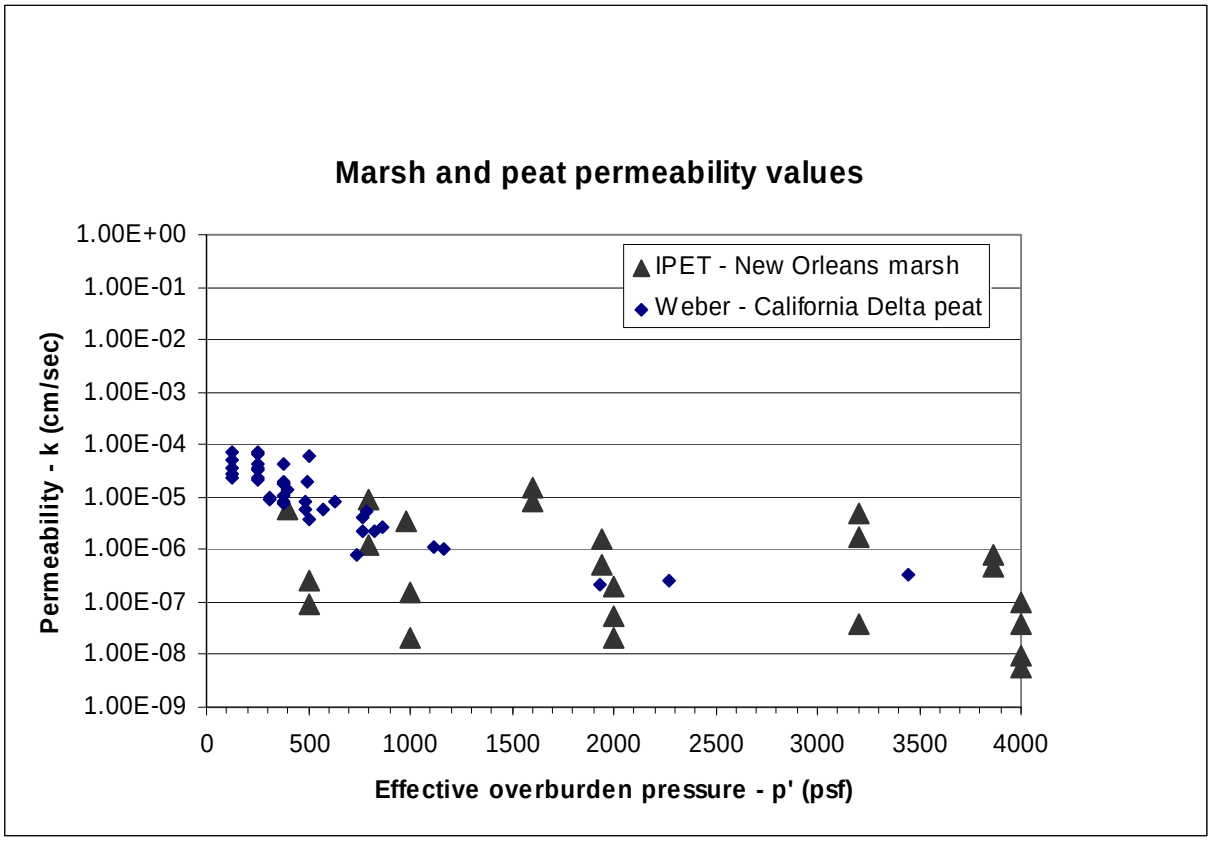


Figure B-1. Values of marsh permeability measured by IPET in consolidation tests on New Orleans marsh material, and by Weber (1969) in field piezometer tests on California Delta peat.

In order to demonstrate the effects of more realistic permeability values for the marsh material on the performance of the IHNC I-wall along the Lower Ninth Ward, the IPET team has conducted a series of transient finite element analyses.

The data available to assess the stratigraphy of the area includes borings from the General Design Memorandum (GDM), borings taken after the failure, and cone penetration tests taken after the failure. The locations of these borings and cone penetration tests are shown in Figure B-2. Note that all borings taken after the failure were at the levee toe. The GDM contains 10 borings on the levee centerline (2-U, 3, 4, 5, 6-U, and 7 in the vicinity of the breach), and four at the levee toe (2-UT, 3T, 4T, and 6UT). A centerline profile under the levee is represented in Figure B-3 and is based on both pre-Katrina and post-Katrina borings. This section shows 60 to 70 ft of predominantly fine-grained Holocene (i.e., less than 10,000 years old) shallow water and terrestrial sediments overlying the Pleistocene surface (i.e., older than 10,000 years). Holocene sediments are separated into various depositional environments in Figure B-3, based on soil texture, organic content, and other physical and engineering properties. Engineering properties of these layers are described in greater detail below.

The GDM borings indicate the levee fill properties for the north and south breach areas are similar, consisting of compacted CL and CH materials. The average moist unit weight of the fill was estimated to be 109 pcf.

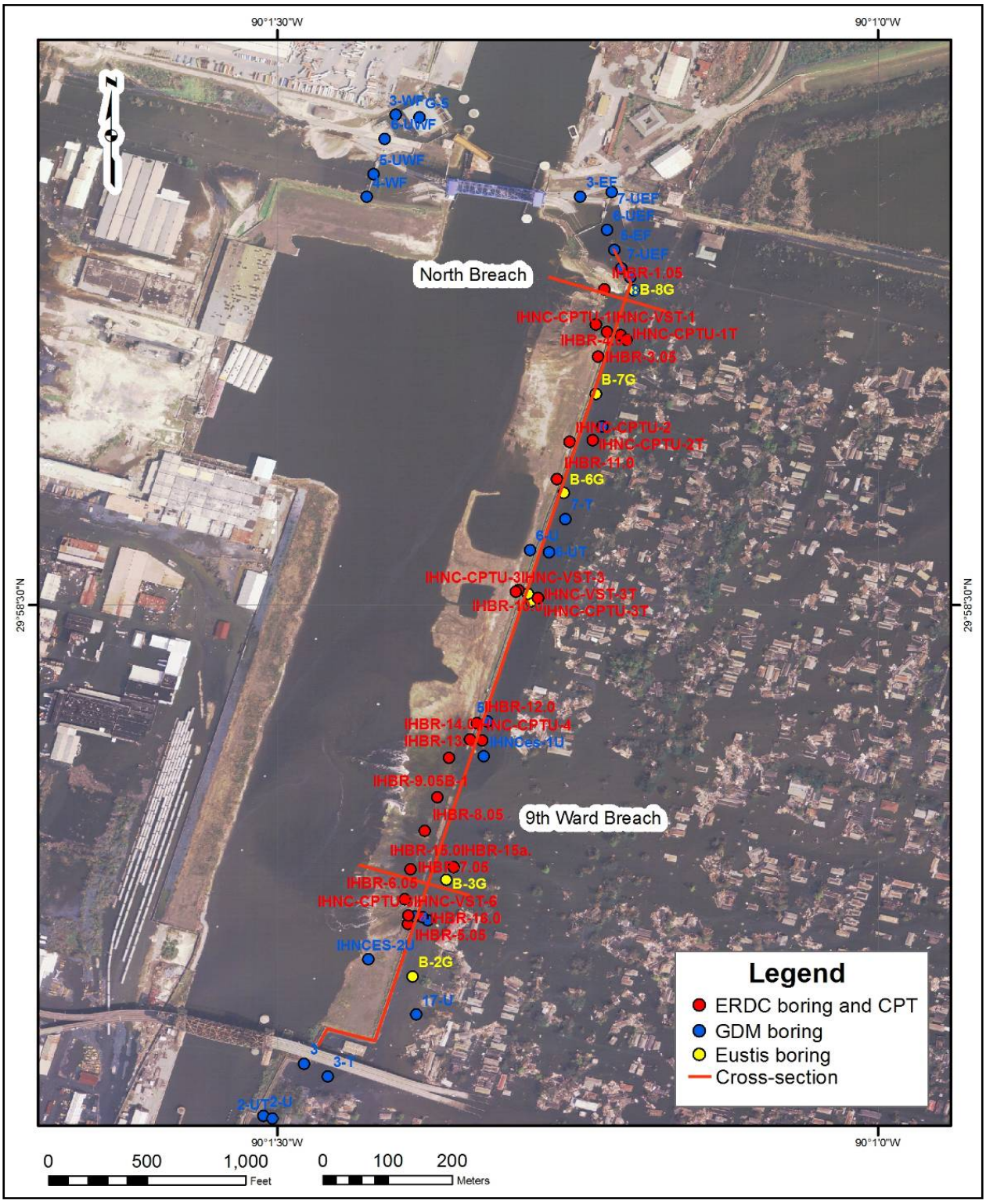


Figure B-2. IHNC – East Bank (Between Florida Ave. and North Claiborne Ave.), Boring and CPTU Location Map

Beneath the fill is a marsh unit about 17 ft thick. The marsh layer is composed of organic material from the cypress swamp that occupied the area, together with silt and clay deposited in the marsh. Because the upper 8 to 9 ft of this unit has different material properties than the lower portion, it was divided into two layers, Marsh 1 and Marsh 2. Water contents and saturated unit weights determined from samples of marsh material taken from the toe are shown in Figures B-4 and B-5, respectively. These figures clearly depict the differences in the marsh layers.

Water contents, unit weights, and undrained shear strengths are shown in Table B-1, and these properties for the Marsh 2 layer are shown in Table B-2. These properties are based on samples from post-Katrina borings at the levee toe. The average saturated unit weight of the Marsh 1 layer is about 105 pcf. Water contents of the Marsh 1 layer are as high as 80%. The average water content of the Marsh 1 layer is approximately 49%. The average saturated unit weight of the Marsh 2 layer is about 80 pcf. Water contents of the Marsh 2 layer are as high as 442%. The average water content of the Marsh 2 layer is approximately 175%. The marsh 1 layer is mostly CH material. The Marsh 2 layer is fibrous at the top, and more amorphous near the bottom, indicating more advanced decomposition of the older organic materials at depth.

Table B-1
Properties of Marsh 1 Layer from Post-Katrina Borings at Toe

Marsh 1 Layer					
Number of Samples = 16					
	Mean	Standard Deviation	COV	Max	Min
%w	49	17	0.342	80.2	21.9
Saturated Unit Weight (pcf)	104	9	0.081	120.5	92.2
S_u (psf)	550	214	0.389	3195	90.0

Table B-2
Properties of Marsh 2 Layer from Post-Katrina Borings at Toe

Marsh 2 Layer					
Number of Samples = 12					
	Mean	Standard Deviation	COV	Max	Min
%w	175	96	0.549	441.6	90.9
Saturated Unit Weight (pcf)	78.4	7	0.091	87.1	63.4
S_u (psf)	195.3	116	0.595	336	64.6

Beneath the marsh layers is a layer of interdistributary clay with an average Liquid Limit of about 79% and an average Plastic Limit of 26%. Based on consolidation test results presented in the GDM, the clay is normally consolidated throughout its depth. The

average saturated unit weight of the clay is about 100 pcf, and the average water content is approximately 60%. Water content and unit weights are summarized in Table B-3.

Table B-3
Properties of Interdistributary Clay from Post-Katrina Borings at Toe

Interdistributary Clay					
Number of Samples = 45					
	Mean	Standard Deviation	COV	Max	Min
%w	60	12	0.208	77.2	25
Saturated Unit Weight (pcf)	101.1	6	0.063	125	93.6

Beneath the clay is a layer of Beach Sand. This layer is not involved in the observed or calculated mechanisms of instability, and its strength is therefore of little importance in stability analyses, except as a more resistant layer beneath the clay.

Figure B-6 shows the cross section of the north IHNC breach selected for the seepage analysis.

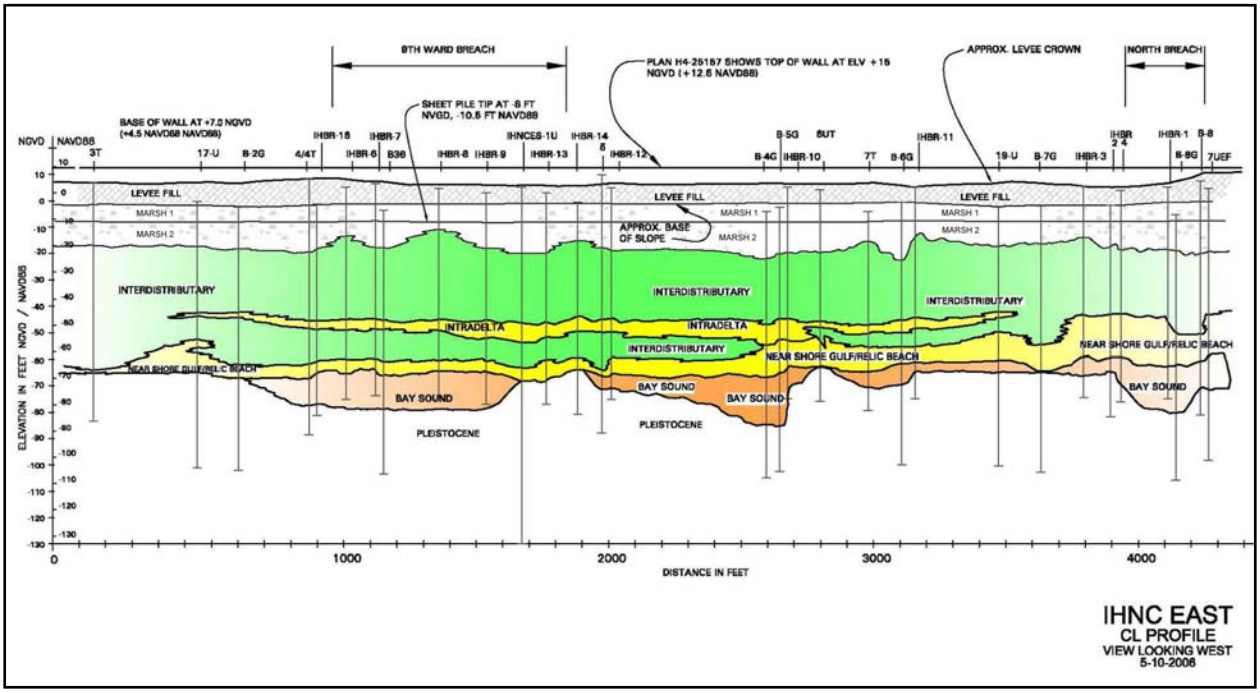


Figure B-3. IHNC East Bank, Centerline Geologic Section Showing South (Lower Ninth Ward) and North Breaches

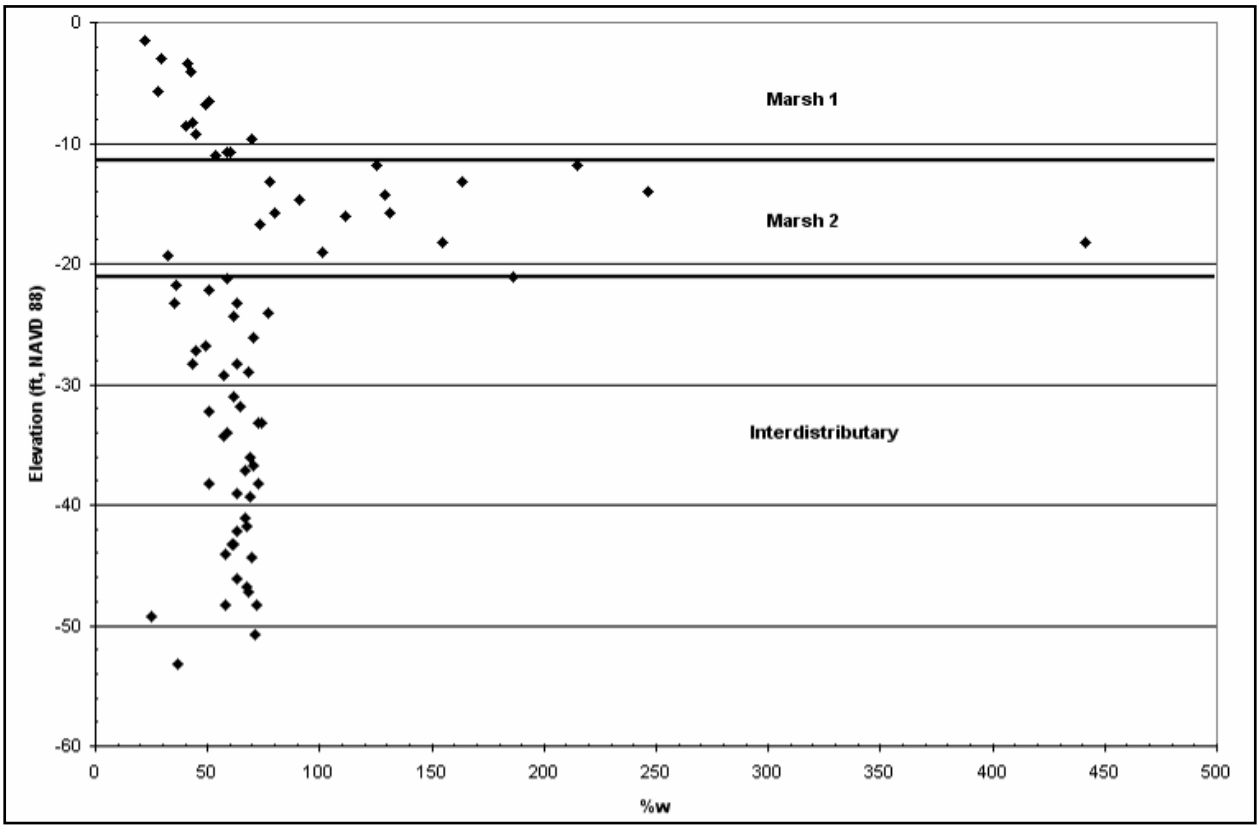


Figure B-4. IHNC – East Bank (Between Florida Ave. and North Claiborne Ave.), % w Versus Elevation (ft, NAVD 88) from Toe Borings

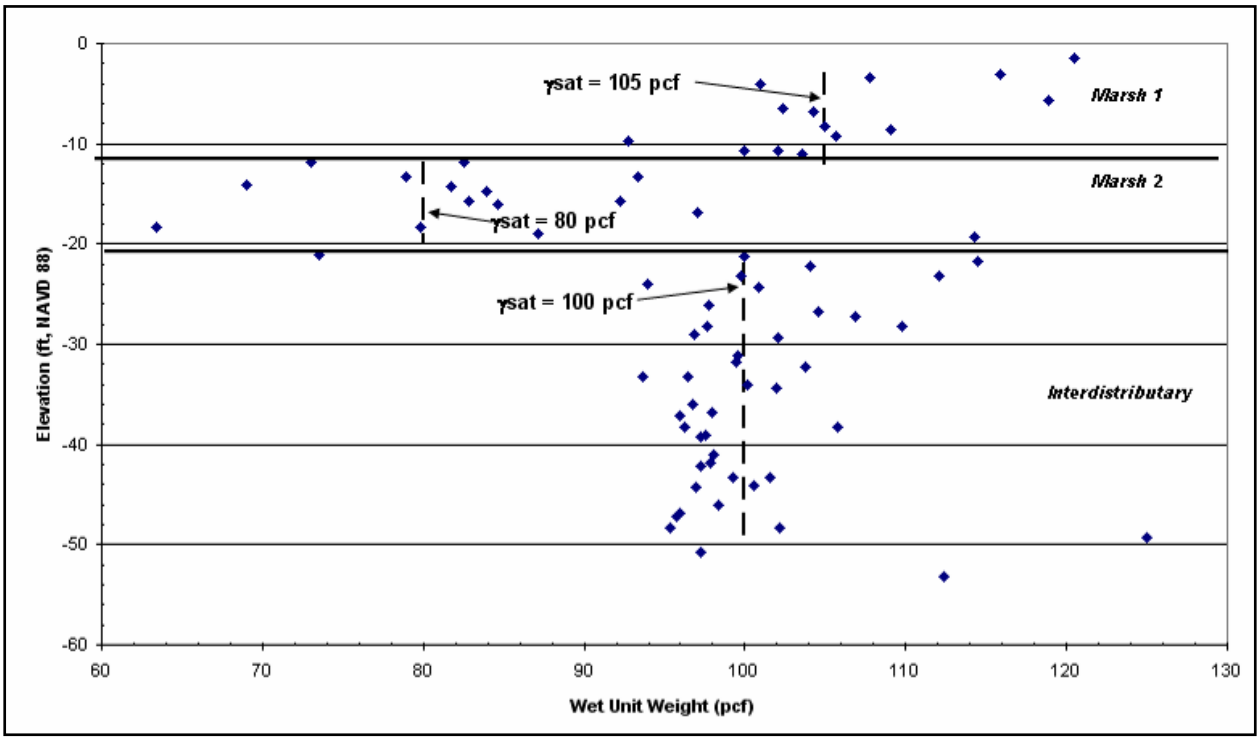


Figure B-5. IHNC – East Bank (Between Florida Ave. and North Claiborne Ave.), Wet Unit Weight versus Elevation (ft, NAVD 88) from Post-Katrina Borings

Figure B-6 shows the cross section of the north IHNC breach selected for the seepage analysis. Figure B-7 shows the finite element mesh used for the seepage analyses performed for the IHNC canal, north breach. Figure B-8 show the materials used in the first series of finite element seepage analyses of the IHNC canal, north breach and the coefficient of permeability values used in the first series of the analyses. Figure B-9 shows the rise portion of the IPET-constructed hydrograph for IHNC canal. This hydrograph is used to specify the water level on the canal side of the model and the time rise during the transient analysis. As the water level rise in the canal, the protected side boundary water is raised from -11.5 to -6.0 to simulate the shut down of the pumps and the heavy rainfall.

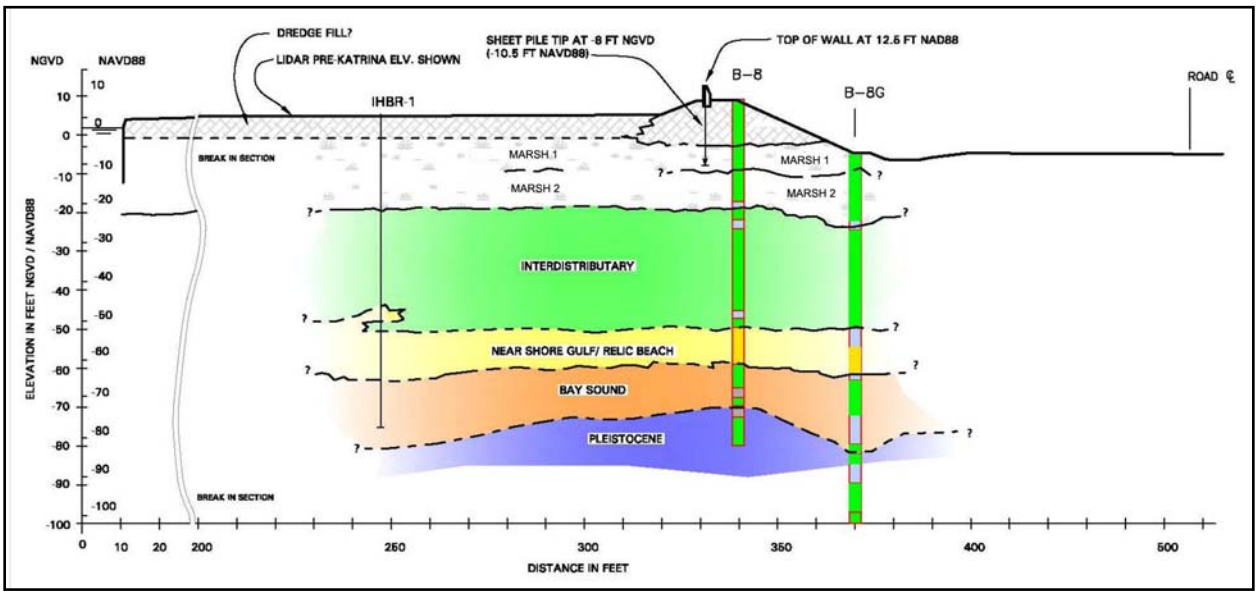
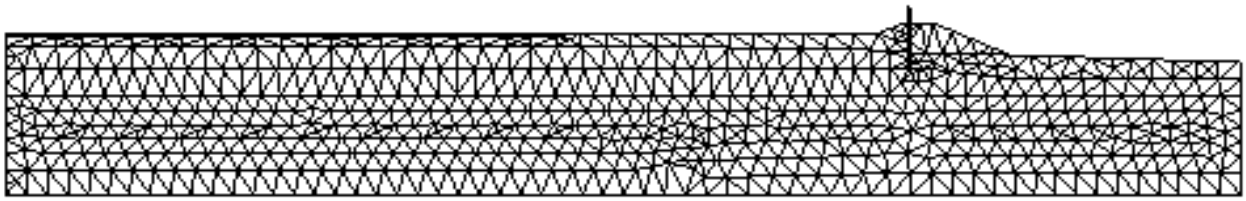
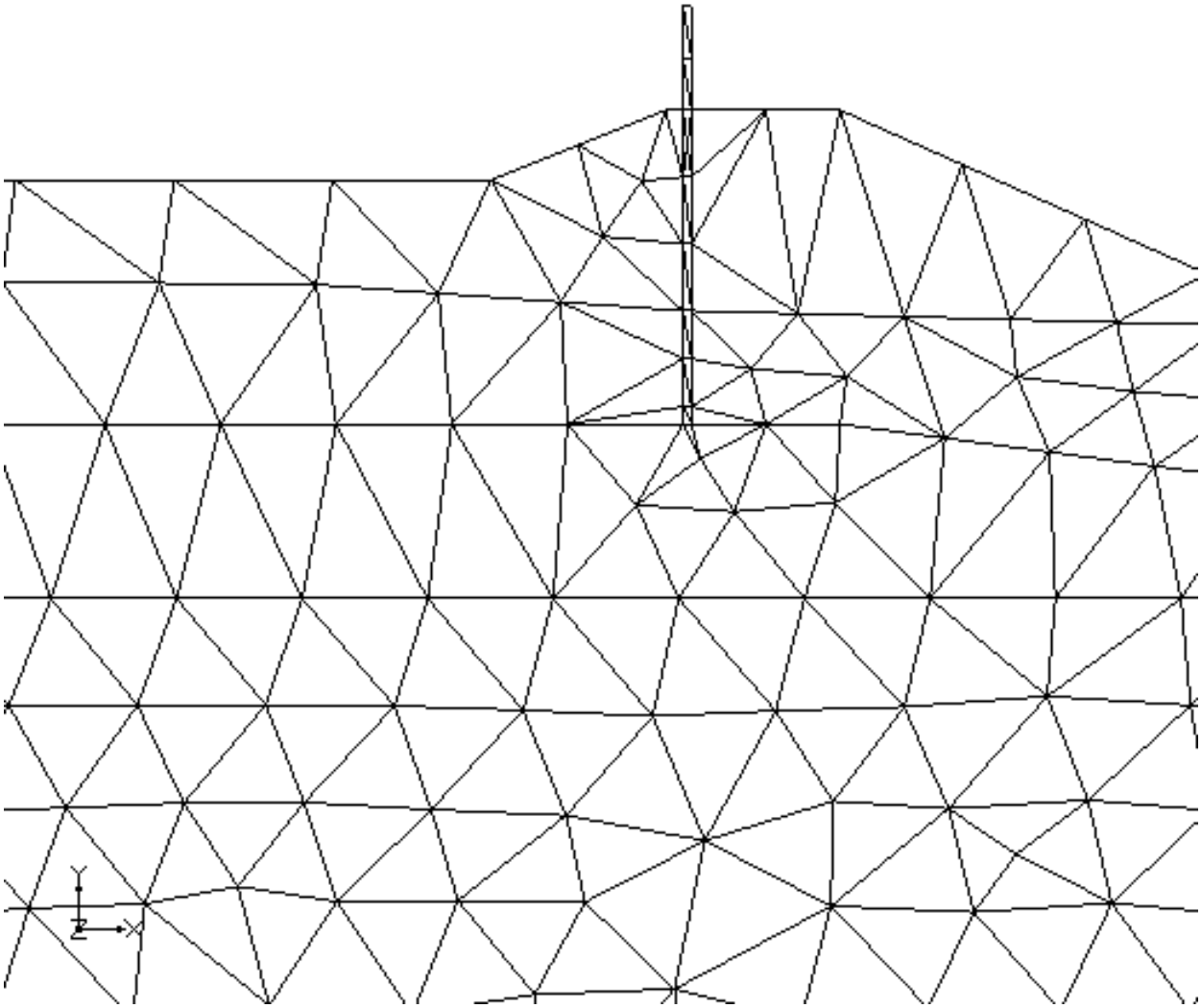


Figure B-6. Profile of the North Breach at IHNC East bank, View Looking North



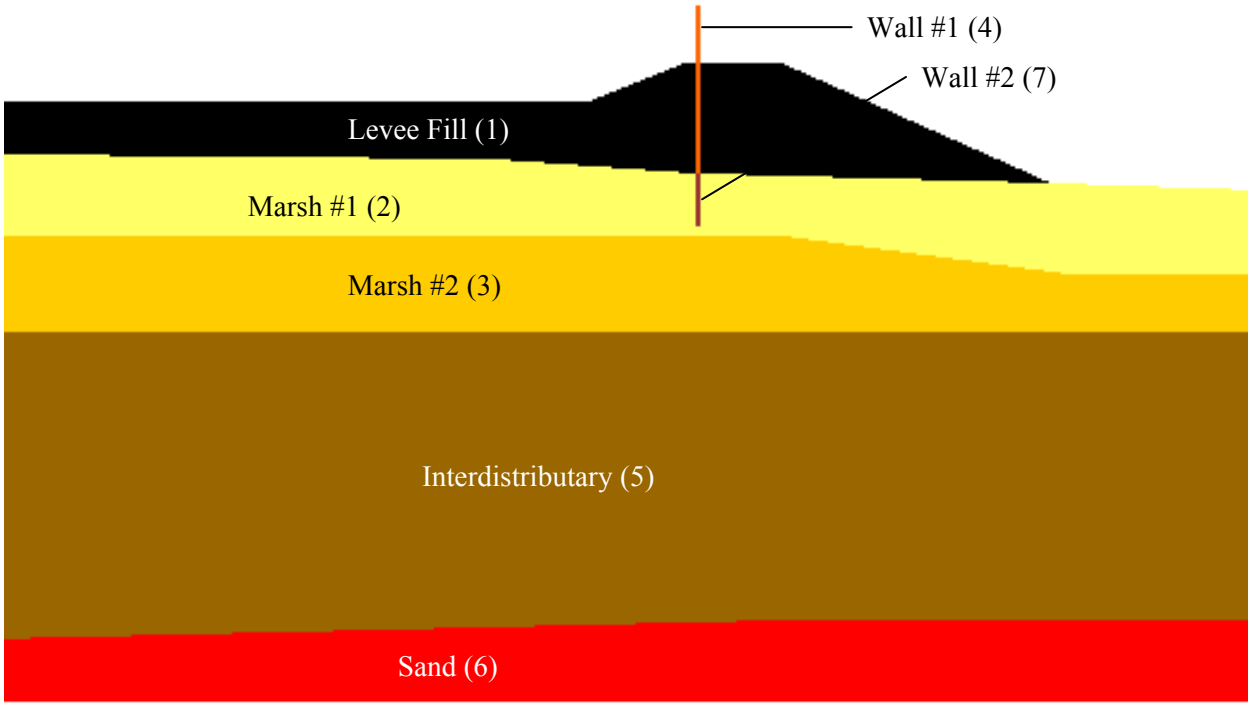
FE Mesh



Zoom of FE Mesh

Figure B-7. Finite element mesh of the north breach of IHNC east bank.

Material Number	Name	K (ft/hr)
1	Levee Fill	0.000118
2	Marsh #1	0.00118
3	Marsh #2	0.00118
4	Wall #1	0.000118
5	Interdistributary	0.000118
6	Sand	1.77
7	Wall #2	0.00118



Zoom of Materials

Figure B-8. Materials and coefficient of permeability values used in the first series of IHNC finite element seepage analyses.

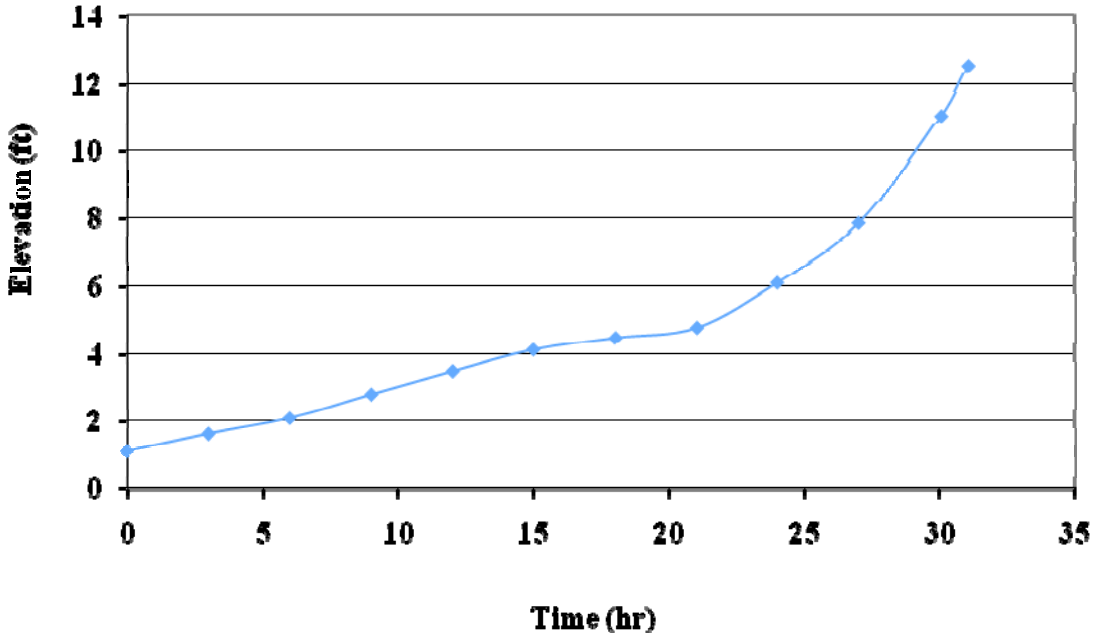


Figure B-9. Hydrograph starting 8/28/2005 at 12:00 AM

Figure B-10 shows the initial steady-state underseepage conditions used for the transient analysis. It is important to keep in mind that soil above the phreatic surface is not fully saturated; and in order for seepage flow to occur, the soil most become fully saturated, which requires time and can only be assessed by a transient analysis. Figure B-11 shows the steady-state solution for the canal water level at 12.5 (top of the wall) and the protected side at -6.0. The phreatic surface in the protected side levee does not intersect the protected side slope. The phreatic surface intersects the protected side water surface (elevation -6.0) at the toe of the levee (elevation -6.0). The exit gradient at the levee toe is less than 0.30.

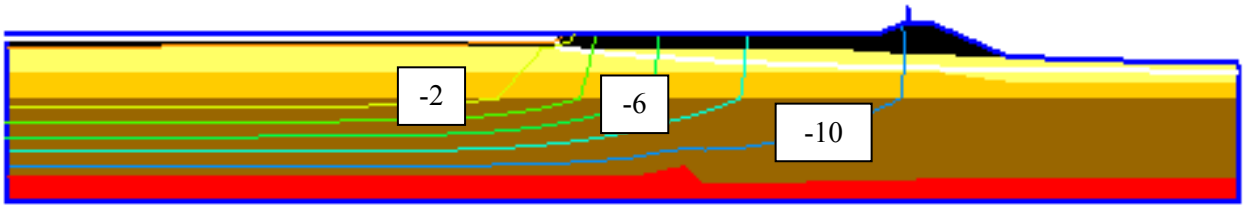


Figure B-10. Contours of Total Head for Steady-State Solution, Canal Elevation = 1.13 ft applied from x=0 to x = 202 ft, Head at Protected Side = -11.5 ft, (Equipotential Lines = -10, -8, -6, -4, -2, 0 ft)

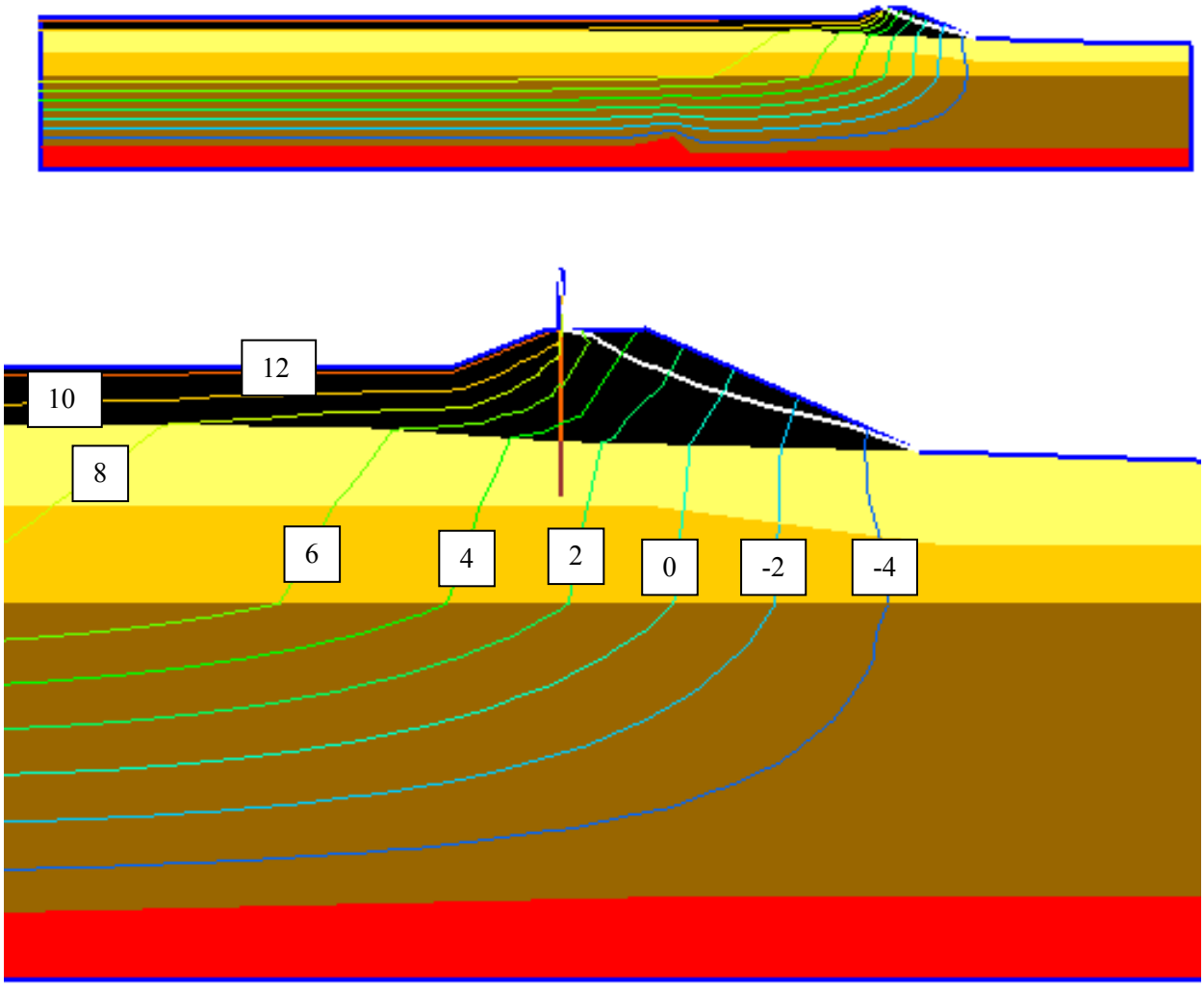


Figure B-11. Contours of Total Head for Steady-State Solution, Canal Elevation = 12.5 ft, Head at Protected Side = -6 ft (Equipotential Lines = -4, -2, 0, 2, 4, 6, 8, 10, 12 ft)

Figure B-12 shows the results of the transient finite element seepage analysis for the most realistic representation of the geometry and material property. It can be seen that the seepage conditions have not reached the steady-state condition. The levee on the canal side has not even reached full saturation.

As designed, the pre-Katrina site conditions were a clay blanket starting at the toe of the levee on the canal side. This is similar to the clay blanket used upstream of a dam to reduce underseepage and seepage pressures down stream. While unlikely, a worst case condition would be that the clay blanket had the same permeability as the marsh material, Figure B-13. Figure B-14 shows the initial steady-state underseepage conditions used for the transient analysis. Figure B-15 shows the steady state solution for the canal water level at 12.5 (top of the wall) and the protected side at -6.0 for no clay blanket. The phreatic surface intersects the protected levee slope.

Figure B-16 shows the results of the transient finite element seepage analysis for the clay blanket with the same permeability as the marsh material. Again, the levee on the canal side does not even reach full saturation.

To demonstrate that the Plaintiff's expert's explanation cannot be supported, another unrealistic set of conditions were assessed. These conditions included no clay blanket, and increasing the permeability of the marsh by 100 times beyond the highest limit of published values. Figure B-17 shows the steady state solution for the canal water level at 12.5 (top of the wall) and the protected side at -6.0 for 100 times increase in permeability. Figure B-18 shows the results of the transient finite element seepage analysis for the 100 times increase in marsh permeability. Even with this completely unrealistically high permeability, the seepage does not reach the steady state conditions.

Table B-4 shows a comparison of the exit gradient for the steady state condition and transient analysis of the storm surge in the canal. The transient solution has a 40 percent reduction in uplift pressure on the protected side as compared to the steady state analysis. The transient solution also has a 48 percent reduction in the exit gradient as compared to the steady state solution.

Table B-4. Comparison of Exit Gradient for steady state condition and transient analysis

	Total Head at Sheetpile on Protected Side (ft)	Uplift Force on Protected Side (kips)	Percent Reduction in Uplift from Steady State	Change in Head at Toe of Levee (ft)	Length of Seepage Path (ft)	Exit Gradient = H/L	Percent Reduction in Gradient from Steady State
Steady State	10	11.4		6-4.59=1.41	10.79-6=4.79	0.29	
Transient	6	6.8	40	6-5.30=0.70	10.79-6=4.79	0.15	48

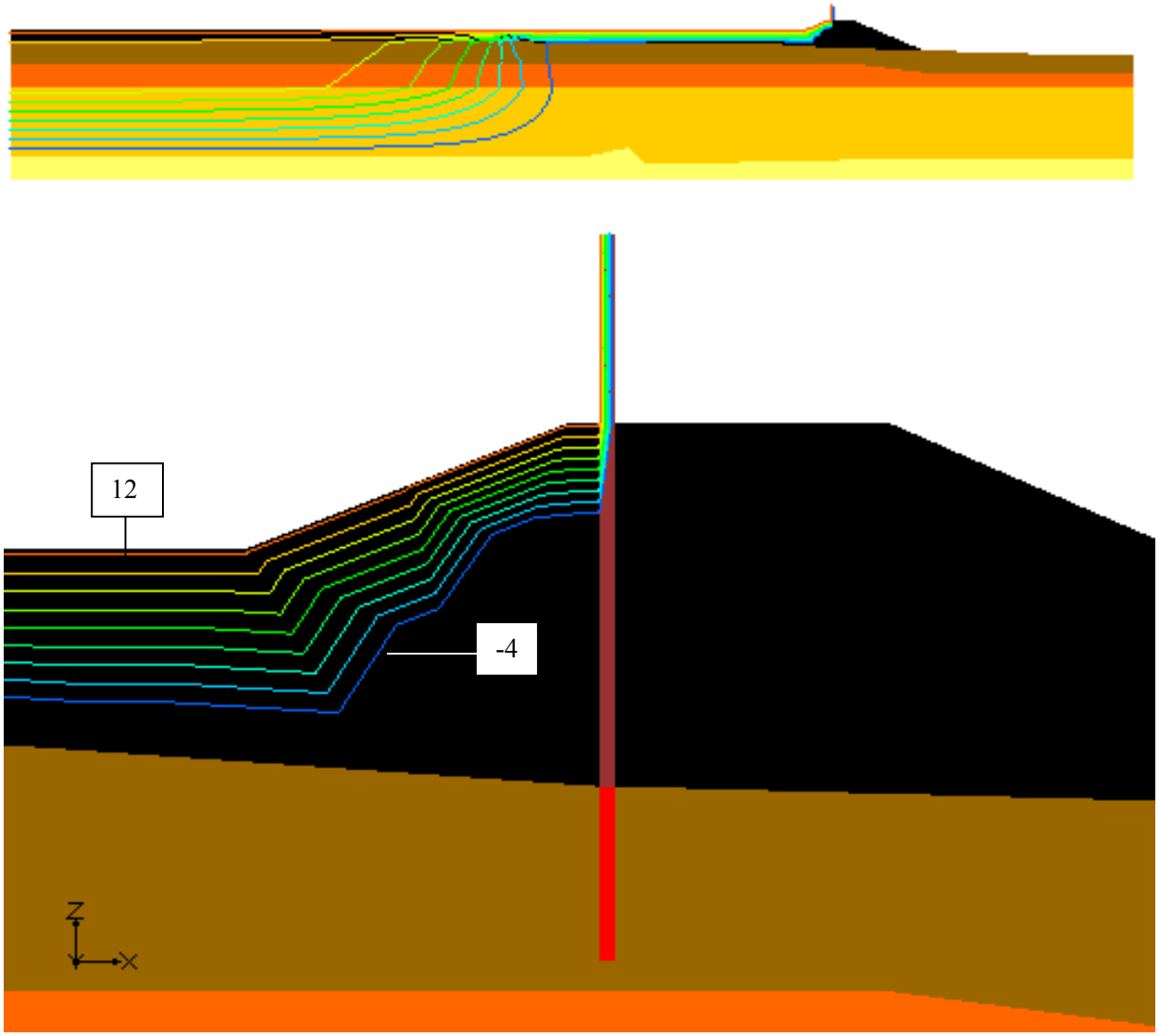


Figure B-12. Contours of Total Head for Transient Solution, Canal Elevation = 12.5 ft, Head at Protected Side = -6 ft (Equipotential Lines = -4, -2, 0, 2, 4, 6, 8, 10, 12 ft)

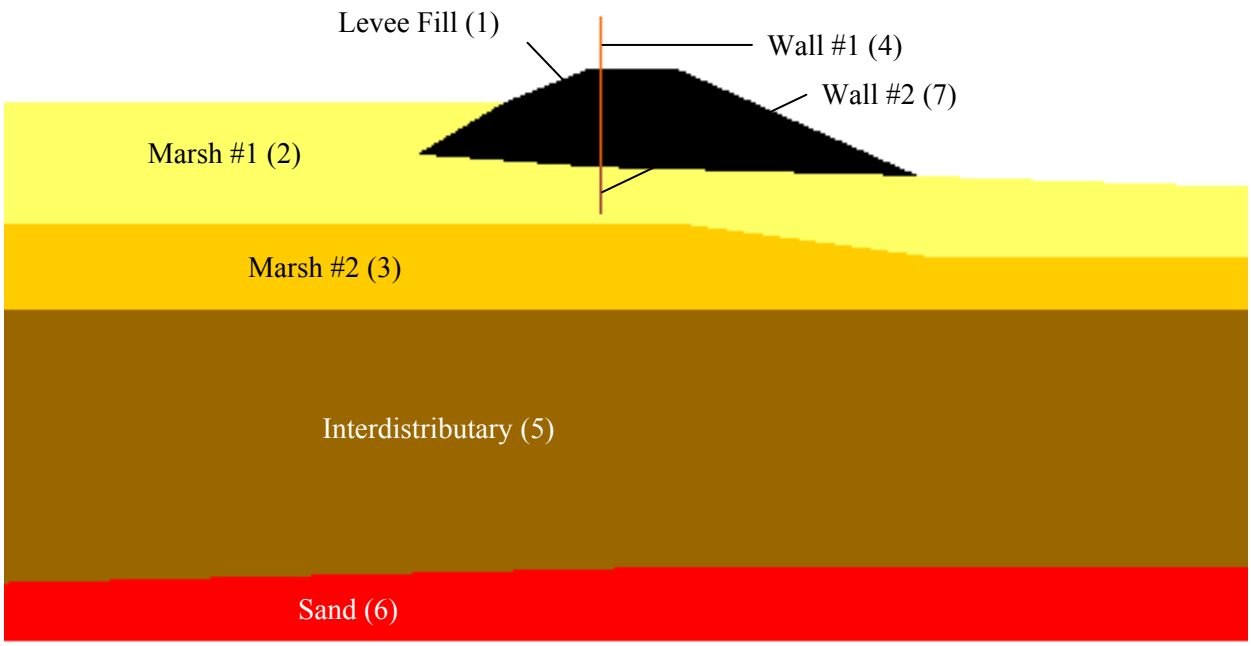


Figure B-13. Clay Blanket Assumed to have the same permeability as Marsh #1

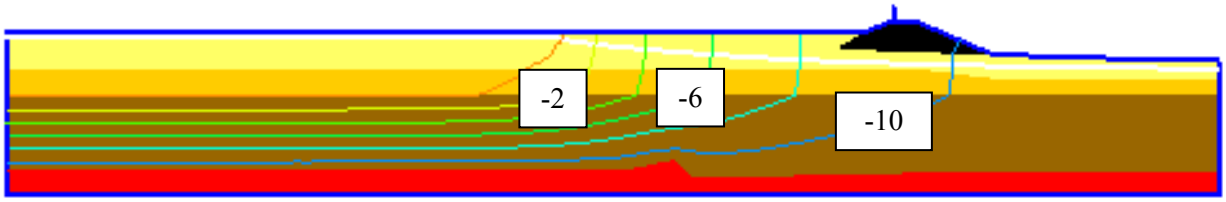


Figure B-14. 2D Contours of Total Head for Steady-State Solution, Canal Elevation = 1.13 ft applied from x=0 to x = 202 ft, Head at Protected Side = -11.5 ft (Equipotential Lines = -10, -8, -6, -4, -2, 0 ft)

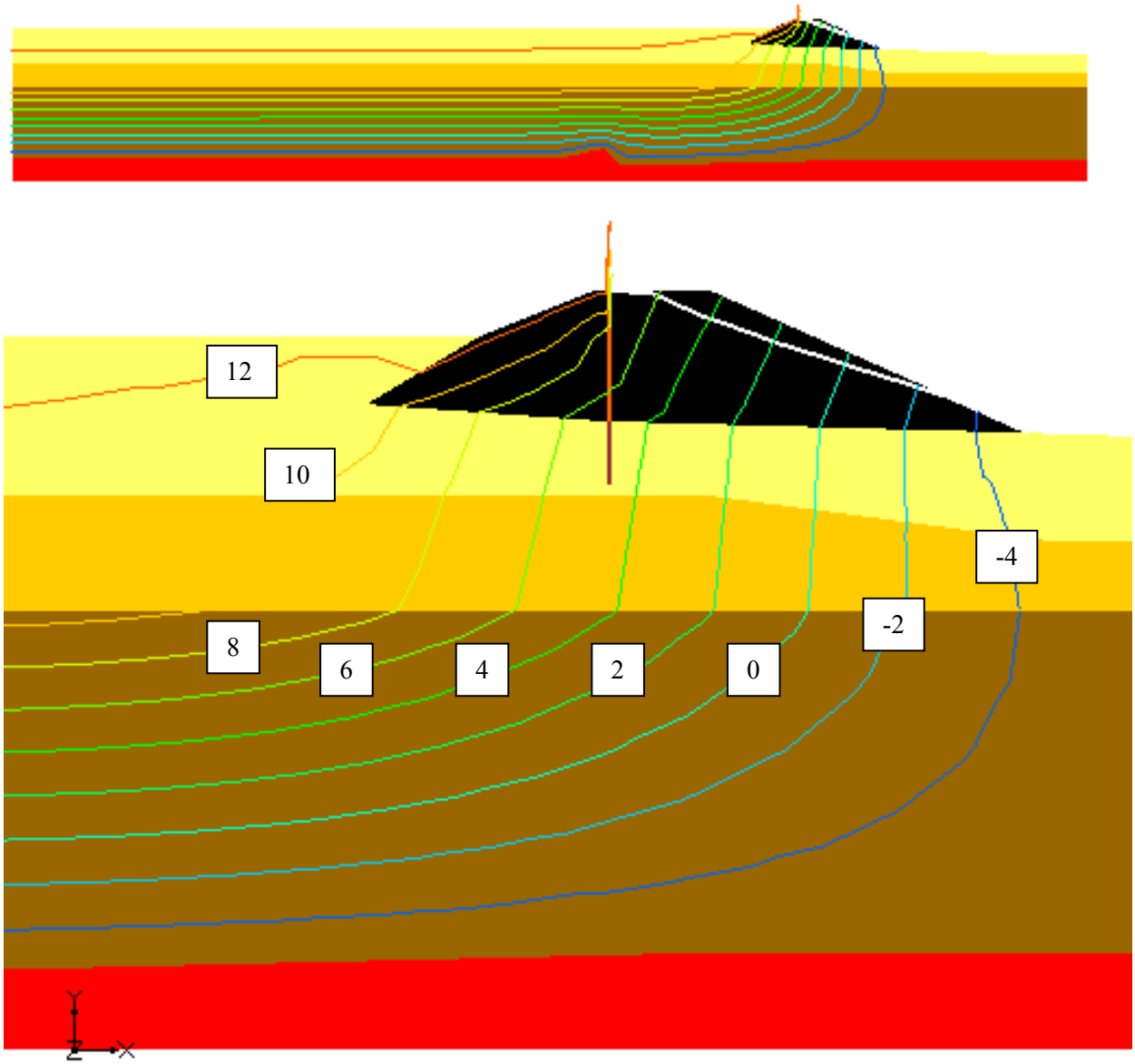


Figure B-15. Contours of Total Head for Steady-State Solution, Canal Elevation = 12.5 ft, Head at Protected Side = -6 ft (Equipotential Lines = -4, -2, 0, 2, 4, 6, 8, 10, 12 ft)

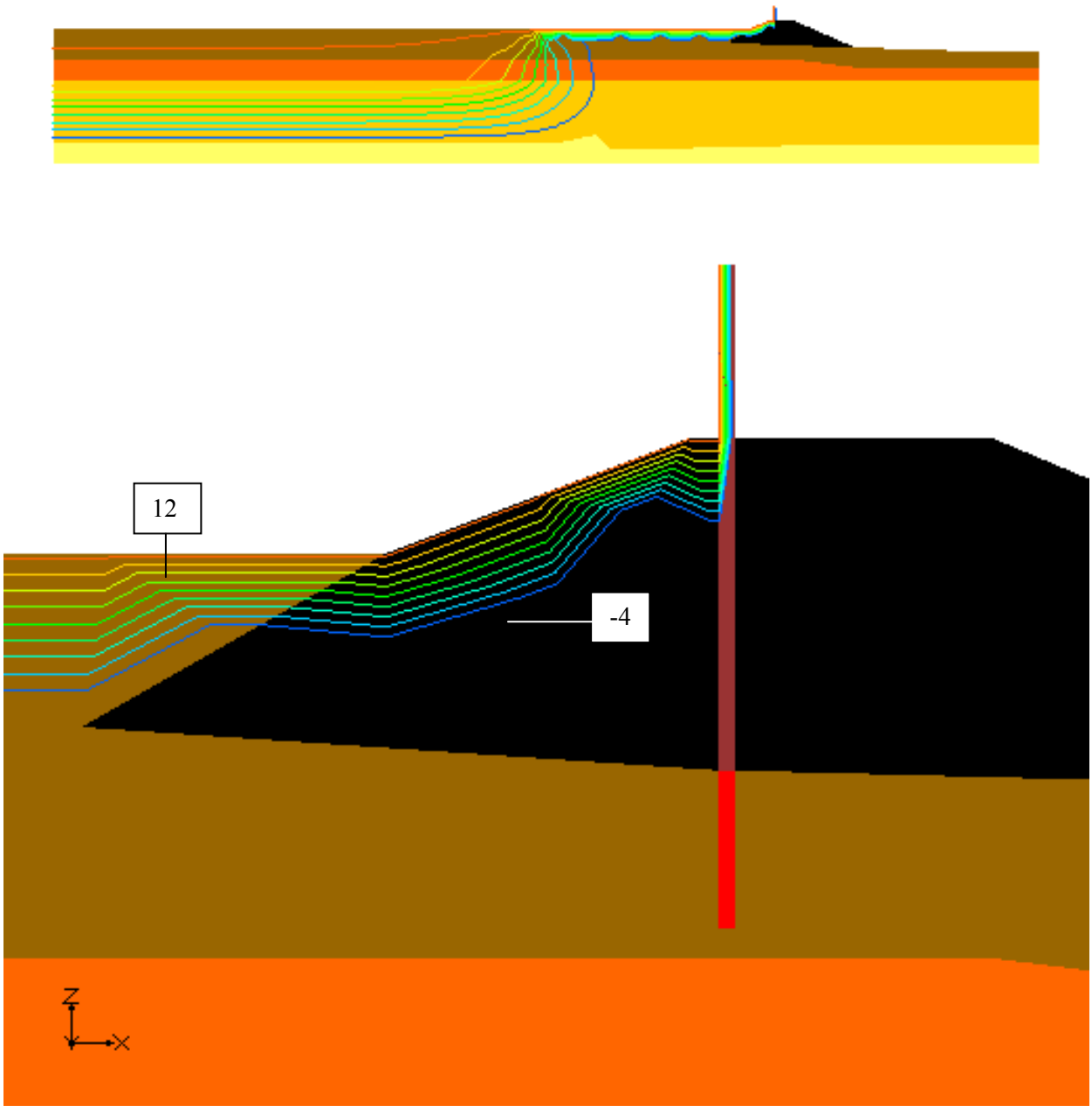


Figure B-16. Contours of Total Head for Transient Solution, Canal Elevation = 12.5 ft, Head at Protected Side = -6 ft (Equipotential Lines = -4, -2, 0, 2, 4, 6, 8, 10, 12 ft)

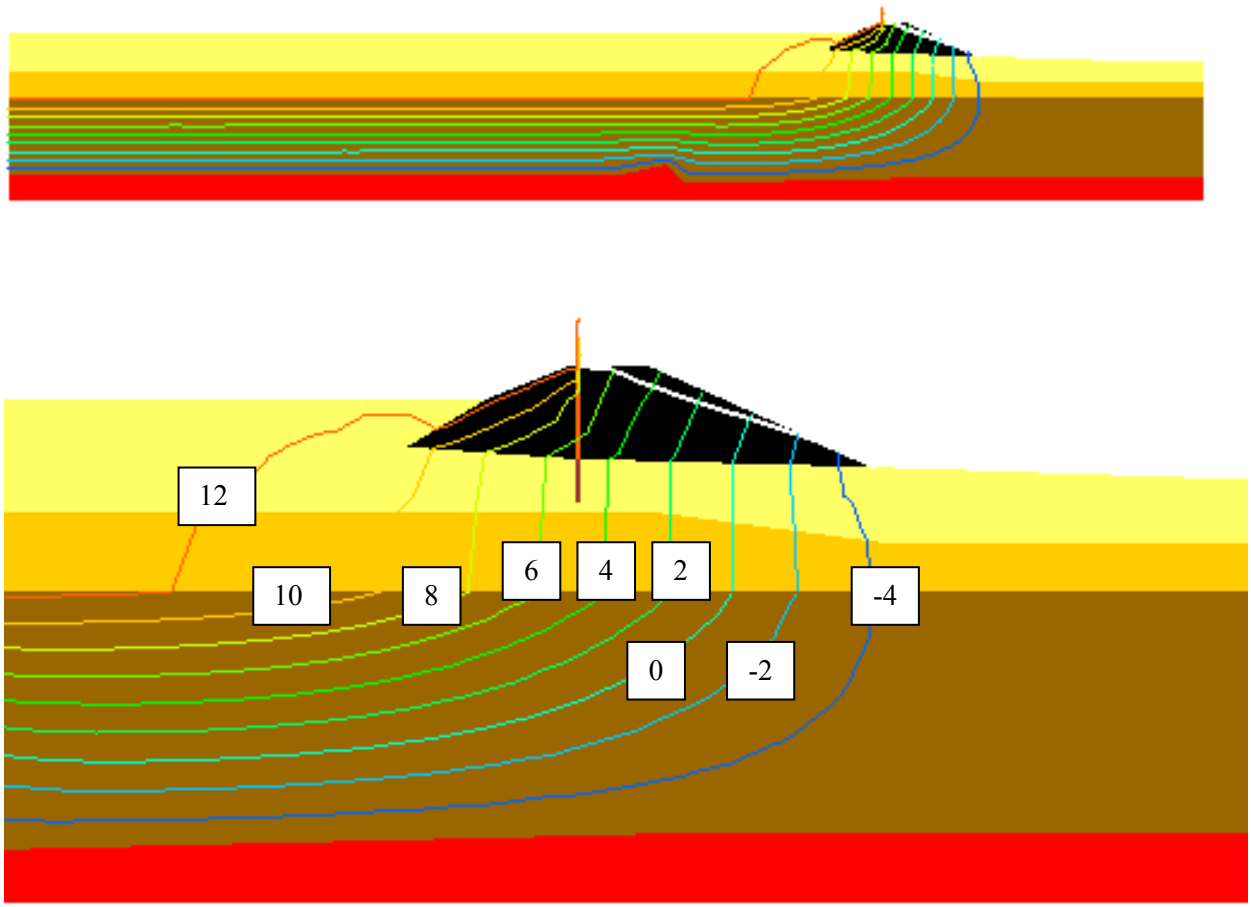


Figure B-17. Contours of Total Head for Steady-State Solution, Canal Elevation = 12.5 ft, Head at Protected Side = -6 ft (Equipotential Lines = -4, -2, 0, 2, 4, 6, 8, 10, 12 ft)

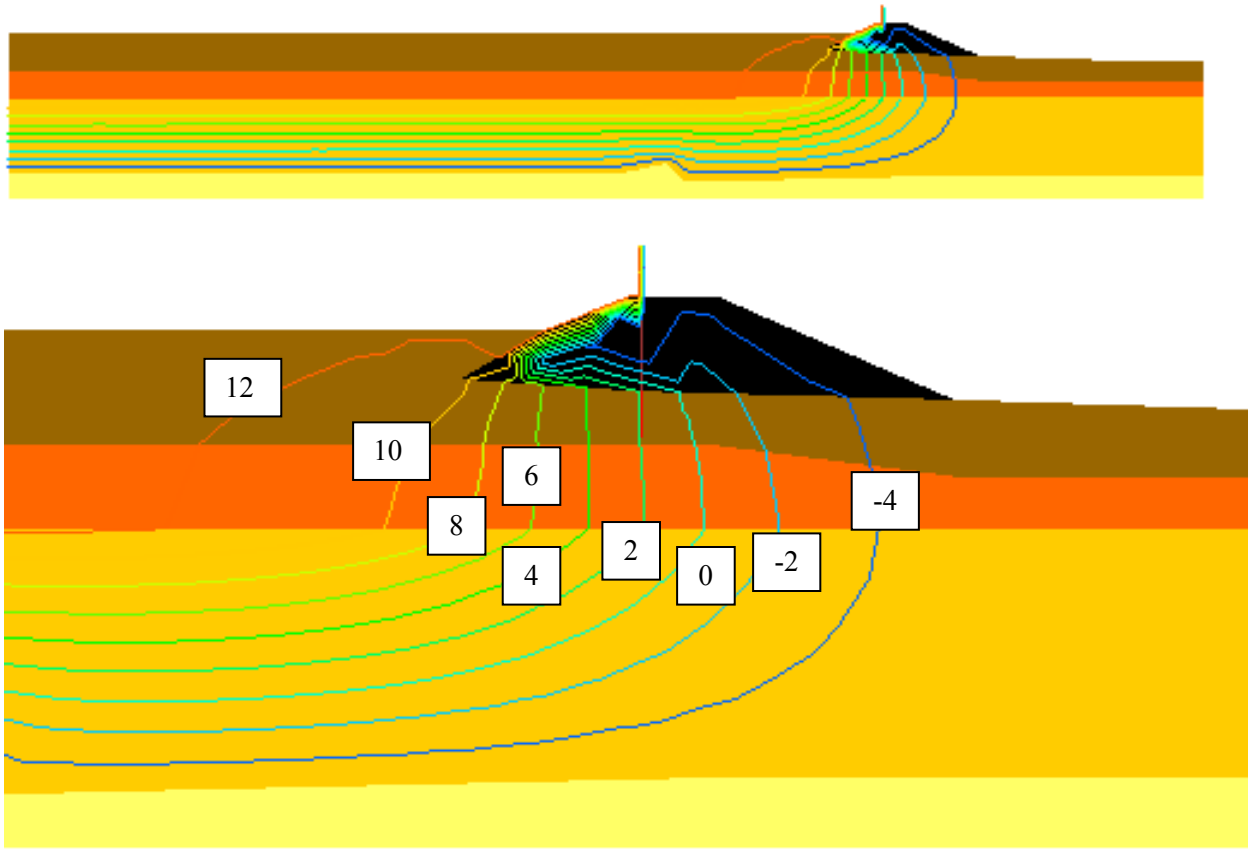


Figure B-18. Contours of Total Head for Transient Solution, Canal Elevation = 12.5 ft, Head at Protected Side = -6 ft (Equipotential Lines = -4, -2, 0, 2, 4, 6, 8, 10, 12 ft)

In conclusion, Dr. Bea findings on underseepage in regard to the IHNC breaches along the Lower Ninth Ward are based on unrealistic and unproven permeability values and unverified and inaccurate soil stratification. This flawed data produced equally flawed results.

IPET's slope stability analyses show that failure of the IHNC East Bank, North Breach at the Lower Ninth Ward could occur before the canal water level reached the top of the wall. There is clear evidence that water levels in the northern region of the Lower Ninth Ward, south of Florida Avenue, were rising early in the morning of August 29, 2005. Several eyewitness accounts had water flowing into houses and down streets between 0430 and 0500. Stopped clock data has the water level in this area at Elevation +3.0 by 0600, which makes the depth of water between 5 to 10 ft. These observed water levels and the associated volume of water needed to achieve them in the northern region of the Lower Ninth Ward, south of Florida Avenue, did not come from underseepage as suggested by Dr. Bea expert report. This can only occur if the levee is breached, which is what the IPET Draft Final Report stated, "*Eyewitness reports indicate that water level in the 9th Ward near Florida Avenue was rising when the water level in the IHNC was still below the top of the wall. Stability analyses indicate that foundation failure would occur before overtopping at the north breach on the east side of the IHNC. This breach*

location is thus the likely source of the early flooding in the 9th Ward." Even with outrageously unrealistically high permeability values used by the Dr. Bea, underseepage could not produce the volume of water observed in this area. This would have been realized if he had reviewed the hydrograph for the Lower Ninth Ward inundation presented here in Figure B-19.

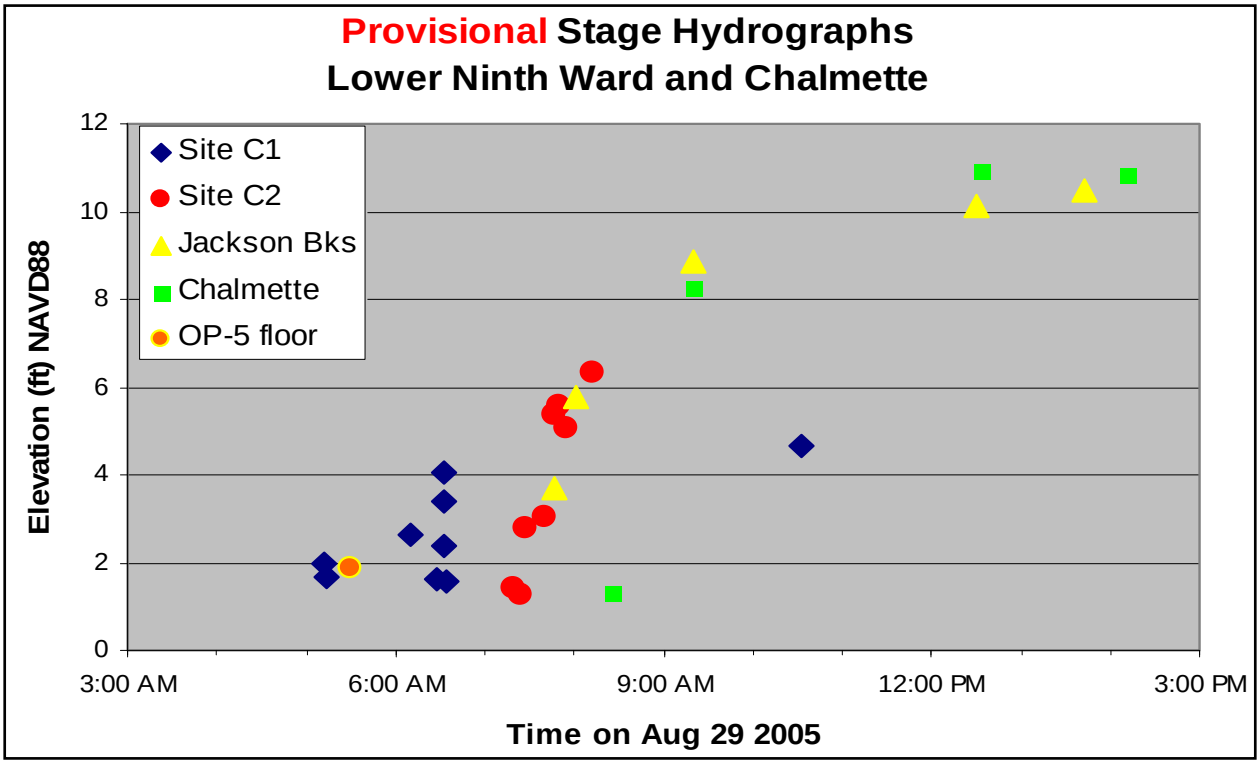


Figure B-19. Hydrograph for the Lower Ninth Ward Inundation

The IPET slope stability analyses show that the levee would become unstable when the water level in the canal reached approximately Elevation +11.2 NAVD 88. Figure B-20 shows the reprint of the hydrograph for the IHNC, Figure 129, IPET Volume IV – Storm, page IV-185. The hydrograph shows that the water level in the canal at 0500 could have been Elevation +11.0, depending on which gage reading is used. Based on the variability of the soil properties and the gage readings that make up the hydrograph, the IPET analyses would appear to provide a probable explanation for the observed water in the neighborhood and foundation failure that resulted in the north breach. In order for this foundation failure to develop, it did not require unrealistic underseepage to occur to cause the breach.

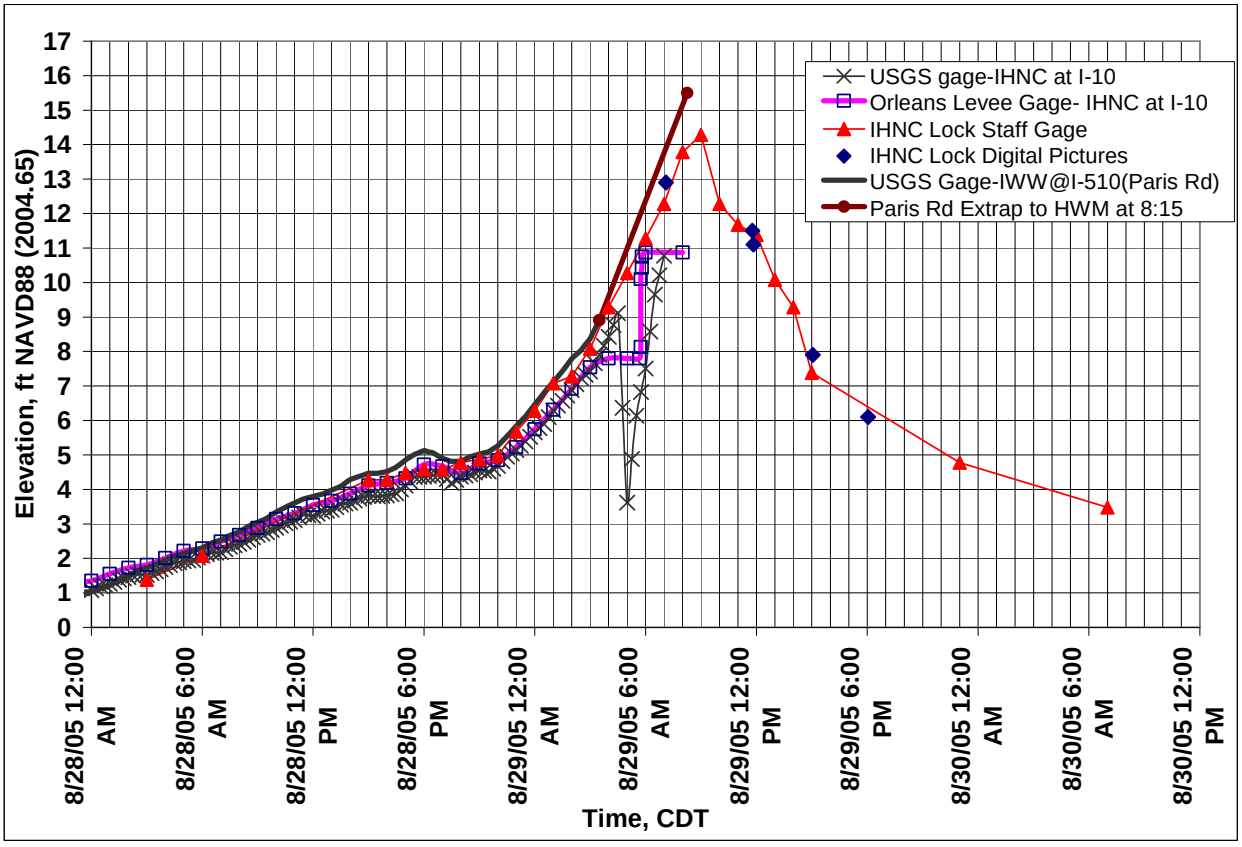


Figure B-20. Hydrograph for IHNC

This calls into question the rest of Dr. Bea's investigation of the breaches along the IHNC east bank Lower Ninth Ward. While Dr. Bea tries to use unclear and compromised evidence from observations to bolster their underseepage hypothesis, he overlooked the direct comparison of field observations between the south breach at the east bank of the IHNC Lower Ninth Ward, Figure B-21, and the I-wall on Citrus back levee along the GIWW, Figures B-22, B-23, and B-24.

Comparing the scour trench located on the protected side of what was the I-wall running along the east bank of IHNC, south breach Lower Ninth Ward shown in Figure B-21, with the scour trench on the protected side of the I-wall of the Citrus Back Levee shown in Figure B-22, and the IPET slope stability analysis for the I-wall at the east bank IHNC at south breach show it to be stable, with water to the top of the wall, one would have to conclude that the most plausible explanation for the breach is scour of the protected side support of the I-wall from overtopping.

Because the unrealistic permeability assigned to the marsh material for Dr. Bea seepage analyses was at least 1,000 times too high, the results of the seepage analyses described in that his report do not reflect the real seepage conditions in the field. Because it was assigned such a high permeability, the marsh layer appeared in those analyses to have very low resistance to seepage, and to respond very quickly to the rise in canal water level. This behavior is not consistent with the actual behavior of marsh material and peat, especially when consolidated under the weight of the levees. Based on this mistaken choice of marsh permeability, and the ensuing unrepresentative analytical results, Dr. Bea's report offered a misguided conclusion for the performance of the I-walls along the IHNC adjacent to the Lower 9th Ward. He further tries to imply that his unrealistic results from seepage analyses have effect on the slope stability analyses he performed. Because he used undrained shear strengths for the marsh soils, he is implicitly stating the marsh soils are so impervious that they will not drain when sheared and strength is not affected by pore pressure during the analysis. He also uses the results of the seepage analyses to calculate a factor of safety for hydraulic uplift by a ratio of effective stress acting at the bottom of the clay blanket and the pore pressure at the same point in the marsh soils. This is misleading because he has characterized the clay and marsh soils as having undrained shear strength, thus unaffected by seepage pore pressures.



Figure B-21. Scour and Erosion Leading to the Failure of the I-Wall on the IHNC adjacent to the South Breach (Lower Ninth Ward)



Figure B-22. Scour trench on the protected side of Citrus Back Levee I-wall. (Figure 7.14, NSF-Berkeley report (ILIT Final Report, July 31, 2006)



Figure B-23. Another section of the Citrus Back Levee I-wall showing erosion of the levee, lateral deflection, and tilting from overtopping



Figure B-24. Deflection and tilting of Citrus Back Levee I-wall



Dr. Mosher

Dr. Reed L. Mosher

Director
Information Technology Laboratory
US Army Engineer Research and Development Center

Dr. Reed L. Mosher serves as the Director of the U.S. Army Engineer Research and Development Center (ERDC) Information Technology Laboratory, the premier Department of Defense laboratory for information technology in support of military engineering and Army civil works. Dr. Mosher oversees the execution of a broad range of research, development, and studies and an operational program that provides technical assistance and operational support in information technology and closely related fields, including the following: automated information systems development, computer-aided engineering, computer-aided design and drafting, geospatial systems, building information modeling, computational science and engineering, high-performance computing, general-purpose computing, software engineering, informatics, sensor and instrumentation systems, and the ERDC library.

Prior to his becoming Director of ITL, Dr. Mosher was the Technical Director for Survivability and Protective Structures and the lead Technical Director for Military Engineering in the Geotechnical and Structures Laboratory. Dr. Mosher has 30 years of experience conducting research at all levels in the field of geotechnical and structural engineering. In 1999, he was the ERDC first selection to be promoted to one of the twenty Army-wide Senior Scientific Technical Manager (SSTM) positions created under the Science and Technology Laboratory Demonstration Project. Dr. Mosher served as the Co-Lead for the Levee and Floodwall Performance team of the Interagency Performance Evaluation Task Force, which investigated the performance of the New Orleans hurricane protection system during Hurricane Katrina. Dr. Mosher received the U.S. Army's Meritorious Civilian Service Award for this effort. Dr. Mosher recently received the Department of Defense Distinguished Civilian Service Award, the highest award given by the Secretary of Defense to a career employee, and the Army Engineer Association's Bronze de Fleury Medal for his leadership in research that has led to the development of innovative products for force protection of our military and civilian personnel worldwide from terrorist bombings and conventional weapons.

A native of Maine, Mosher earned his bachelor's degree in civil engineering from Worcester Polytechnic Institute in Worcester, Mass. He holds a master's degree in civil engineering from Mississippi State University and a doctorate in civil engineering from Virginia Polytechnic Institute and State University in Blacksburg, Va. He has been an adjunct professor at Mississippi State University, University of Puerto Rico, Virginia Polytechnic Institute and State University, and Louisiana State University.

ERDC is the premier research and development facility for the U.S. Army Corps of Engineers with more than 2,000 employees, $1.2 billion in facilities, and an annual research program

exceeding $1 billion. It conducts research in both military and civil works mission areas for the Department of Defense and the nation.

Publications:

(1) Papers:

Ebeling, R. M., Peters, J. F., and Mosher, R. L., *Nonlinear Deformation Analysis in the Design Reinforced Soil Berm at Red River U-Frame Lock No. 1*, International Journal of Numerical and Analytical Methods Geomechanics, Vol. 21, 1997, 753-787.

Peters, J. F., Ebeling, R. M., and Mosher, R. L., *Analysis of Dense Geotextile Grids*, International Journal of Numerical and Analytical Methods Geomechanics, Vol.21, 1997, 801-810.

Ebeling, R. M. and Mosher, R. L., *Red River U-Frame Lock No. 1 Backfill-Structure-Foundation Interaction*, ASCE Journal of Geotechnical Engineering, Vol. 122, No. 3, March 1996, pages 216-225.

Chakravorty, M., Frangopol, D. M., Mosher, R. L., and Pytte, J. E., *Time-Dependent Reliability of Rock-Anchored Structures,* International Journal, **Reliability Engineering & System Safety**, Vol. 47, Technical Note, 1995, Elsevier Applied Science.

Mosher, R. L., and Rossow, M. P., *Design of Cellular Cofferdams by the CCELL Computer Program,* An International Journal, **Computers & Structures**, Vol. 42, No. 6, 17 March 1992, Pergamon Press, Elmsford, New York.

Mosher, R. L., *Axial Capacity of Vibratory-Driven versus Impact-Driven Piles,* **Transportation Research Record,** No. 1277 (Soils, Geology, and Foundations), ***Modern Geotechnical Methods: Instrumentation and Vibratory Hammers 1990***, Transportation Research Board, National Research Council, Washington, D.C., 1990.

(2) Books:

Design of Sheet Pile Walls, **Technical Engineering and Design Guides as Adapted from the US Army Corps of Engineers, No. 15**, ASCE Press, New York, NY, 1996

Design of Pile Foundations, **Technical Engineering and Design Guides as Adapted from the US Army Corps of Engineers, No. 1**, ASCE Press, New York, NY, 1993

Rossow, M., Demsky, E., and Mosher, R. L., *Theoretical Manual for Design of Cellular Cofferdams,* **Cellular Cofferdam**, Pile Buck, Inc, Jupiter, FL, 1990

b. Publications published (refereed or not) in proceedings of professional conferences:

Coltharp, D. R., and Mosher, R. L., *Blast Loading of a Full-Scale, Five-Story Building,* Proceeding of 9th International Symposium of Effects of Munitions with Structures, Berlin, Germany, May 1999

Patev, R. C., Mosher, R. L., and Leggett, M. A., *Reliability Model for Concrete Deterioration of Lock Walls due to Freeze-Thaw Damage and Abrasion,* Proceeding of ASCE Engineering Mechanics and Structural Division, **Seventh Specialty Conference on Probabilistic Mechanics and Structural Reliability,** Worcester, MA, August, 1996

Isenhower, W. M., and Mosher, R. L., *Reliability Analysis and Evaluation of Deep-Seated Stability for Pile-Supported Structures,* Proceeding of the ASCE Geotechnical Engineering Division Specialty Conference, **Uncertainty in the Geologic Environment: From Theory to Practice**, Madison, Wisconsin, June, 1996.

Padula, J. A., Mosher, R. L., Mlakar, P. F., Chasten, C. P., and Stough, W. R., *A Reliability Model for Fatigue and Corrosion Degradation of Hydraulic Steel Structures*, invited paper for the ASCE 1994 Material Engineering Conference, November, 1994, San Diego, CA.

Chakravorty, M., Pytte, J. E., Frangopol, D. M., and Mosher, R. L., *Reliability of Navigation Structures Under Time-Dependent Effects*, **Proceeding PSAM - II International Conference**, Elsevier, March 1994.

Leggett, M. A., and Mosher, R. L., *Reliability-Based Assessment of Navigation Structures,* **ASCE Specialty Conference: Fifth International Conference on Computing in Civil Engineering,** Anaheim, CA, June 1993.

Banafa, A., Frangopol, D. M., and Mosher, R. L., *Reliability Model for Cost Estimation of Pile Foundations*, **Second International Symposium on Uncertainty Modeling and Analysis**, University of Maryland, College Park, MD, April 1993.

Kuppusamy, T., Zerco, M., and Mosher, R. L. *Soil-Structure Interaction Analysis by Coupled BEM-FEM,* **International Conference on Geotechnics and Computers**, Paris, France, October 1992.

Ebeling, R. M., Peters, J. F., and Mosher, R. L., *Finite Element Analysis of Slopes with Reinforcement, Proceeding,* **ASCE Specialty Conference on Stability and Performance of Slopes and Embankments - II**, ASCE Geotechnical Division, July 1992.

Mosher, R. L., *Computer Applications in Geotechnical Engineering: In a High-Performance Computer Environment,* **Geotechnical News**, Vol 9, No. 4, BiTech Publishers Ltd., Vancouver, British Columbia, Canada, December 1991.

Nogami, T., Mosher, R. L., and Jones, H. W., *Seismic Response Analysis of Pile-Supported Structures: Assessment of Commonly Used Approximations,* **Proceedings Second International Conference on Recent Advances in Geotechnical Earthquake Engineering and Soil Dynamics**, St. Louis, MO, March 1991.

Mosher, R. L., *Axial Capacity of Vibratory-Driven versus Impact-Driven Piles,* **Transportation Research Board 69th Annual Meeting**, National Research Council, Washington, D.C., January 1990.

Mosher, R. L., *Review of Tests on Vibro-Driven Piles,* Proceedings of 1989 Annual Deep Foundations Institute Conference, Baltimore, MD, October 89.

Mosher, R. L., Mlakar, P. F., and Jones, H. W., *Simplified Seismic Analysis of Pile Foundations,* **ASCE Proceedings, Foundation Engineering Congress,** Evanston, IL, June, 1989.

Mosher, R. L., *Load-Transfer Criteria for Sands,* **ASME Proceedings, Energy-Sources Technology Conference, Offshore and Arctic Operations Symposium**, New Orleans, LA, January, 1988. (refereed)

Mosher, R. L. and Radhakrishnan, N., *The Government and the PC - The Corps of Engineers' Experience,* **Microcomputers in Engineering Practice - Version 2.0**, BSCES/ASCE Computer Group Lectures Series, MIT, Boston, MA, September, 1987.

Clough, G. W., Mosher, R. M., Singh, Y., and Kuppusamy, T., *Two- and Three-Dimensional Finite Element Analysis of Cellular Cofferdams,* **International Conference of Soil-Structure Interaction**, Paris, May, 1987.

Mosher, R. L. and Urzua, A., *Microcomputer Program for Bearing Capacity Analyses of Shallow Foundation,* **Proceedings of the ASCE Fourth Conference on Computing in Civil Engineering**, Boston, MA, October 1986.

c. Other publications:

Secretary of Defense, **Report to the President and Congress on *Protection U.S. Forces Deployed Abroad,*** Annex C: Defense Special Agency (DSWA) Report of Khobar Tower Bomb Damage, September 1996, Washington, D.C.

Ebeling, R. M., Patev, R. C., and Mosher, R. L., *Case Histories of Earth Pressure-Induced Cracking of Locks,* **Technical Report ITL-96-3,** U. S. Army Engineer Waterways Experiment Station, CE, Vicksburg, MS, September 1996.

Department of the Army, Corps of Engineers, *Seismic Design and Analysis for Corps Projects*, **Engineer Regulation 1110-2-1806,** May 1996, USACE HQ, Washington, D.C.

Ebeling, R. M., Morrison, R. L., and Mosher, R. L., *Stability of Existing Concrete Structures*, **The REMR Bulletin Vol. 13, No.1,** U. S. Army Engineer Waterways Experiment Station, CE, Vicksburg, MS, February 1996.

Department of the Army, Corps of Engineers, *Seismic Analysis and Design of Reinforced Concrete Locks*, **Engineer Technical Letter 1110-2-342,** October 1993, USACE HQ, Washington, D.C.

Ebeling, R. M., Mosher, R. L., Abraham, K., and Peters, J. F., *Soil-Structure Interaction Study of Red River Lock and Dam No. 1 Subject to Sediment Loading*, **Technical Report ITL-93-3,** U. S. Army Engineer Waterways Experiment Station, CE, Vicksburg, MS, September 1993.

Department of the Army, Corps of Engineers, *Design of Sheet Pile Walls,* **Engineer Manual 1110-2-2504,** September 1993, USACE HQ, Washington, D.C.

Mosher, R. L., *Three-Dimensional Finite Element Analysis of Sheet-Pile Cellular Cofferdams*, **Technical Report ITL-92-1**,U. S. Army Engineer Waterways Experiment Station, CE, Vicksburg, MS, April 1992.

Mosher, R. L., ***Three-Dimensional Finite Element Analysis of Sheet-Pile Cellular Cofferdams***, Ph.D., Dissertation, Virginia Polytechnic Institute and State University, Blacksburg, VA, December 1991.

Mosher, R. L., Bevins, T. L., and Neeley, B. D., *Structural Evaluation of Eisenhower and Snell Locks, Saint Lawrence Seaway, Massena, New York*, **Technical Report ITL-91-4,** U. S. Army Engineer Waterways Experiment Station, CE, Vicksburg, MS, November 1991.

Department of the Army, Corps of Engineers, *Design of Pile Foundations,* **Engineer Manual 1110-2-2506,** 1 June 1990, USACE HQ, Washington, D.C.

Mosher, R. L. and Knowles, V., *Finite Element Study of Tieback Wall for Bonneville Navigation Lock,* **Technical Report-ITL-90-4,** U. S. Army Engineer Waterways Experiment Station, CE, Vicksburg, MS, May 1990.

Department of the Army, Corps of Engineers, *Design of Sheet Pile Cellular Structures,* **Engineer Manual 1110-2-2503,** 29 September 1989, USACE HQ, Washington, D.C.

Jones, H. W., Mosher, R. L., and Mlakar, P. F., *Dynamic Group Pile Analysis,* **Proceedings of Corps of Engineers Structural Engineering Conference,** USACE HQ, St. Louis, MO, June, 1988.

Mosher, R. L., *Recent Developments in the Stability of Concrete Gravity Structures,* **Proceedings of Corps of Engineers Structural Engineering Conference**, USACE HQ, St. Louis, MO, June, 1988.

Mosher, R. L., *Recent Developments in Sheet Pile Cellular Cofferdam Design,* **Proceedings of Corps of Engineers Structural Engineering Conference**, USACE HQ, St. Louis, MO, June, 1988.

Mosher, R. L. and Knowles, V., *Finite Element Study of Tieback Wall for Bonneville Navigation Lock,* **Proceedings of Corps of Engineers Structural Engineering Conference**, USACE HQ, St. Louis, MO, June, 1988.

Mosher, R. L., *Effects of Vibratory Driving on Axial Load Capacity,* **Technical Report-ITL-87-7,** September, 1987, U.S. Army Engineer Waterways Experiment Station, CE, Vicksburg, MS.

Rossow, M., Demsky, E., and Mosher, R. L., *Theoretical Manual for Design of Cellular Cofferdams,* **Technical Report-ITL-87-5,** May, 1987, U.S. Army Engineer Waterways Experiment Station, CE, Vicksburg, MS.

Pace, M., Mosher, R. L., Williams, D., *Seepage Analysis of Confined Flow Problems by the Method of Fragments (CFRAG),* **Instruction Report K-84-3**, June 1984, U.S. Army Engineer Waterways Experiment Station, CE, Vicksburg, MS.

Mosher, R. L., *Load-Transfer Criteria for Numerical Analysis of Axially Loaded Piles in Sand,* **Technical Report K-84-1**, January 1984, U.S. Army Engineer Waterways Experiment Station, CE, Vicksburg, MS.

Mosher, R. L., ***Load-Transfer Criteria for Axially Loaded Piles in Sand***, M.S. Thesis, September 1982, Mississippi State University, Mississippi State, MS.

Mosher, R. L., and Pace, M., *Documentation of Computer Program for Bearing Capacity Analysis, (CBEAR),* **Instruction Report K-82-7**, June 1982, U.S. Army Engineer Waterways Experiment Station, CE, Vicksburg, MS.

Price, W. A., Hall, R. L., Mosher, R. L., WES, Hamby, C. C., and Vesselka, R., *Validation Report: Computer Program for Design and Analysis of Inverted-T Retaining Walls and Floodwalls (TWALL),* **Instruction Report K-81-3,** February 1981, U.S. Army Engineer Waterways Experiment Station, CE, Vicksburg, MS.

Price, W. A., Hall, R. L., Mosher, R. L., Jones, H. and George, M. E., *Users Reference Manual: Computer Program for Design and Analysis of Inverted-T Retaining*

Walls and Floodwalls (TWALL), **Instruction Report K-80-7**, U.S. Army Engineer Waterways Experiment Station, CE, Vicksburg, MS.

Price, W. A., Hall, R. L., Mosher, R. L., Jones, H. and George, M. E., *Basic User' s Guide: Computer Program for Design and Analysis of Inverted-T Retaining Walls and Floodwalls (TWALL),* **Instruction Report K-80-6**, April 1980, U.S. Army Engineer Waterways Experiment Station, CE, Vicksburg, MS.

Mosher, R. L. and Radhakrishnan, N., *Computer Programs for Settlement Analysis,* **Instruction Report K-80-5, February 1980,** U.S. Army Engineer Waterways Experiment Station, CE, Vicksburg, MS.

Training

Large Deformation Finite Plasticity, Dr. K. C. Valanis, Vicksburg, MS, 32 hrs, July 1990.

Multiphase Flow and Transport through Soils, Dr. T. Kuppusamy, VPI, Vicksburg, MS, 40 hrs, November 1991.

Introduction to Supervision, OPM, Denver, CO, 80 hrs, March 1992.

Dynamics of Structures and Structure-Foundation Soil Systems, University of Missouri-Rolla, Atlanta, GA, 40 hrs, March 1993.

Leadership for A Democratic Society, The Federal Executive Institute, Charlottesville, VA, 160 hrs, June 1995.

Position Classification for Supervisors, Managers, and Non-Classifiers, Graduate School, U.S. Department of Agriculture, Vicksburg, MS, 16 hrs, January 1996.

Polytechnic University Continuing Education & Professional Training, in conjunction with PLAXIS, 30 hrs, January 2006.

Professional or Technical Societies/Organizations:

American Society of Civil Engineers.

Society of American Military Engineers.
International Society of Soil Mechanics and Foundation Engineers.

Membership on committees or panels:

Organizer, Session on Computer Applications in Geotechnical Engineering, ASCE National Convention, 1987, Alexandria, VA.

Member, ASCE Geo-Institute's Computer Applications Committee, 1988-1994.

Organizer, Session on Computer Applications, ASCE Foundation Engineering Congress, June 1989, Northwestern University, Evanston, IL.

Member, ASCE Technical Council on Computer Practices Publication Committee, 1990-1994.

Member, Organizing Committee, Geotechnical Engineering Congress, June 1991, Boulder, CO.

Member, National Research Council, Transportation Research Board Committee on Modeling Techniques in Geomechanics, A2K05, 1992-present.

Member, Advisory Board, International Specialty Symposium on Structures Response to Impact and Blast – Theory, Experiments and Practice, Tel Aviv, Israel, 1995-1996.

Member, Editorial Board, Shock and Vibration Critical Technology Journal, Shock and Vibration Information Analysis Center (SAVIAC), 1998-present.

National and international meetings of non-governmental societies or organizations:

National Science Foundation Workshop on Research Needs for Experimental Soil Engineering Virginia Polytechnic Institute and State University, Blacksburg, VA, August 1983.

ASCE National Convention, Denver, CO, May 1985, technical committee member).

ASCE Fourth Conference on Computing in Civil Engineering, Boston, MA, October 1986 (technical committee member and presented paper).

ASCE National Convention, Atlantic City, May 1987 (technical committee member).

BSCES/ASCE Computer Group Lectures Series, MIT, Boston, MA, September 1987 (invited speaker).

ASME Energy-Sources Technology Conference, Offshore and Arctic Operations Symposium, New Orleans, LA, January 1988 (presented paper).

ASCE National Convention, Nashville, TN, May 1988 (technical committee member).

ASCE Foundation Engineering Congress, Evanston, IL, June 1989 (session organizer, technical committee member, and presented paper).

Deep Foundations Institute Conference and Annual Meeting, October 1989 (invited speaker).

Transportation Research Board Annual Meeting, January 1990 (presented a paper).

Geotechnical Engineering Congress, June 1991, Boulder, CO (chaired a session).

Transportation Research Board Annual Committee Meeting, January 1993.

Fifth International Conference on Computing Civil and Building Engineering (V-ICCCBE), Anaheim, CA, June 1993 (presented paper).

Engineering Foundation Conference on Risk-Based Decision-Making VI, Santa Barbara, CA, July 1993.

Transportation Research Board Annual Meeting, Committee Meeting, January 1994.

Settlement '94 ASCE Conference at Texas A&M University, College Station, TX, June 16-18, 1994 (organized and chaired two sessions).

Transportation Research Board Annual Meeting, Committee Meeting, January 1995.

65th Shock and Vibration Symposium, Biloxi, MS,
1-4 November 1995 (official delegate and session chair).

Transportation Research Board Annual Committee Meeting, January 1996 (chaired session).

International Specialty Symposium on Structures Response to Impact and Blast – Theory, Experiments & Practice, Tel Aviv, Israel, 6-10 October 1996 (Presented Keynote Address and chaired two sessions).

Graduate Seminar, Civil Engineering Department, Louisiana State University, Presentation on Sheet Pile Circular Cofferdams, Baton Rouge, LA, 7 November 1996.

ASCE Student Chapter Meeting, Louisiana State University, Presentation on Force Protection, Baton Rouge, LA,
7 November 1996.

66th Shock and Vibration Symposium, Monterey, CA, 19-21 November 1996 (official delegate and session chair).

Transportation Research Board Annual Committee Meeting, January 1997.

8th International Symposium on Interaction of Effects of Munitions with Structures, McLean, VA, 22-25 April 1997 (chaired two session).

National Research Council Workshop on Structural Blast Mitigation, Washington, September 1997 (Invited speaker).

Mechanical Engineering Seminar, University of Minnesota, Presentation entitled "Survivability and Protective Structure: Force Protection Research", Minneapolis, MN, 22 October 1997.

67th Shock and Vibration Symposium, Hunt Valley, MD, 3-7 November 1997 (official delegate and session chair).

Transportation Research Board Annual Committee Meeting, January 1998.

University of Minnesota Structural Engineering Seminar Series, seminar entitled "Static and Seismic Design of Sheet Pile Walls", 9 April 1998, St. Paul, MN.

Physical Protection Seminar, Eilat, Israel, 25-
28 May 1998, (Invited speaker).

68th Shock and Vibration Symposium, St. Paul, MN, 12-14 October 1998 (Official delegate and session chair).

International Physical Security Forum hosted by the Israeli Security Agency, Tel Aviv, Israel, 6-10 December 1998 (Invited speaker).

Transportation Research Board Annual Committee Meeting, January 1999.

9th International Symposium on Interaction of Effects of Munitions with Structures, Berlin, Germany, 22-25 May 1999 (Invited speaker and chaired two session).

69th Shock and Vibration Symposium, Albuquerque, NM, 14-17 October 1999 (Official delegate and session chair).

Transportation Research Board Annual Committee Meeting, January 2000.

International Physical Security Forum hosted by the U.S. Department of State, 17-
19 February 2000 (Invited speaker).

70th Shock and Vibration Symposium, Alexanader, VA, 13-

15 November 2000 (official delegate and session chair).

National Research Council Workshop on Protection against Terrorist Attacks, Washington, November 2000 (Invited speaker).

Interactions with academia:

Lecturer – Mississippi State University – 1982-1991.

Adjunct Professor - Mississippi State University – 1991-present.

Adjunct Professor - University of Puerto Rico – 1991-1993.

Adjunct Professor - Virginia Polytechnic Institute and State University – 1992-1996.

Adjunct Professor – Louisiana State University – 1996-present.

Advisory Board Member for the Protection Center – Univ. of Florida – 1998-2006

Advisory Board Member for the Protection Center – Penn State Univ. – 2006-Present

Classes taught (graduate/undergraduate level):

Finite-Element Analysis (graduate level), Spring of 81 and Spring of 86.

Soil-Structure Interaction (graduate level), Fall of 85 and Spring of 88.

Engineering Mechanics 1 (undergraduate level), Fall of 93.

Mechanics of Materials (undergraduate level), Spring of 94.

Introduction to Finite-Element Method (graduate level), Fall of 99.

Service on PhD/MS Committees:

MS Committee, WES Graduate Center Advisor, Ms. Virginia Knowles, Civil Engineering Department, Mississippi State University, 1990-1992.

MS Committee, Local Advisor, Mr. Riv, Civil Engineering Department, University of Puerto Rico, 1991-1993.

MS Committee, WES Graduate Center Advisor, Mr. Kevin Abraham, Civil Engineering Department, Mississippi State University, 1993-1996.

PhD Committee, Dr. Kord Wissmann, Civil Engineering Department, Virginia Polytechnic Institute and State University, 1995.

PhD Committee Local Advisor, Mr. John Weathersby, Civil Engineering Department, Louisiana State University, 1996-2001

Service on Academic Boards:

Civil Engineering Technology Advisory Board, Hinds Junior College, 1985-1992

Government-sponsored national meetings and/or membership on government-sponsored technical committees, panels, etc. or serving as an instructor for a government-sponsored training course:

Twelfth Interagency Research Coordination Conference, 1981.

Invited speaker, CE Structural Engineering Conference, Portland, OR, June 1985.

Invited speaker, CE Geotechnical Engineering Conference, St. Louis, MO, 1986.

REMR Workshop on Sliding of Concrete Structures, 1986.

Fifteenth Interagency Research Coordination Conference, 1987.

Invited speaker, CE Geotechnical Engineering Conference, Jacksonville, FL, April 1988.

Invited speaker, CE Structural Engineering Conference, St. Louis, MO, June 1988 (presented four technical papers).

Invited speaker, CE Structural Engineering Conference, Jacksonville, FL, July 1991 (presented three papers).

Invited speaker, Material Management Workshop on Research Needs for Pile Foundations (The only invited speaker from WES), Vicksburg, MS, July 1993.

Invited Speaker, DOE Workshop on Concrete Beaching, Lawrence Livermore National Laboratory, Livermore, CA, May 1998.

Instructed over 1,200 students from Corps offices throughout the country in the Corps PROSPECT training program from 1980 to 1994 in over 35+ short course.

Membership on Government Committees:

WES coordinator for Task Group on Geotechnical Aspect of Computer-Aided Structural Engineering, 1980-1992.

Member of the GCASE/CAGE Task Group on Slope Stability, 1982-1986.

WES coordinator for the CASE Task Group on Pile Foundations and Substructures, 1984-1994.

Member of the CASE Task Group on Massive Concrete Structures, 1986-1993.

Member of Engineer Manual Committee on the Design of Pile Foundations-sponsored by USACE HQ, 1986-1990.

Member of Engineer Manual Committee on Sheet Pile Cellular Cofferdams sponsored by USACE HQ, 1987-1989.

Member of Engineer Manual Committee on Sheet Pile Walls sponsored by USACE HQ, 1990-1993.

Chairman, DOE Soil-Structure Interaction Expert Review Committee for the In-Tank Precipitation/H-Tank Farm at Savannah River Site, May-December 1994.

Member of Engineer Regulation Committee on Earthquake Design and Evaluation for Civil Works Projects sponsored by USACE HQ, 1994-1995.

Chairman, Tri-Service Reliance Committee on Survivability and Protective Structures, 1996-2008.

Invited Member, DOD Concrete Beaching Advisory Group, (Other members were DOD SES's level and a retired Major General), December 1996–October 1997.

Member of the Advisory Group for the Tri-Service Technical Manual on "The Design and Analysis of Hardened Structures to Conventional Weapons Effects," 1996–2008.

Independent Technical Review Committee for TVA's Chickamauga Lock, Lead for the Review of the Finite Element Analysis, December 1997-May 1998

Independent Technical Review Committee for New Gated Dam at Braddock Lock and Dam on the Monongahela River, Review of the Foundation Design, December 1997-2000.

Special recognitions, honors and awards:

Chi Epsilon, 1975-1977, Worcester Polytechnic Institute, Student, Vice President

Technology Advancement Award, Society of American Military Engineers, Vicksburg Post – 93.

Commander and Director's Research and Development Achievement Award, 1990.

Nominated for the Department of Army Research and Development Award, 1990.

Nominated for the Department of Army Researcher of the Year Award, 1990.

Meritorious Civilian Service Award, 2007.